Zircon U–Pb and Lu–Hf isotopic systems in ediacaran to Fortunian "Taourirt" granitic ring complexes (Silet and In Tedeini terranes, Tuareg shield, Algeria)

Abla Azzouni-Sekkal, Bernard Bonin, Peter Bowden, Faten Bechiri-Benmerzoug, Yassamina Meddi

Zircon U-Pb and Lu-Hf isotopic systems in Ediacaran to Fortunian "Taourirt" granitic ring complexes (Silet and In Tedeini terranes, Tuareg shield, Algeria)

Abla Azzouni-Sekkal[1,2], Bernard Bonin[3], Peter Bowden[4], Faten Bechiri-Benmerzoug[2,5], Yassamina Meddi[2]

1 Université Abou Bekr Belkaid, 13000 Tlemcen, Algérie (asazzouni@hotmail.com)
2 LMMA, FSTGAT, USTHB, BP 32, El Alia, 16111 Bab Ezzouar, Alger, Algérie (meddiyasmina@outlook.com)
3 "GEOPS", Université Paris-Saclay, CNRS, 91405 Orsay Cedex, France (bernard.bonin@universite-paris-saclay.fr)
4 Département de Géologie, Université Jean Monnet, 42023 Saint-Etienne, France (Peter.Bowden@univ-st-etienne.fr)
5 École Normale Supérieure, Kouba, Alger, Algérie (faty_benmerzoug@yahoo.fr)

Corresponding author: Prof. Bernard Bonin (bernard.bonin@universite-paris-saclay.fr)
ORCID number 0000-0002-2981-4046

Abstract: The Tuareg shield in North-West Africa is composed of an assembly of Neoproterozoic continental and oceanic terranes, as well as Archean and Paleoproterozoic terranes separated by major continental shear zones. In the Silet terrane, the igneous suite of Silet-Taourirts is composed of post-collisional ring-complexes of ferroan alkaline and alkali-calcic granites. Six ring-complexes have been dated using the U-Pb SHRIMP technique on zircon. The alkaline Tin Erit (584.8 ± 2.0 Ma), Tihoiiarene (569.8 ± 4.8 Ma) and Tioueine (561 ± 6 Ma) complexes are older than the alkali-calcic Issedienne (538.7 ± 2.9 Ma), Tesnou (536.5 ± 6.7 Ma) and Ait Oklan (529.3 ± 3.1 Ma) complexes. Sharing an enriched mantle source, the complexes display a secular variation of crustal contamination marked by decreasing εHf(t). The oldest alkaline complexes are related to the tectonic escape of the Tuareg terranes to the north after the climax of Pan-African orogeny, while the youngest alkali-calcic complexes were emplaced after the 575-555 Ma intra-continental Murzukian event.

Keywords: U/Pb geochronology, Lu-Hf isotopes, zircon, "Taourirt" granite ring complexes, Silet and In Tedeini terranes, Tuareg shield.

Introduction.

The post-collisional stage of an orogenic episode corresponds to the welding of micro-continents forming new mega-continents. Granitoids emplaced during that stage form a large volume of the upper crust. Coeval igneous events comprise (Bonin, 2004): (i) crustally derived strongly peraluminous granitoids, (ii) magnesian high-K calc-alkaline and shoshonitic to ultrapotassic suites, (iii) ferroan alkali-calcic to alkaline bimodal suites, with metaluminous, slightly peraluminous and peralkaline felsic end-members, known as A-type granites (Bonin, 2007), or ferroan granitoids (Frost and frost, 2011). A-type ferroan granites constitute a significant proportion of post-collisional massifs.

Zircon, the major carrier of Zr, contains also a number of radioactive and radiogenic trace elements. The mineral zircon is a powerful tool because it may be dated accurately with the uranium-to-lead (U–Pb) isotopic decay system and is variously resistant to subsequent alteration. Moreover, given the high concentration of hafnium in zircon, the lutetium-to-hafnium (^{176}Lu–^{176}Hf) isotopic decay system may be used to determine the nature and formation timescale of its source reservoir (e.g., Hawkesworth and Kemp, 2006).

The aim of this paper is to present and discuss new U-Pb and Lu-Hf isotopic data on zircon crystals extracted from six A-type ferroan granitic ring complexes – Ait Oklan, Issedienne, Tesnou, Tin Erit, Tihoiiarene, Tioueine – of the Silet-Taourirt group emplaced within and around the Silet terrane of the Tuareg Shield.

Geodynamic settings

In the West Saharan Desert, the Tuareg Shield, comprising Adrar des Iforas, Hoggar and Aïr, is made up of an assemblage of numerous displaced terranes (Black et al., 1994; Liégeois, 2019). It resulted from the welding of Neoproterozoic ophiolite-bearing juvenile terranes (e.g., Silet, In Tedeini, Tin Zaouatene terranes) emplaced onto or along Archean – Paleoproterozoic metacratonic basement (e.g., LATEA Metacraton, Liégeois et al., 2003), trapped in between two large Archean – Paleoproterozoic continental areas, the West African Craton and the East Saharan Metacraton (Abdelsalam et al., 2002; Liégeois et al., 2013) (Figure 1). Neoproterozoic orogenic episodes shaped the shield. The long-lasting Pan-African orogeny resulted ~650-630 Ma ago into inter-continental collision, whose impact affected the entire shield, while the short-lived (~575-555 Ma) intra-continental Murzukian orogenic event was identified more recently (Fezaa et al., 2010) in the Eastern Hoggar terranes.

The Silet, In Tedeini and Tin Zaouatene terranes constitute the Pharusian belt defined by Lelubre (1952). They are characterised by volcano-sedimentary sequences corresponding to Pharusian I and II formations (Bertrand et al., 1966), related to the Tonian and the Cryogenian periods, respectively (Liégeois, 2019). The two series were crosscut by voluminous calcic to calc-alkaline batholiths (Béchiri-Benmerzoug, 2009) and late bimodal complexes of mafic-ultramafic layered igneous rocks and alkaline to alkali-calcic A-type granite complexes.

The Silet and In Tedeini terranes are connected by the extensive 4°10'E shear zone. They are considered as juvenile island arcs (Black et al., 1994; Brahimi et al., 2018) accreted onto the LATEA metacraton. Zircon U-Pb ages ranging from 870 Ma to 638 Ma of calcic to calc-alkaline granitic batholiths in the Silet terrane substantiate Tonian and Cryogenian episodes of arc accretion (Béchiri-Benmerzoug, 2009; Béchiri-Benmerzoug et al., 2011, 2017). All successive intrusive units display juvenile signatures (positive εNd, low Sr_i), with the exception of the 638 Ma Eheli batholith (negative εNd and high Sr_i).

The Taourirt granite province

Post-collisional plutonic complexes constitute the Taourirt province. "Taourirt" is a local Tuareg word defining an isolated mountain clearly visible in the distance. In the original definition, all roughly circular igneous complexes intruding the Tuareg Shield formations characterized by a sugarloaf shaped topographic feature were named Taourirt by Lelubre (1952). Later on, the usage of the term Taourirt was restricted to the younger complexes emplaced in Central Hoggar (Boissonnas, 1974). Indeed, they are the only plutons that cut the dyke swarms subsequent to the main Pan-African igneous activity in Hoggar, indicating a distinctly late event. The high-level sub-circular, often nested, Taourirt complexes are mostly aligned along mega-shear zones delimiting terranes. They are composed of alkali-calcic and (per)alkaline granites. Post-collisional mafic-ultramafic layered igneous complexes, whose type locality is Laouni (Cottin et al., 1998), occur in association with Taourirt granite complexes, e.g., Allioum with Oukcem (Aïdrous-Belhocine, 2010; Ikhlef-Debabha, 2011), Aguelmam between Iskel and Tihoiiarene (Kheloui et al., 2014), and Edikel with Taessa (Ikhlef-Debabha et al., 2016).

Three sub-provinces – Silet-Taourirts, Laouni-Taourirts, and Tamanrasset-Taourirts – were identified on the basis of their locations (Azzouni-Sekkal et al., 2003). Silet-Taourirts crosscut the Pan-African island arc assemblages of Silet and In Tedeini terranes, and occur preferentially along north-south trending shear zones (Figure 2), whereas Laouni-Taourirts and Tamanrasset-Taourirts were emplaced within the LATEA metacraton.

Three granite groups – GI, GII (a and b) and GIII – were distinguished in the Silet-Taourirts sub-province (Azzouni-Sekkal and Boissonnas, 1993) and, more recently, recognized in the whole province (Azzouni-Sekkal et al., 2003) on the basis of their mineralogy and geochemistry. They constitute two discrete ferroan A-type suites: (i) an extensive alkali-calcic suite comprising amphibole-biotite monzogranite (GI), biotite monzogranite and syenogranite (GIIa), and alkali feldspar granite (alaskite) characterized by secondary albite and lithian mica (GIIb), (ii) and an alkaline suite consisting of hedenbergite-biotite-amphibole alkali feldspar syenite and alkali feldspar granite (GIII).

Mineralogical and geochemical characteristics of the three Taourirt granite groups are summarised in Table 1. The feldspar mineralogy is fairly simple and diagnostic: (i) [alkali feldspar + oligoclase] subsolvus assemblage in GI and GIIa monzogranite and syenogranite, (ii) [K-feldspar + albite] assemblage in GIIb alaskite, (iii) mesoperthite hypersolvus assemblage in GIII alkali feldspar syenite and alkali feldspar granite. Mafic mineralogy is always ferroan: hedenbergite in GIII, amphibole (ferro-hornblende to ferro-edenite in GI and GIIa, hastingsite to ferro-hornblende ± grünerite ± riebeckite in GIII) and mica (annite in GI, GIIa and GIII, protolithionite to zinnwaldite in GIIb).

Abundant accessory minerals are represented by a variety of silicate minerals (zircon, thorite, allanite, chevkinite, titanite), oxides (magnetite, ilmenite, fergusonite), fluorine-bearing minerals (fluorite, topaz) and phosphates (apatite, monazite) (Azzouni-Sekkal and Bonin, 1998).

In GI and GIIa groups, the [titanite + magnetite + ilmenite + quartz] assemblage (Wones, 1989) indicates a more oxidizing environment than in the GIII group characterized by the [hedenbergite + magnetite + ilmenite + quartz] assemblage. Accessory Y-rich minerals form two groups: (1) LREE-rich allanite, chevkinite and monazite, (2) HREE-rich zircon, thorite, titanite and fergusonite. As a result, all rock compositions are rich in LILE, REE and HFSE, a typical feature of A-type granites (Bonin, 2007; Collins et al., 2020).

Zircon crystals are stubby to elongate, and millimetre-sized, with specific morphologies (Azzouni, 1995). In GI, they display dominant pyramids corresponding to S18 and P3-P4 types defined by Pupin (1980), S14 and P2-P3 types in GIIa, and P1-P2 and G1 types in GIIb. In GIII, long, limpid and coloured crystals yield D (K1-K3 sub-types) and P5 (T13-T14 sub-types) types. High zircon saturation temperatures (780-940°C) suggest early crystallization in hot magmas.

Geology and Rb-Sr data of six Silet-Taourirt complexes

Samples from six Silet-Taourirt ring complexes were analysed at Ait Oklan, Issedienne, Tesnou, Tin Erit, Tihoiiarene and Tioueine (Figures 2 and 3).

The Ait Oklan ring complex was emplaced into the In Tedeini terrane, where it crosscuts the undated Tidjelamine calc-alkaline batholith. It is made up of two GIIa concentric units, the outer one is composed of syenogranite, where AO24 sample was collected (Figure 3). An imprecise whole-rock Rb-Sr isochron age of 511 ± 39 Ma ($\lambda^{87}Rb = 1.42*10^{-11}$ a^{-1}) with $^{87}Sr/^{86}Sr = 0.703 \pm 0.013$, MSWD = 4.4, is interpreted as having been disturbed by the interaction with hydrothermal fluids (Azzouni-Sekkal et al., 2003).

The Issedienne ring complex was emplaced south of the Imhellatene nested complex, within the Silet terrane, near the contact between Pharusian II volcano-sedimentary formations and the undated Louine Harane calc-alkaline batholith. It consists of several GIIa concentric units and one GIIb peripheral unit. I26 sample was collected in a GIIa monzogranite unit set between the outer and central intrusions (Figure 3). A biotite Rb-Sr age of 470 ± 15 Ma ($\lambda^{87}Rb = 1.47*10^{-11}$ a^{-1}), recalculated at 487 ± 15 Ma ($\lambda^{87}Rb = 1.42*10^{-11}$ a^{-1}), was published by Lay and Ledent (1963), evidencing likely hydrothermal alteration.

The Tesnou ring complex was emplaced along the 4°10'E shear zone, which marks the In Tedeini – Silet terrane boundary. Cross-cutting Pharusian II volcano-sedimentary formations, and elongated parallel to the north-south trending regional schistosity, it is a nested complex formed from a number of GIIa and GIIb intrusive units. TES52 sample is composed of GIIa monzogranite (Figure 3). An associated lepidolite pegmatite yields a composite mineral Rb-Sr age of 522 ± 11 Ma ($\lambda^{87}Rb = 1.47*10^{-11}$ a^{-1}), recalculated at 540 ± 11 Ma ($\lambda^{87}Rb = 1.42*10^{-11}$ a^{-1}). It may approximate the crystallisation age (Boissonnas et al., 1964). A more imprecise age of 537 ± 30 Ma age was also obtained by K-Ar on pegmatitic muscovite (Boissonnas, 1974).

The Tin Erit ring complex was emplaced within the Silet terrane, where it crosscuts the undated Louine Harane calc-alkaline batholith, and Pharusian I volcano-sedimentary formations. It is composed of a GIIa central unit, and a GIII peripheral crescent unit (Boissonnas, 1974, Bechiri-Benmerzoug, 1998). The TE26 sample was collected in the GIIa syenogranite central unit (Figure 3).

The Tihoiiarene ring complex (Boissonnas and Gravelle, 1961; Meddi, 2011) was emplaced within the In Tedeini terrane, in between the Imezzarene calc-alkaline batholith, dated as 583 ± 7 Ma by U-Pb zircon ID-TIMS method (Bertrand et al., 1986), Pharusian II volcano-sedimentary formations, and the Aguelmam gabbro complex (Kheloui et al., 2014). It comprises a central GIIa intrusive unit surrounded by an outer GIII alkali feldspar granite intrusive unit, where the TH24 sample was collected (Figure 3). The nearby Iskel complex yields an imprecise whole-rock Rb-Sr isochron age at 564 ± 40 Ma ($\lambda^{87}Rb = 1.47*10^{-11}$ a^{-1}) (Boissonnas et al., 1969), recalculated at 592 ± 20 Ma ($\lambda^{87}Rb = 1.42*10^{-11}$ a^{-1}) by Cahen et al. (1984).

The Tioueine ring complex was emplaced close to the 4°10'E shear zone, within the Silet terrane, where it crosscuts Pharusian I volcano-sedimentary formations. GI, GIIa and GIII intrusive units are concentrically arranged (Azzouni-Sekkal and Boissonnas, 1987). The major ring intrusion, where the Ti52 sample was collected, is composed of GIII alkali feldspar granite (Figure 3). An imprecise whole-rock Rb-Sr isochron age ($\lambda^{87}Rb = 1.47*10^{-11}$ a^{-1}) of 560 ± 40 Ma with $^{87}Sr/^{86}Sr = 0.705$ and a biotite Rb-Sr age of 551 ± 17 Ma (Boissonnas et al., 1969), were recalculated at 580 ± 41 Ma and 571 ± 18 Ma ($\lambda^{87}Rb = 1.42*10^{-11}$ a^{-1}), respectively, by Cahen et al. (1984). A narrow GIII quartz alkali feldspar syenite ring dyke, crosscutting GIIa and GIII granitic intrusive units, yields a zircon ID-TIMS U-Pb age of 523 ± 1 Ma (Paquette et al, 1998).

Analytical methods

All analyses were completed in the Geochemical Analysis Unit (GAU) of the GEMOC Key Centre in the Department of Earth and Planetary Sciences, Macquarie University, Australia. Analytical methods are described in Belousova et al. (2006).

Hf contents of the zircon grains were determined by a CAMEBAX SX50 electron microprobe. An accelerating voltage of 15 kV and a beam current of 20 nA were used for all analyses.

Hf isotope analyses were carried out in situ with either a Merchantek/New Wave Research 213 nm or a 193 nm EXCIMER laser-ablation microprobe attached to a Nu Plasma multi- collector ICPMS system. For the calculation of εHf values, we have adopted the values of Blichert-Toft et al. (1997).

Zircon U-Pb isotopic geochronology

Analytical data are listed in Table 2. Almost all crystals yield a core – mantle – rim texture and display oscillatory zoning and, more rarely, sector zoning, all indicative of an igneous origin. U and Th concentrations may be very high, with Th/U ratios generally higher than 0.20. For periods more recent than 1.5 Ga, apparent $^{206}Pb/^{238}U$ data yield lower uncertainties than $^{207}Pb/^{206}Pb$ data (Spencer et al., 2016). Thus, they will be examined preferably to determine the most geologically appropriate ages. Crystals exhibiting discordance higher than 10% were discarded in age calculations. Large variations of discordance are not related to U and Th concentrations.

Ait Oklan (AO24)

Zircon crystals are euhedral and brown with iron staining. One homogeneous crystal is entirely dark. Grain shapes vary from stubby to elongate. Crystals are 1000-3000 µm-long and 750 µm-wide (length/width ratios varying from 1.5:1 to 4:1) and display oscillatory zoning around cores. In a total of 30 analysed grains, 9 crystals satisfy the lower than 10% discordance criteria and 21 crystals are strongly discordant with discordance up to 51%.

Zircon crystals are highly radioactive, with U and Th contents ranging from 877 to 27550 ppm (average 6035 ppm) and from 580 to 6790 ppm (average 1723 ppm), respectively. Th/U ratios vary from 0.14 up to 1.15. Ratios higher than 0.20, which indicate an igneous origin, were found in both concordant and discordant spots. The lowermost ratios (0.14-0.17) were found in discordant spots, and may result from solid-state diffusion.

Apparent $^{206}Pb/^{238}U$ ages range from 593 ± 7 Ma to 290 ± 4 Ma, with a peak at 514 Ma (Figure 4A). A group of 4 concordant spots yielded a Concordia age of 529.3 ± 3.1 Ma, MSWD = 1.3, representing the age of emplacement of the ring-dyke. Two spots yield older apparent $^{206}Pb/^{238}U$ ages of 593 ± 7 Ma and 581 ± 6 Ma, which are interpreted as inherited. Three other spots yielded younger apparent $^{206}Pb/^{238}U$ ages of 483 ± 7 Ma, 453 ± 5 Ma and 333 ± 4 Ma, which may reflect late hydrothermal events (Figure 5A).

Issedienne (I26)

Zircon crystals are euhedral and brown with iron staining. Grain shapes vary from stubby to elongate. Crystals are 1000-4000 µm-long and 500-1500 µm-wide (length/width ratios varying from 1.5:1 to 5:1) and display oscillatory zoning around cores. In a total of 31 analysed grains, 11 crystals satisfy the lower than 10% discordance criteria and 20 crystals are strongly discordant with discordance up to 71%.

Crystals are variably radioactive, with U and Th contents ranging from 3 to 10187 ppm (average 1519 ppm) and from 13 to 9534 ppm (average 967 ppm), respectively. Th/U ratios vary from 0.20 up to 3.95, indicating an igneous origin.

Apparent $^{206}Pb/^{238}U$ ages range from 1441 ± 6 Ma to 418 ± 5 Ma, with a peak at 538 Ma (Figure 4B). A first group of 4 spots yielded a Concordia age of 558.9 ± 3.2 Ma, MSWD = 0.021, and a second group of 5 spots yields a Concordia age of 538.7 ± 2.9 Ma, MSWD = 3.4 (Figure 5B). The interpretation of the two age groups is not straightforward. They might represent two discrete igneous episodes. Chronological data on the other intrusions of the complex are not available, and it is not possible to select the correct age. For now, the younger age is assumed to represent the age of igneous emplacement of the intrusive unit and the older age to remobilized antecrysts. An older

concordant spot ($^{206}Pb/^{238}U$ age of 588 ± 8 Ma) is interpreted as inherited. A younger $^{206}Pb/^{238}U$ age of 480 ± 5 Ma may reflect late hydrothermal effects.

Tesnou (TES52)

Zircon crystals are euhedral and translucent to milky yellow. Grain shapes vary from stubby to elongate. Crystals are 1000-6000 μm-long and 500-1500 μm-wide (length/width ratios varying from 1.5:1 to 6:1) and display oscillatory zoning around cores. In a total of 22 analysed grains, 8 crystals satisfy the lower than 10% discordance criteria and 14 crystals are strongly discordant with discordance up to 62%.

Crystals are highly radioactive, with U and Th contents ranging from 164 to 41833 ppm (average 2951 ppm) and from 93 to 5511 ppm (average 693 ppm), respectively. Th/U ratios vary from 0.12 to 0.57. Concordant crystals have Th/U ratios ranging from 0.28 to 0.57, indicating an igneous origin.

Apparent $^{206}Pb/^{238}U$ ages range from 583 ± 6 Ma to 306 ± 5 Ma, with two major peaks at 524 Ma and 478 Ma (Figure 4D). A group of 5 concordant spots yielded a Concordia age of 536.5 ± 6.7 Ma, MSWD = 16 (Figure 5D), which is consistent with the less precise mineral ages of 540 ± 11 Ma (Rb-Sr) and 537 ± 30 Ma (K-Ar) determined on muscovite. It is interpreted as the age of igneous emplacement. A $^{206}Pb/^{238}U$ age of 583 ± 6 Ma is interpreted as inherited. Two younger $^{206}Pb/^{238}U$ ages of 494 ± 6 Ma and 475 ± 5 Ma may evidence late hydrothermal disturbance.

Tin Erit (TE26)

Zircon crystals are euhedral, stubby and translucent to orange yellow with iron staining. They are 1000-2000 μm-long and 500-750 μm-wide (length/width ratios varying from 1.5:1 to 2:1) and display oscillatory zoning around cores. In a total of 20 analysed crystals, 14 spots satisfy the lower than 10% discordance criteria and 6 spots are strongly discordant with discordance up to 45%.

Crystals are highly radioactive, with U and Th contents ranging from 127 to 6993 ppm (average 2404 ppm) and from 68 to 7853 ppm (average 1300 ppm), respectively. Th/U ratios vary from 0.33 to 1.08, indicating an igneous origin.

Apparent $^{206}Pb/^{238}U$ ages range from 639 ± 6 Ma to 510 ± 7 Ma (Figure 4C). Two groups of concordant spots provide two Concordia ages. A first group of 9 spots yielded a Concordia age of 584.8 ± 2.8 Ma, MSWD = 6.2, whereas the second group of 4 spots yields a Concordia age of 600.4 ± 3.4 Ma, MSWD = 3.9 (Figure 5C). From field evidence, the 585 ± 3 Ma age is considered as

representing the age of igneous emplacement and the 600 Ma age is interpreted as inherited. A crystal with a $^{206}Pb/^{238}U$ age of 639 ± 6 Ma is clearly inherited.

Tihoiiarene (TH24)

Zircon crystals are euhedral, stubby and translucent to pale yellow. They are 1000-1500 μm-long and 500-750 μm-wide (length/width ratios varying from 1.5:1 to 2:1) and display oscillatory zoning around cores. In a total of 30 analysed grains, 8 crystals satisfy the lower than 10% discordance criteria and 22 spots are strongly discordant with discordance up to 93%.

Crystals are highly radioactive, with U and Th contents ranging from 441 to 45162 ppm (average 9926 ppm) and from 162 to 26678 ppm (average 4581 ppm), respectively. Th/U ratios vary from 0.23 to 0.96, indicating an igneous origin.

Apparent $^{206}Pb/^{238}U$ ages range from 607 ± 8 Ma to 93 ± 3 Ma, with 19 spots yielding ages higher than 550 Ma. A group of 5 concordant spots yielded a Concordia age of 569.8 ± 4.8 Ma, MSWD = 0.46 (Figure 5E). Two older $^{206}Pb/^{238}U$ ages of 579 ± 8 Ma and 577 ± 8 Ma are interpreted as inherited. Three younger $^{206}Pb/^{238}U$ ages of 537 ± 7 Ma, 498 ± 6 Ma, and 452 ± 6 Ma may evidence late hydrothermal disturbance.

Tioueine (Ti59)

Zircon crystals are euhedral, stubby and pale yellow, with sparse deep red staining. They are 1000-2500 μm-long and 500-750 μm-wide (length/width ratios varying from 1.5:1 to 3:1) and display oscillatory zoning around cores. In a total of 30 analysed grains, 17 crystals satisfy the lower than 10% discordance criteria, 12 spots are discordant with discordance up to 42% and one spot yields a discordance of 70% (Figure 4F).

Three spots are moderately radioactive (154-514 ppm U, 72-335 ppm Th) spots. Other crystals are more radioactive, with U and Th contents ranging from 1526 to 7640 ppm (average 4905 ppm) and from 466 to 5705 ppm (average 2807 ppm), respectively. Th/U ratios vary from 0.27 to 0.78, indicating an igneous origin.

Apparent $^{206}Pb/^{238}U$ ages range from 609 ± 6 Ma to 532 ± 6 Ma. A group of 16 concordant spots yielded a Concordia age of 561 ± 6 Ma, MSWD = 0.57 (Figure 5F). A poorly radioactive concordant crystal yielding an older $^{206}Pb/^{238}U$ age of 609 ± 6 Ma is interpreted as inherited.

Zircon Hf isotopic compositions

In Table 3, $^{206}Pb/^{238}U$ ages, Lu-Hf isotopic data, εHf(t), single-stage (TDM1) and 2-stage (TDM2) model ages are listed.

Ait Oklan (AO24)

From the total of 30 crystals analysed for U-Pb geochronology, 19 crystals were analysed for Lu-Hf isotopes. εHf(t) are constantly negative and range between -6.57 and -0.15 (Fig. 6A), TDM1 between 1.08 and 0.92 Ga and TDM2 between 1.40 and 1.16 Ga. The four concordant crystals at 529.3 ± 3.1 Ma yield a more restricted range, with εHf(t) between -2.65 and -0.86, TDM1 between 1.22 and 1.14 Ga and TDM2 between 1.60 and 1.50 Ga. The two concordant crystals at 483 ± 7 and 482 ± 6 Ma display similar results, with εHf(t) = -3.44 and -2.42, TDM1 = 1.21 and 1.15 Ga and TDM2 = 1.62 and 1.55 Ga, respectively. The 13 other crystals, which are discordant, give scattered results within the whole range of values.

Issedienne (I26)

From the total of 31 crystals analysed for U-Pb geochronology, 17 crystals were analysed for Lu-Hf isotopes. εHf(t) are constantly positive and range between +0.68 and +4.84 (Fig. 6B), TDM1 between 1.55 and 1.12 Ga and TDM2 between 1.45 and 1.84 Ga. The four concordant crystals at 558.9 ± 3.2 Ma display the highest values of εHf(t), ranging from +2.51 to +4.84, and the lowest values of TDM1 from 1.03 to 0.92 Ga and of TDM2 from 1.31 to 1.16 Ga. The five concordant crystals at 538.7 ± 2.9 Ma display similar values of εHf(t), ranging between +2.16 and +4.01, of TDM1 between 1.03 and 0.95 Ga and TDM2 between 1.32 and 1.20 Ga. The older crystal yielding a 588 ± 8 Ma age displays again nearly identical values with εHf(t) = +3.26, TDM1 = 1.02 Ga and TDM2 = 1.28 Ga. The younger crystal yielding an apparent 480 ± 5 Ma age displays a lower value of εHf(t) = +0.99, with TDM1 = 1.04 Ga and TDM2 = 1.34 Ga. The six discordant crystals display various results with the lowest εHf(t) of +0.68 and +0.84 and the highest TDM1 of 1.08 Ga and TDM2 of 1.40 Ga, as well as medium values (εHf(t) between +1.91 and +3.04, TDM1 between 1.03 and 0.98 Ga, TDM2 between 1.33 and 1.26 Ga).

Tesnou (TES52)

From a total of 22 crystals analysed for U-Pb geochronology, 12 crystals were analysed for Lu-Hf isotopes. εHf(t) are highly variable, ranging between -6.01 and +11.19 (Fig. 6C), corresponding to TDM1 between 1.54 and 0.68 Ga and TDM2 between 1.77 and 0.98 Ga. The four concordant

crystals at 536.5 ± 6.7 Ma display εHf(t) ranging between -1.08 and +11.19, TDM1 between 1.14 and 0.68 Ga and TDM2 between 1.50 and 0.75. The concordant crystal yielding a younger apparent age of 494 ± 6 Ma displays εHf(t) = -2.77, TDM1 = 1.20 Ga and TDM2 = 1.60 Ga. In the group of seven discordant crystals, one crystal yields high εHf(t) = +7.45, low TDM1 = 0.81 and TDM2 = 0.98 Ga, another crystals yields the lowest values of εHf(t) and the highest TDM1 and TDM2, while four others yield values near CHUR (εHf(t) between -0.39 and +0.61, TDM1 between 1.08 and 1.05 Ga, TDM2 between 1.42 and 1.37 Ga).

Tin Erit (TE26)

From a total of 20 crystals analysed for U-Pb geochronology, 16 crystals were analysed for Lu-Hf isotopes. εHf(t) are constantly positive and yield a huge range of values, between +5.59 and +30.27, four of which plot well above the DM trend (Fig. 6D) and give unrealistic low TDM1 and TDM2. These four crystals are the most radioactive and display the highest $^{176}Lu/^{177}Hf$ and $^{176}Yb/^{177}Hf$ ratios.

The first group of eight concordant crystals at 584.8 ± 2.8 Ma show the widest range of εHf(t) from +5.67 up to +27.89, among which the five crystals having εHf(t) values below the DM trend show TDM1 between 0.94 Ga and 0.69 Ga and TDM2 between 1.16 Ga and 0.76 Ga. The second group of five concordant crystals at 600.4 ± 3.4 Ma displays a more restricted range of εHf(t) between +5.59 and +12.58, TDM1 between 0.96 Ga and 0.68 Ga, TDM2 between 1.16 Ga and 0.73 Ga. Two discordant crystals display lower εHf(t) (+5.54 and +9.44), with TDM1 of 0.93 Ga and 0.78 Ga and TDM2 of 1.16 Ga and 0.91 Ga, respectively, while another one shows the highest value of εHf(t) of +30.27.

Tihoiiarene (TH24)

From a total of 30 crystals analysed for U-Pb geochronology, 20 crystals were analysed for Lu-Hf isotopes. εHf(t) are dominantly positive and yield again a large range of values, between -2.93 and +22.15, two of which plot well above the DM trend (Fig. 6E), giving unrealistic low TDM1 and TDM2. These two crystals are discordant and not highly radioactive, one crystal displays the highest $^{176}Lu/^{177}Hf$ and $^{176}Yb/^{177}Hf$ ratios.

The group of five concordant crystals at 569.8 ± 4.8 Ma displays εHf(t) ranging between +1.55 and +8.59, TDM1 between 1.08 and 0.81 Ga and TDM2 between 1.37 and 0.93 Ga. The older (579 ± 8 Ma) concordant crystal displays highly radiogenic εHf(t) of +12.84, TDM1 of 0.64 Ga, TDM of 0.68 Ga, indicating a juvenile source. Two younger (537 ± 7 Ma and 498 ± 6 Ma) concordant

crystals display εHf(t) of +4.17 and +9.59, TDM1 between 0.94 and 0.76 Ga and TDM2 between 1.19 and 0.83 Ga, respectively. The twelve discordant crystals show the largest variations of εHf(t) from negative (-2.93, corresponding to TDM1 = 1.24 Ga and TDM = 1.63 Ga) to highly positive values (+22.15, with unrealistic low TDM1 and TDM2).

Tioueine (Ti59)

From the total of 30 crystals analysed for U-Pb geochronology, 22 crystals were analysed for Lu-Hf isotopes. εHf(t) are constantly positive and range between +2.20 and +7.06 (Fig. 6F), TDM1 between 1.08 and 0.88 Ga and TDM2 between 1.33 and 1.06 Ga. Fifteen crystals in the group of concordant crystals at 561 ± 6 Ma yield fairly grouped results, with εHf(t) between +2.20 and +4.72, TDM1 between 1.08 and 0.95 Ga and TDM2 between 1.33 and 1.17 Ga. Three discordant crystals, with similar (565-560 Ma) apparent ages, yield the same results, with εHf(t) between +3.10 and +3.85, TDM1 between 1.03 and 1.01 Ga and TDM2 between 1.27 and 1.23 Ga. An older (609 ± 6 Ma) concordant crystal displays more juvenile results, with εHf(t) = +7.06, TDM1 = 0.88 Ga and TDM2 = 1.06 Ga. Two discordant crystals with similar old (597 Ma and 605 Ma) apparent ages yield close results, with εHf(t) = +6.12 and 7.01, TDM1 = 0.92 and 0.89 Ga and TDM2 = 1.11 and 1.06 Ga, respectively.

Discussion

Unravelling precise ages of granitic episodes require zircon U-Pb isotopic analyses. Modern techniques enable simultaneous determination of Hf isotopes. It is not the scope of this paper to review all occurrences of postorogenic granitic suites resembling the Taourirt granite province.

Unfortunately, if post-collisional igneous episodes in the Pan-African orogen are currently more and more dated by zircon U-Pb isotopic system, combined U-Pb-Lu-Hf isotopic studies remain scarce (e.g., Montero et al., 2017, and references therein). Thus, we will concentrate the discussion on the Taourirt granite province and, afterwards, we will consider postorogenic granite magmatism emplaced after the Pan-African orogenic episodes in the Hoggar.

Rb-Sr (and $^{40}Ar/^{39}Ar$) age conundrum

Previous attempts using rock-mineral and/or whole-rock Rb-Sr methods (Boissonnas et al., 1964, 1969; Azzouni-Sekkal et al., 2003) have failed to date accurately and/or precisely the emplacement

ages of Silet-Taourirts, due to isotopic disturbance by hydrothermal fluids active along shear zones until the Early Ordovician epoch.

In the Laouni terrane, in the Tamanrasset-Taourirt sub-province, the In Tounine massif displays consistent Early Cambrian ages (Cheilletz et al., 1992), i.e. 521 ± 7 Ma (recalculated at 502 ± 40 Ma, Azzouni-Sekkal et al., 2003) by whole-rock Rb-Sr isochron and 534.5 ± 2.5 Ma by $^{40}Ar/^{39}Ar$ on biotite (Cheilletz et al., 1992). Similarly, in the Laouni-Taourirt sub-province, the Bahouinet North massif yields an imprecise whole-rock Rb-Sr isochron age of 524 ± 43 Ma (Zaimen, 1994, Azzouni-Sekkal et al., 2003).

Elsewhere in Hoggar, whole-rock Rb-Sr isochron ages of granite complexes akin to the Taourirt suite are in the same range. Whole-rock Rb-Sr isochron ages of 536 ± 16 Ma (Tihodaïne, Abdallah, 2008) and 555 ± 15 Ma (Tisseliline, Liégeois et al., 2003) relate to complexes emplaced along the Ounane major shear zone separating the LATEA Metacraton and the Orosirian Stripe (Liégeois, 2019) and may be related to isotopic disturbance by hydrothermal fluids percolating along the shear zone.

However, the precise zircon U-Pb ID-TIMS age of 523 ± 1 Ma measured in a quartz alkali feldspar syenite ring dyke of Tioueine (Paquette et al., 1998) was consistent with average biotite $^{40}Ar/^{39}Ar$ age of 534.5 ± 2.5 Ma of Tamanrasset-Taourirts (Cheilletz et al., 1992). Thus, until the beginning of the 21st century, the entire Taourirt province was collectively assumed to be emplaced during the Early Cambrian (Azzouni-Sekkal et al., 2003).

Igneous emplacement ages

The age conundrum became more obvious, when a zircon U-Pb SHRIMP age of 552 ± 3 Ma was determined in the In Tounine complex, in variance with the former Rb-Sr and $^{40}Ar/^{39}Ar$ ages (Idir et al., 2014). Accordingly, the Late Ediacaran zircon U-Pb age was interpreted as dating igneous emplacement, while the Early Cambrian ages may relate to late hydrothermal events.

Our zircon U-Pb SHRIMP isotopic study of Silet-Taourirts ring complexes confirmed that Rb-Sr ages are systematically lower. We identified two groups of zircon U-Pb ages. The older group of GIII-bearing ring complexes display Middle Ediacaran ages: Tin Erit (585 ± 2 Ma), Tihoiiarene (570 ± 5 Ma) and Tioueine (561 ± 6 Ma). The younger group of GIII-free ring complexes yields a larger range of ages from Late Ediacaran to Fortunian (Early Cambrian): Issedienne (559 ± 3 Ma and 539 ± 3 Ma), Tesnou (536.5 ± 7 Ma, vs. 506 ± 16 Ma by Rb-Sr) and Ait Oklan (529 ± 3 Ma, vs. 511 ± 39 Ma by Rb-Sr). The 523 ± 1 Ma Tioueine quartz alkali feldspar syenite ring dyke (Paquette et al., 1998) is probably related to this second group.

The two igneous episodes occurred well after the final Pan-African collision estimated at 650-

630 Ma. The first 585-560 Ma intra-continental event accompanied dextral displacements along the 4°10'E transcurrent shear zone. Associated with the northward tectonic escape of Pharusian terranes due to West African Craton indentation, these post-collisional movements ended at around 580 Ma (Brahimi et al., 2018; Liégeois, 2019). The second 560-520 Ma intra-continental event may be related either to vanishing stress generated by the end of convergence with West African Craton, and/or to the far-distant Murzukian (~575-555 Ma) effect (Fezaa et al., 2010), when the stress coming from the west became negligible.

Inheritance

Scarce inherited crystals occur in all samples. They may shed light on igneous episodes predating Silet-Taourirts emplacement. The older Middle Ediacaran group displays concordant xenocrysts at ~639 Ma (Tin Erit), ~612 Ma (Tioueine) and ~600 Ma (Tihoiiarene). The Cryogenian (639 Ma) xenocryst may have been extracted from the undated Louine Harane calc-alkaline batholith, which Tin Erit crosscuts. The Early Ediacaran (612 Ma and 600 Ma) ages are so far unknown in Silet and In Tedeini terranes. In the younger Late Ediacaran-Fortunian group, concordant crystals at 588 ± 8 Ma (Issedienne), 585.4 ± 4.3 Ma (Ait Oklan) and at 583 ± 6 Ma (Tesnou) remind ages of the first group.

Late hydrothermal episodes

In Taourirt ring complexes, except Tin Erit and Tioueine, scarce concordant crystals record isotopic disturbance in the Early Paleozoic. However, they show by cathodoluminescence imagery the same characteristics as the remainder of concordant crystals and do not represent newly formed crystals. In Ait Oklan, a unique crystal dated at 453 ± 5 Ma (AO24-20) is entirely dark (Figure 6A), as a consequence of metamictisation due to radioactive decay and/or resulting from high contents of non-stoichiometric trace elements (Troch et al., 2018).

Five episodes – ~535 Ma (Fortunian), ~500 Ma (Furongian), ~480 Ma (Tremadocian), ~ 450 Ma (Katian), ~330 Ma (Mississipian) – may be identified. The first episode, recorded in Tihoiiarene only, was coeval to Tesnou emplacement and may reflect hydrothermal fluid percolation within the large shear zone at the Silet – In Tedeini terrane boundary, along which Tihoiiarene and Tesnou were emplaced.

The other episodes were not coeval to igneous events known to date in the Hoggar, but they are recorded in disturbed isotopic clocks of many igneous complexes (for an overview, see Bechiri-Benmerzoug et al., 2017). The Cambrian episode is associated with orogenic collapse and molasse

deposition (Fabre, 2005). Interestingly, two types of zircon crystals – igneous and hydrothermal – were distinguished in the Tamlalt-Menhouhou gold deposit of High Atlas (Morocco) (Pelleter et al., 2007). Ediacaran potassic rhyolites, with a ferroan (A-type) alkali-calcic chemistry, were erupted at 569 ± 8 Ma, i.e. coevally with Tihoiiarene. They were albitized during the Tremadocian, like in Ait Oklan and Tihoiiarene. The Ordovician episodes are associated with transtensional to extensional movements along north-south trending shear zones, evidenced by the so-called "Arenigian" and "Taconic" unconformities (Zazoun and Mahdjoub, 2011).

Last, a unique crystal (AO24-38) in Ait Oklan yields a more intriguing 333 ± 4 Ma Visean age, reminiscent of the Variscan orogeny, developed in Northwestern Sahara only (Fabre, 2005). Early Permian compressional deformations (Haddoum et al., 2001) resulted in the Hoggar basement into renewed dextral movements along north-south trending shear zones.

Sources

The two groups exhibit a wide range of εHf(t) in zircon. In the Middle Ediacaran group, concordant and discordant crystals yield positive εHf(t), except two discordant spots in TH24 sample. Crystals with high $^{176}Yb/^{177}Hf$ (> 0.09) show the largest range of εHf(t), from +0.1 up to +30.3, some spots plotting well above the DM evolutionary curve. These extremely high εHf(t) do not reflect igneous signatures, but may indicate fluid-induced Lu-Hf isotopic disturbance.

There is no simple correlation of $^{176}Yb/^{177}Hf$ ratios with εHf(t) values. In crystals with low $^{176}Yb/^{177}Hf$ (< 0.09), εHf(t) values plot between CHUR and DM evolutionary curves and vary from Tin Erit (between +5.5 and +8.9, average εHf = +7.3) to Tihoiiarene (between +0.6 and +7.3, average = +3.8) to Tioueine (between +2.2 and +4.7, average = +3.6). Positive values of εHf(t) suggest that zircon crystallized in juvenile liquids formed by fractionation of mantle-derived magmas. The OIB-type mantle source was enriched, as shown by fairly young Neoproterozoic TDM ages of ~0.65 Ga (Tin Erit), ~0.91 Ga (Tihoiiarene) and ~0.99 Ga (Tioueine). The secular variation from 585 to 560 Ma marked by decreasing εHf(t) (Figure 7) suggests increasing, yet slight, contamination by old crustal components.

In the Late Ediacaran to Fortunian group, concordant and discordant crystals yield both negative and positive εHf(t). In the three crystals yielding high $^{176}Yb/^{177}Hf$ (> 0.09), two discordant crystals exhibit low negative values of -6.0 and -6.6 and one concordant crystal a high positive value of +11.2. In crystals with low $^{176}Yb/^{177}Hf$ (< 0.09), εHf(t) values plot both above and below the CHUR evolutionary curve and show a secular variation of εHf(t) decreasing from Issedienne (between +0.7 and +4.8, average = +2.6) to Tesnou (between -2.8 and +1.8, average = +0.0) to Ait Oklan (between -4.4 and -0.1, average = -1.8) (Figure 7). Compared to the older Middle Ediacaran group, the

younger Late Ediacaran to Fortunian group shares the same OIB-type mantle source, but is little more and more contaminated by crustal materials.

Sm-Nd isotopic data are available on the youngest (Fortunian) Tesnou and Ait Oklan complexes. Whole rock εNd, calculated at 525 Ma, are negative, from -2.13 down to -5.20 and from -1.25 down to -5.21, respectively (Azzouni-Sekkal et al., 2003). As the country rocks, made up of Cryogenian Pharusian II volcano-sedimentary formations, yield positive εNd calculated at 530 Ma from +1.23 up to +3.03 (Dupont, 1987), the negative εNd in the Silet-Taourirts imply contamination by an old basement. Sm-Nd isotopic data are consistent with Lu-Hf isotopic data and identify the Archean – Paleoproterozoic LATEA metacraton, which the Silet terrane was overthrusted onto, as the likely contaminant.

Post-orogenic granitic massifs in the Hoggar

The Taourirt province, as defined by Azzouni-Sekkal et al. (2003), is confined to a restricted quadrangle delimited by 4°E – 6°E longitudes and 20°N – 26°N latitudes. Many igneous complexes containing ferroan alkali-calcic and alkaline granites identical to Taourirt granites, but not always with ring structures, occur throughout the Tuareg Shield (Liégeois, 2019). Several ferroan alkali-calcic and alkaline granite massifs in the Hoggar have been dated by U-Pb on zircon, mostly by SHRIMP and LA-ICP-MS methods. Yet, no Lu-Hf isotopic compositions were determined.

The In Ouzzal terrane, Western Hoggar, displays the oldest dated "Taourirt-like" granitic massif (Fezaa et al., 2019). The North Tihimatine massif analysed by two zircon U-Pb methods used on the same sample yields mean $^{206}Pb/^{238}U$ ages of 600 ± 5 Ma, MSWD = 0.87 (LA-ICP-MS method), and 602 ± 4 Ma, MSWD = 0.37 (SHRIMP method). Combined data yield an age of 601 ± 4 Ma, interpreted as the age of emplacement. Whole-rock Rb-Sr isochrons, obtained with samples of eight massifs of the In Ouzzal terrane, give less precise and lower ages of 579 ± 11 Ma (4 massifs including North Tihimatine, 15 samples), 576 ± 9 Ma (North and South Tihimatine, 11 samples), 581 ± 28 Ma (5 massifs, 9 samples), 510 ± 11 Ma (5 samples), questioning the reliability of Rb-Sr system in post-collisional magmatism in case of incipient hydrothermal alteration. The Tin Zebane peralkaline dyke swarm yields a reliable whole-rock Rb-Sr isochron age of 592 ± 6 Ma and a PREMA Sr-Nd signature (Sr_i = 0.7028, εNd(t) = +6.2), which might represent the mantle source of post-collisional magmatism (Hadj Kaddour et al., 1998). Whole-rock Nd isotopic data on the In Ouzzal granitic massifs display εNd(t) values ranging from -4 to -30, implying varying amounts of contamination by the In Ouzzal (-35 < εNd(601 Ma) < -23) Archean formations reworked by 2.0 Ga granulitic metamorphism.

In Central Hoggar, the LATEA metacraton, named from the Laouni – Aouilene – Tefedest – Egéré-Aleksod – Azrou n'Fad group of lithospheric terranes (Liégeois, 2019), is crosscut by Ediacaran ferroan alkali-calcic granitic massifs. Some of them were dated by zircon U-Pb SHRIMP methods, namely from north to south (i) Tihodaïne (582 ± 4 Ma), Tisselliline (572 ± 5 Ma), both in Egéré-Aleksod terrane (Abdallah, 2008), (ii) Temaguessine (582 ± 5 Ma) in Azrou n'Fad terrane (Abdallah et al., 2007), and (iii) In Tounine Tamanrasset-Taourirt complex (552 ± 3 Ma, Idir et al., 2014).

In the Eastern Hoggar, Ediacaran post-collisional ferroan alkali-calcic to alkaline granite massifs occur in the three terranes composing the western edge of the Saharan Metacraton (Liégeois et al., 2013). Westward, the Raghane 8°30'E major shear zone separates Assodé-Issalane, forming the easternmost terrane of the Orosirian Stripe to the west, and Aouzegueur, forming the westernmost terrane of the Saharan Metacraton, to the west (Liégeois, 2019). A number of ferroan alkali-calcic to (per)alkaline granites constitutes an igneous suite emplaced along the shear zone. The Arigher massif yields a zircon U-Pb LA-ICP-MS age of 554 ± 5 Ma (Henry et al., 2009), consistent with a less precise whole rock isochron Rb-Sr age of 553 ± 20 Ma (Zeghouane, 2006). Eastward, in the Djanet terrane, the Djanet batholith – Tin Bedjane massif – Tin Amali dyke swarm igneous suite yields zircon U-Pb LA-ICP-MS ages of 571 ± 16 Ma, 568 ± 5 Ma and 558 ± 6 Ma, respectively (Fezaa et al., 2010). The central Edembo terrane displays a similar granitic suite, but no ages have been published so far.

The sequence of emplacement ages started well after the ~650-630 Ma climax of Pan-African compressional events and overthrusting of juvenile arc terranes, like Silet and Tedeini terranes, over continental cratonic blocks, like the LATEA Metacraton. Igneous emplacements occurred during a general post-collisional tectonic escape of all Tuareg terranes to the north. Lateral translations along north-south trending dextral shear zones were coeval with metacratonization of formerly cratonic blocks and induced large offsets estimated to hundreds of kilometres in response to West African Craton indentation. When the West African Craton convergence was finished, the final Murzukian compressional event (575–555 Ma) concerned only the margin of the Saharan Metacraton, resulting into intra-continental metacratonization of Eastern Hoggar.

To sum up, post-collisional ferroan alkali-calcic to alkaline granitic massifs constitute a single "Taourirt-like" igneous suite emplaced during three periods of time. All terranes of the Tuareg Shield (for reviews, Brahimi et al., 2018, Liégeois, 2019) were affected. The ~600-585 Ma first episode took place in the Iforas Cordillera, westernmost Hoggar. The ~585-560 Ma second episode affected all terranes located east of the Iforas Cordillera, i.e. from west to east the Pharusian Belt (Silet and In Tedeini terranes), the LATEA Metacraton, the Orosirian Stripe and the Saharan Metacraton (Eastern Hoggar terranes). It was quickly followed by the ~560-520 Ma third episode,

585 which affected only the Pharusian Belt (Silet and In Tedeini terranes) and the LATEA Metacraton.
586
587 ## Conclusion
588
589 Six Silet-Taourirt massifs (Ait Oklan, Tesnou 1, Issedienne, Tin Erit, Tihoiiarene and Tioueine)
590 have been analysed by U-Pb zircon SHRIMP and Lu-Hf isotopes. The first Middle Ediacaran
591 igneous episode comprises 585 ± 2 Ma Tin Erit, 570 ± 5 Ma Tihoiiarene and 561 ± 6 Ma Tioueine
592 alkaline massifs. The second Late Ediacaran-Fortunian episode comprises 559 ± 3 Ma – 539 ± 3 Ma
593 Issedienne, 537 ± 7 Ma Tesnou and 529 ± 3 Ma Ait Oklan alkali-calcic massifs and the 523 ± 1 Ma
594 alkaline syenite dyke of Tioueine. The younger ages recorded in scarce crystals reflect hydrothermal
595 episodes associated with renewed movements along large north-south trending shear zones.
596 Hf isotopic data show a secular variation of decreasing εHf(t) from positive values (all massifs of
597 the first igneous episode, Issedienne and partly Tesnou massifs of the second igneous episode) to
598 negative values (partly Tesnou and Ait Oklan massifs of the second igneous episode), suggesting an
599 enriched mantle source and increasing contamination by Archean – Paleoproterozoic continental
600 materials of the LATEA Metacraton.
601 The first ~585-560 Ma igneous episode of emplacement of Silet-Taourirts reflects a major event
602 of tectonic escape to the north, while the second ~560-520 Ma igneous episode is likely related to
603 the intra-continental Murzukian event.
604
605 **Acknowledgements**
606 The manuscript has benefitted from two anonymous reviewers. Elena Belousova, Yves Greau and
607 William L. Griffin, who performed the isotopic analyses in the Geochemical Analysis Unit (GAU),
608 GEMOC Key Centre, Department of Earth and Planetary Sciences, Macquarie University,
609 Australia, deserve special thanks. We are indebted to Jean Boissonnas, for having shared his
610 passion and knowledge of the Taourirt problematic. Moreover, he went with one of the authors
611 (AAZ) during field missions in Tesnou, Issedienne, Ait Oklan and Tioueiine ring complexes.
612 Additional thanks to Amina Louni, Hamid Bechiri and Rekia Kheloui for having helped AAZ, FBB
613 and YM in field studies of Tin Erit and Tihoïarène ring complexes.

References

Abdallah, N., 2008. Géochimie et géochronologie des intrusions magmatiques panafricaines du terrane Egéré-Aleksod: exemple des massifs granitiques de l'Ounane, Tihoudaïne et Tisselliline (Hoggar central, Algérie). Thèse de doctorat, USTHB-FSTGAT, 191 p.

Abdallah, N., Liégeois, J.P., De Waele, B., Fezaa, N., Ouabadi, A., 2007. The Temaguessine Fe-cordierite orbicular granite (Central Hoggar, Algeria): U–Pb SHRIMP age, petrology, origin and geodynamical consequences for the late Pan-African magmatism of the Tuareg shield. Journal of African Earth Sciences, 49, 153–178.

Abdelsalam et al., 2002. The Saharan metacraton. Journal of African Earth Sciences, 34, 119–136.

Aïdrous-Belhocine K., 2010. Étude pétrologique des granitoïdes panafricains de la partie Nord du bloc d'Azrou-N 'Fad (régions du col d'Azrou et du Manzaz). Thèse de magister, USTHB-FSTGAT, Alger, 147 p.

Azzouni-Sekkal, A., 1995. Le zircon, marqueur de la transition calco-alcalin – alcalin dans les complexes granitiques « Taourirt » du Hoggar – Algérie. Bulletin du Service Géologique de l'Algérie, 6, 179–193.

Azzouni-Sekkal, A., Boissonnas, J., 1987. Geochemistry of the Tioueine Pan-African granite complex (Hoggar, Algeria). Geological Journal, 22, 213–224.

Azzouni-Sekkal, A., Boissonnas, J., 1993. Une province magmatique de transition du calco-alcalin à l'alcalin: les granitoïdes panafricains à structure annulaire de la chaîne pharusienne du Hoggar (Algérie). Bulletin de la Société Géologique de France, 164, 597–608.

Azzouni-Sekkal, A., Bonin, B., 1998. Les minéraux accessoires des granitoïdes de la suite Taourirt, Hoggar (Algérie): conséquences pétrogénétiques. Journal of African Earth Sciences, 26, 65–87.

Azzouni-Sekkal, A., Liégeois, J.-P., Bechiri-Benmerzoug, F., Belaidi-Zinet, S., Bonin, B., 2003. The "Taourirt" magmatic province, a marker of the closing stage of the Pan- African orogeny in the Tuareg shield: review of available data and Sr–Nd isotope evidence. Journal of African Earth Sciences, 37, 331–350.

Bechiri-Benmerzoug, F., 1998. Le complexe granitique du Tin-Erit: Cartographie, pétrologie, minéralogie et géochimie (Hoggar occidental, Algérie). Thèse de magister, IST/USTHB, Alger, 165 p.

Bechiri-Benmerzoug, F., 2009. Pétrologie, géochimie isotopique et géochronologie des granitoïdes Pan-africains de type TTG de Silet: contribution à la connaissance de la structuration du bloc d'Iskel (Silet, Hoggar occidental) Algérie. Thèse de doctorat, FSTGAT/USTHB, Alger, 386 p.

Bechiri-Benmerzoug, F., Liégeois, J.-P., Bonin, B., Azzouni-Sekkal, A., Bechiri, H., Kheloui, R., Matukov, D.I., Sergeev, S.A., 2011. The plutons from the Cryogenian Iskel composite oceanic

649 island arc (Hoggar, Tuareg Shield, Algeria): U–Pb on zircon SHRIMP geochronology,
650 geochemistry and geodynamical setting. In: Seventh Hutton symposium on granites and related
651 rocks, Avila, Spain, 4-9 July 2011, abstract, 17–18.
652 Bechiri-Benmerzoug, F., Bonin, B., Bechiri, H., Khéloui, R., Talmat-Bouzeguella, S., Bouzid, K.,
653 2017. Hoggar geochronology: a historical review of published isotopic data. Arabian Journal of
654 Geosciences, 10, 351–383.
655 Belousova, E.A., Griffin, W.L., O'Reilly, S.Y., 2006. Zircon crystal morphology, trace element
656 signatures and Hf isotope composition as a tool for petrogenesis modelling: examples from
657 Eastern Australian granitoids. Journal of Petrology, 47, n°2, 329–353.
658 Bertrand, J.M.L., Boissonnas, J., Caby, R., Gravelle, M., Lelubre, M. 1966. Existence d'une
659 discordance dans l'antécambrien du "fossé" pharusien de l'Ahaggar occidental (Sahara central).
660 Comptes Rendus de l'Académie des Sciences de Paris, 262, 2197–2200.
661 Bertrand, J.M., Meriem, D., Lapique, F., Michard, A., Dautel, D., Gravelle, M. 1986. Nouvelles
662 données radiométriques sur l'âge de la tectonique Pan-Africaine dans le rameau oriental de la
663 chaîne pharusienne (région de Timgaouine, Hoggar, Algérie). Comptes Rendus de l'Académie
664 des Sciences de Paris, 302, 437–440.
665 Beuf, S., Biju-Duval, B., de Charpal, O., Rognon, P., Gariel, O., Bennacef, A., 1971. Les grès du
666 Paléozoïque inférieur au Sahara. In: Collection ''Science et techniques du pétrole''. Publication
667 IFP, Paris. 464 pp.
668 Black, R., Latouche, L., Liégeois, J.-P., Caby, R., Bertrand, J.M., 1994. Pan-African displaced
669 terranes in the Tuareg shield (Central Sahara). Geology, 22, 641–644.
670 Blichert-Toft, J., Chauvel, C., Albarède, F., 1997. The Lu–Hf geochemistry of chondrites and the
671 evolution of the mantle–crust system. Earth and Planetary Science Letters, 148, 243–258.
672 Boissonnas, J. 1974. Les granites à structures concentriques et quelques autres granites tardifs de la
673 chaîne pan-africaine en Ahaggar (Sahara central, Algérie). Paris, Mémoires hors série B.R.G.M,
674 2 volumes, 662 p. Orléans.
675 Boissonnas, J., Gravelle, M., 1961. Un massif granitique de l'Ahaggar à mode de gisement hybride:
676 le Tihoiiarene. Bulletin de la Société géologique de France, S7-III, 152–256.
677 Boissonnas, J., Duplan, L., Maisonneuve, J., Vachette, M., Vialette, Y., 1964. Étude géologique et
678 géochronologique des roches du compartiment suggarien du Hoggar central (Algérie). Annales
679 de la Faculté des Sciences, Université de Clermont-Ferrand, 25(8), 73–90.
680 Boissonnas, J., Borsi, S., Ferrara, G., Fabre, J., Fabriès, J., Gravelle, M., 1969. On the Early
681 Cambrian age of two late orogenic granites from west-central Ahaggar (Algerian Sahara).
682 Canadian Journal of Earth Sciences, 6, 25–27.

683 Bonin, B., 2004. Do coeval mafic and felsic magmas in post-collisional to within-plate regimes
684 necessarily imply two contrasting, mantle and crustal, sources ? A review**.** Lithos, 78, 1–24.
685 Bonin, B., 2007. A-type granites and related rocks: evolution of a concept, problems and prospects.
686 Lithos, 97, 1–29.
687 Bonin, B., Azzouni-Sekkal et al., Bussy, F., Ferrag, S., 1998. Alkali-calcic and alkaline post-
688 orogenic (PO) magmatism: petrologic constraints and geodynamic settings. Lithos, 45, 45-70.
689 Brahimi, S., Liégeois, J.-P., Ghienne, J.F., Munschy, M., Bourmatte, A., 2018. The Tuareg shield
690 terranes revisited and extended towards the northern Gondwana margin: Magnetic and
691 gravimetric constraints. Earth Science Reviews, 185, 572–599.
692 Cahen, L., Snelling, N.J., Delhal, J., Vail, J.R., Bonhomme, M., Ledent, D., 1984. The
693 geochronology and evolution of Africa. Clarendon Press, Oxford, 508 p.
694 Cheilletz, A., Bertrand, J.M.L., Charoy, B., Moulahoum, O., Bouabsa, L., Farrar, E., Zimmerman,
695 J.L., Dautel, D., Archibald, D.A., Boullier, A.M., 1992. Géochimie et géochronologie Rb-Sr, K-
696 Ar et $^{40}Ar/^{39}Ar$ des complexes granitiques panafricains de la région de Tamanrasset (Algérie):
697 relations avec les minéralisations Sn-W associées et l'évolution tectonique du Hoggar central.
698 Bulletin de la Société Géologique de France, 163, 733–750.
699 Collins, W.J., Huang, H.Q., Bowden (2020). Repeated S- I- A-type granite trilogy in the Lachlan
700 Orogen, and geochemical contrasts with A-type granites in Nigeria: Implications for
701 petrogenesis and tectonic discrimination. In: V. Janoušek, B. Bonin, W.J. Collins, F. Farina, P.
702 Bowden (Editors), "Post-Archaean Granitic Rocks: Petrogenetic Processes and Tectonic
703 Environments", Geological Society, London, Special Publication 491, in press.
704 Cottin, J.Y., Lorand, J.P., Agrinier, P., Bodinier, J.L., Liégeois, J.-P., 1998. Isotopic (O, Sr, Nd) and
705 trace element geochemistry of the Laouni layered intrusions (Pan-African belt, Hoggar, Algeria):
706 evidence for post-collisional tholeiitic magmas variably contaminated by continental crust.
707 Lithos, 45, 197–222.
708 Dupont, P.L., 1987. Pétrologie et géochimie des ensembles magmatiques Pharusien I et Pharusien II
709 dans le rameau oriental de la chaîne pharusienne (Hoggar, Algérie). Thèse Doctorat, Université
710 de Nancy I, France, 283 p.
711 Fabre, J., editor, 2005. Géologie du Sahara occidental et central. Tervuren African Geoscience
712 Collection, 108, Musée Royal de l'Afrique Centrale, Tervuren, Belgium, 572 p.
713 Fezaa, N., Liégeois, J.-P., Abdallah, N., Cherfouh, E.H., De Waele, B., Bruguier, O., Ouabadi, A.,
714 2010. Late Ediacaran geological evolution (575–555 Ma) of the Djanet Terrane, Eastern Hoggar,
715 Algeria, evidence for a Murzukian intracontinental episode. Precambrian Research, 180, 299–
716 327.

717 Fezaa, N., Liégeois, J.-P., Abdallah, N., Bruguier, O., De Waele, B., Ouabadi, A., 2019. The 600
718 Ma-old Pan-African magmatism in the In Ouzzal terrane (Tuareg Shield, Algeria): Witness of
719 the metacratonisation of a rigid block. In: Bendaoud, A., Hamimi, Z., Hamoudi, M., Djemai, S.,
720 Zoheir, B. (editors), The Geology of the Arab World – An overview. Springer Geology, Berlin –
721 Heidelberg – New York, 109–148.

722 Frost, C.D., Frost, B.R., 2011. On ferroan (A-type) granitoids: their compositional variability and
723 modes of origin. Journal of Petrology, 52, 39-53.
724 Haddoum, H., Guiraud, R., Moussine-Pouchkine, A., 2011. Hercynian compressional deformations
725 of the Ahnet-Mouydir Basin, Algerian Saharan Platform: far-field stress effects of the Late
726 Palaeozoic orogeny. Terra Nova, 13, 220-226.
727 Hadj Kaddour, Z., Demaiffe, D., Liégeois, J.-P., Caby, R., 1998. The alkaline-peralkaline granitic
728 post-collisional tin Zebane dyke swarm (Pan-African Tuareg shield, Algeria): prevalent mantle
729 signature and late agpaitic differentiation. Lithos, 45, 223-243.
730 Hawkesworth, C.J., Kemp, A.I.S., 2006. Using hafnium and oxygen isotopes in zircons to unravel
731 the record of crustal evolution. Chemical Geology, 226, 144-162.
732 Henry, B., Liégeois, J.-P., Nouar, O., Derder, M.E.M., Bayou, B., Bruguier, O., Ouabadi, A.,
733 Belhai, D., Amenna, M., Hemmi, A., Ayache, M., 2009. Repeated granitoid intrusions during the
734 Neoproterozoic along the western boundary of the Saharan metacraton, eastern Hoggar, Tuareg
735 shield, Algeria: an AMS and U–Pb zircon age study. Tectonophysics, 474, 417–434.
736 Idir, T., Abdallah, N., Ouabadi, A., Boissonnas, J., Liégeois, J.-P., Fezaa, N., 2014. Géochimie et
737 géochronologie du massif tardif d'In Tounine (Terrane de Laouni, Hoggar central). Colloque
738 national sur la géologie et les ressources minérales du Hoggar, USTHB, FSTGAT, Alger.
739 Ikhlef-Debabha, F., 2011. Pétrologie et minéralogie du complexe basique d'Allioum et de son
740 satellite, région de Mertoutek (Hoggar central, Algérie). Thèse de magister, USTHB-FSTGAT,
741 142 p.
742 Ikhlef-Debabha, F., Azzouni-Sekkal, A., Benhallou, A-Z., Ben el Khaznadji, R., Dautria, J.M.,
743 Bonin, B., 2016. Données pétrographiques préliminaires sur les gabbros du massif mafique-
744 ultramafique d'Edikel (Laouni, Hoggar Central, Algérie). First Arab Geosciences Union
745 (ArabGU) International Conference (AIC-1), 17-18 February 2016, USTHB, Algiers, Algeria,
746 abstract, 16-17.
747 Kheloui, R., Azzouni-Sekkal, A., Bechiri-Benmerzoug, F., Liégeois, J.-P., Bechiri, H., Bonin, B.,
748 2014. Étude pétrographique et géochimique du massif mafique–ultramafique d'Aguelmam (Bloc
749 de Silet, Hoggar, Algérie). Colloque national sur la géologie et les ressources minérales du
750 Hoggar, Alger, Algérie, 2014.
751 Lay, C., Ledent, D., 1963. Mesures d'âges absolus de minéraux et de roches du Hoggar (Sahara

central). Comptes Rendus Académie des Sciences, Paris, 257, 3188–3191.

Lelubre, M., 1952. Recherches sur la géologie de l'Ahaggar central et occidental (Sahara central). Bulletin du Service de la Carte Géologique de l'Algérie, 22, tome 1, 354 p., tome 2, 387 p.

Liégeois, J.-P., 2019. A new synthetic geological map of the Tuareg Shield: An overview of its global structure and geological evolution. In: Bendaoud, A., Hamimi, Z., Hamoudi, M., Djemai, S., Zoheir, B. (editors), The Geology of the Arab World – An overview. Springer Geology, Berlin – Heidelberg – New York, 83–107.

Liégeois, J.-P., Latouche, L., Boughrara, M., Navez, J., Guiraud, M., 2003. The LATEA metacraton (Central Hoggar, Tuareg shield, Algeria): behaviour of an old passive margin during the Panafrican orogeny. Journal of African Earth Sciences, 37, 161–190.

Liégeois, J.-P., Abdelsalam, M.G., Ennih, N., and Ouabadi, A., 2013, Metacraton: Nature, genesis and behavior. Gondwana Research, 23, 220–237.

Meddi, Y., 2011. Pétrologie des granitoïdes du massif de Tihoiiarene (bloc d'In Tedeini, Hoggar occidental, Algérie). Thèse de magister, FSTGAT/USTHB, Alger, 156 p.

Montero, P., Talavera, C., Bea, F., 2017. Geochemical, isotopic, and zircon (U-Pb, O, Hf isotopes) evidence for the magmatic sources of the volcano-plutonic Ollo de Sapo Formation, Central Iberia. Geologica Acta, 15, 245-260.

Paquette, J.L., Caby, R., Djouadi, M.T., Bouchez, J.L., 1998. U–Pb dating of the end of Pan-African orogeny in the Tuareg shield: the post-collisional syn-shear Tioueine pluton (Western Hoggar, Algeria). Lithos 45, 245–253.

Pelleter, E., Cheilletz, A., Gasquet, D., Mouttaqi, A., Annich, M., El Hakour, A., Deloule, E., Féraud, G., 2007. Hydrothermal zircons: A tool for ion microprobe U–Pb dating of gold mineralization (Tamlalt–Menhouhou gold deposit – Morocco). Chemical Geology, 245, 135-161.

Pupin, J.P., 1980. Zircon and granite petrology. Contributions to Mineralogy and Petrology, 73, 207–220.

Spencer, C.J., Kirkland C.L., Taylor, R.J.M., 2016. Strategies towards statistically robust interpretations of in situ U-Pb zircon geochronology. Geoscience Frontiers, 7, 581-589.

Troch, J., Ellis, B.S., Schmitt, A.K., Bouvier, A.-S., Bachmann, O., 2018. The dark side of zircon: textural, age, oxygen isotopic and trace element evidence of fluid saturation in the subvolcanic reservoir of the Island Park-Mount Jackson Rhyolite, Yellowstone (USA). Contributions to Mineralogy and Petrology, 173, 54-70.

Wones, D.R., 1989. Significance of the assemblage titanite + magnetite + quartz in granitic rocks; American Mineralogist, 74, 744–749.

Zaimen, F., 1994. Mise en évidence de plusieurs suites magmatiques dans la partie occidentale du

terrain de Laouni (Hoggar, Algérie). Unpublished PhD Thesis, Université de Paris-Sud, Orsay, 175 p.

Zazoun R.S., Mahdjoub, Y., 2011. Strain analysis of Late Ordovician tectonic events in the In-Tahouite and Tamadjert Formations (Tassili-n-Ajjers area, Algeria). Journal of African Earth Sciences, 60, 63–78.

Zeghouane, H., 2006. Pétrologie, géochimie, géochimie isotopique et géochronologie Rb/Sr du massif granitique d'Arirer (terrane Aouzegueur, Hoggar oriental) Algérie. Thèse Magister, USTHB-FSTGAT, Alger, 126 p.

795 **Figure captions**

796 Figure 1: Map of the Tuareg shield terranes (Black et al., 1994; Liégeois, 2019).

797 Figure 2: Sketch map of the Central Hoggar and Silet terrane, with localization of Taourirt plutons
798 (updated from Azzouni et al., 2003). I: Silet-Taourirts; II: Laouni-Taourirts; III: Tamanrasset-
799 Taourirts. Taourirt plutons are shown in yellow.

800 Figure 3: A. Sketch maps of studied massifs with localization of the studied samples. B. Pictures of
801 Taourirt landscapes: Ait Oklan, Issedienne, Tesnou, Tioueine.

802 Figure 4: Probability curves. A, Ait Oklan (AO24), B, Issedienne (I26), C, Tin Erit (TE26), D,
803 Tesnou (TES52).

804 Fig. 5: Cathodoluminescence images and U-Pb concordia diagrams: A, Ait Oklan (AO24), B,
805 Issedienne (I26), C, Tesnou (TES52), D, Tin Erit (TE26), E, Tihoiiarene (TH24), F, Tioueine
806 (TI59).

807 Figure 6: εHf(t) versus $^{206}Pb/^{238}U$ apparent ages and εHf(t) versus discordance. A, Ait Oklan
808 (AO24), B, Issedienne (I26), C, Tesnou (TES52), D, Tin Erit (TE26), E, Tihoiiarene (TH24), F,
809 Tioueine (TI59). Symbols: pink circle – concordant crystals, yellow circles – reset crystals, blue
810 circles – inherited crystals, black circles – discordant crystals.

811 Figure 7: εHf(t) versus $^{206}Pb/^{238}U$ apparent ages of concordant crystals.

812

813 **Table captions**

814 Table 1. Summary of major features of the Taourirt suite of Hoggar, Algeria.

815 Table 2. Zircon U-Pb isotopic data.

816 Table 3. Zircon Lu-Hf isotopic data.

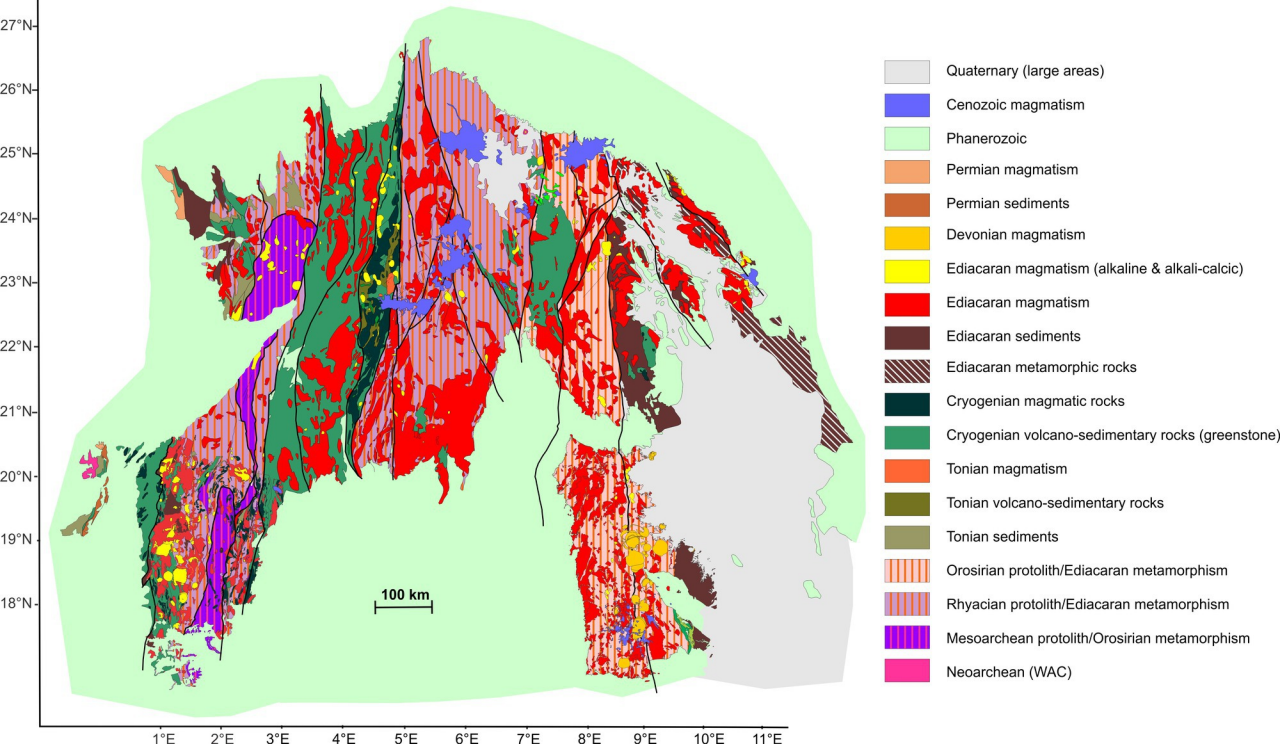
27°N
26°N
25°N
24°N
23°N
22°N
21°N
20°N
19°N
18°N
1°E
2°E
3°E
4°E
5°E
6°E
7°E
8°E
9°E
10°E
11°E
100 km
Quaternary (large areas)
Cenozoic magmatism
Phanerozoic
Permian magmatism
Permian sediments
Devonian magmatism
Ediacaran magmatism (alkaline & alkali-calcic)
Ediacaran magmatism
Ediacaran sediments
Ediacaran metamorphic rocks
Cryogenian magmatic rocks
Cryogenian volcano-sedimentary rocks (greenstone)
Tonian magmatism
Tonian volcano-sedimentary rocks
Tonian sediments
Orosirian protolith/Ediacaran metamorphism
Rhyacian protolith/Ediacaran metamorphism
Mesoarchean protolith/Orosirian metamorphism
Neoarchean (WAC)

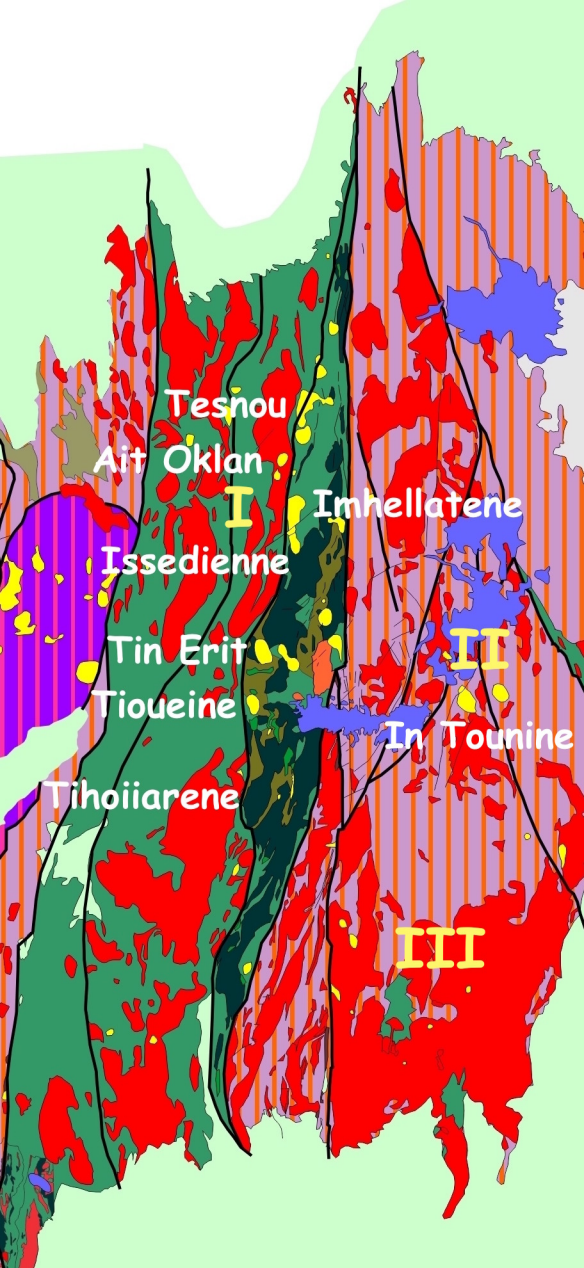
Tesnou
Ait Oklan
I
Imhellatene
Issedienne
Tin Erit
II
Tioueine
In Tounine
Tihoiiarene
III

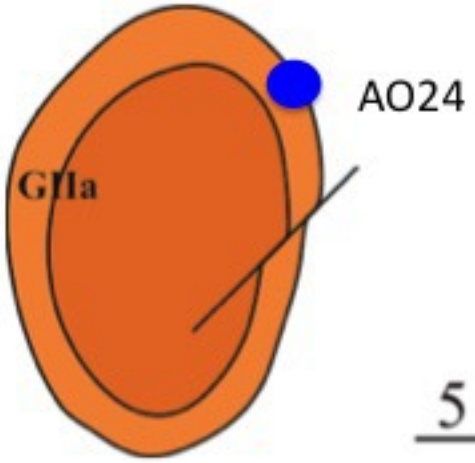

Ait Oklan

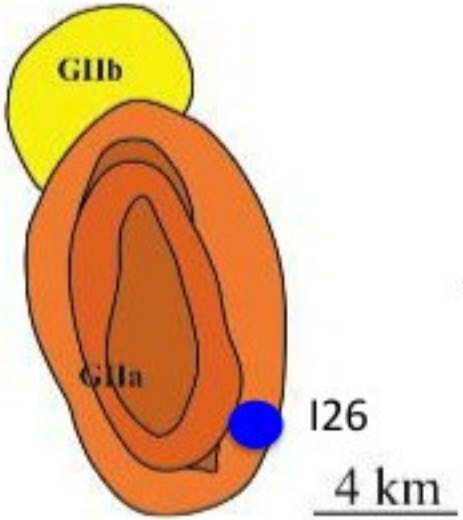

Issedienne

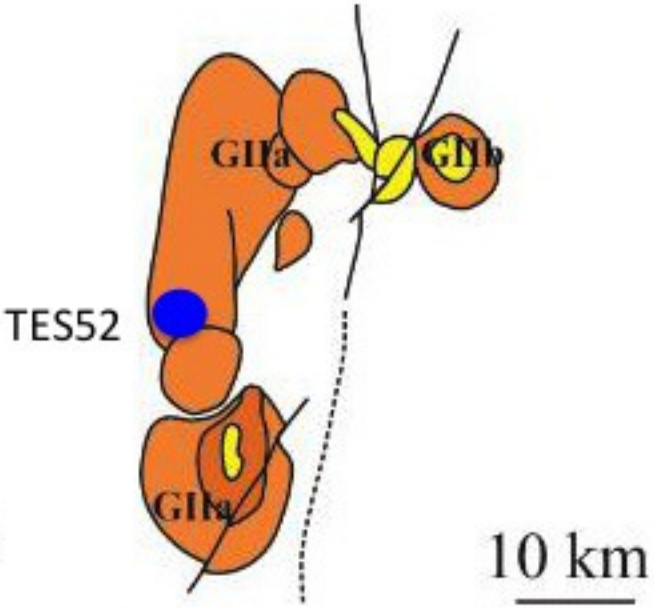

Tesnou

Tin Erit

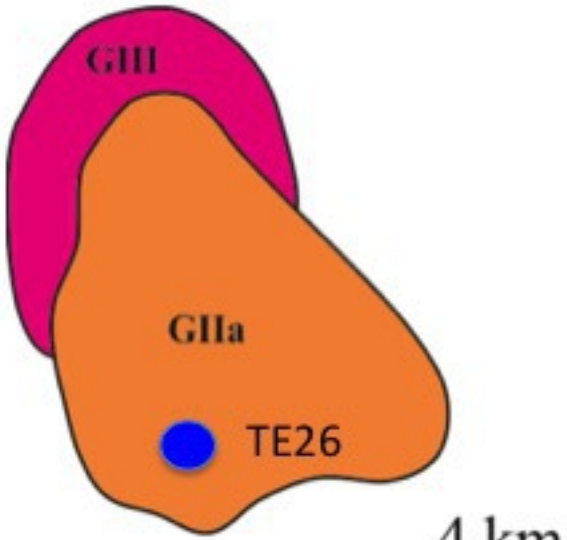

Tihoiiarene

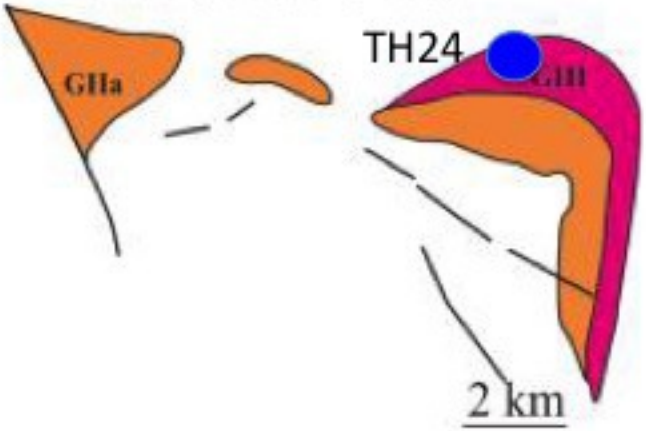

Tioueine

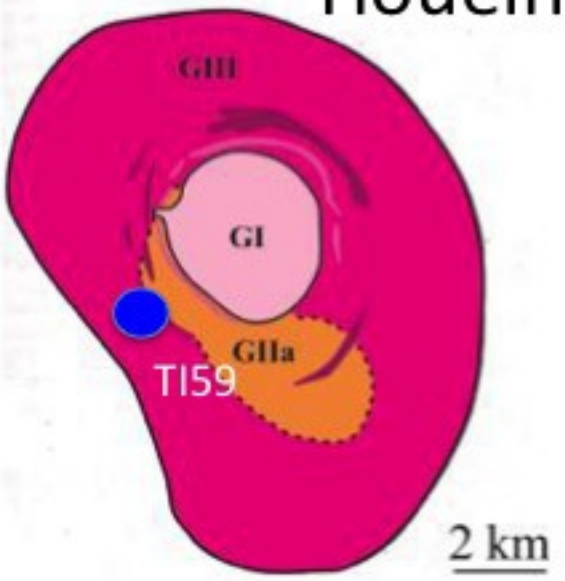


Ait Oklan


Issedienne


Tesnou


Tioueine

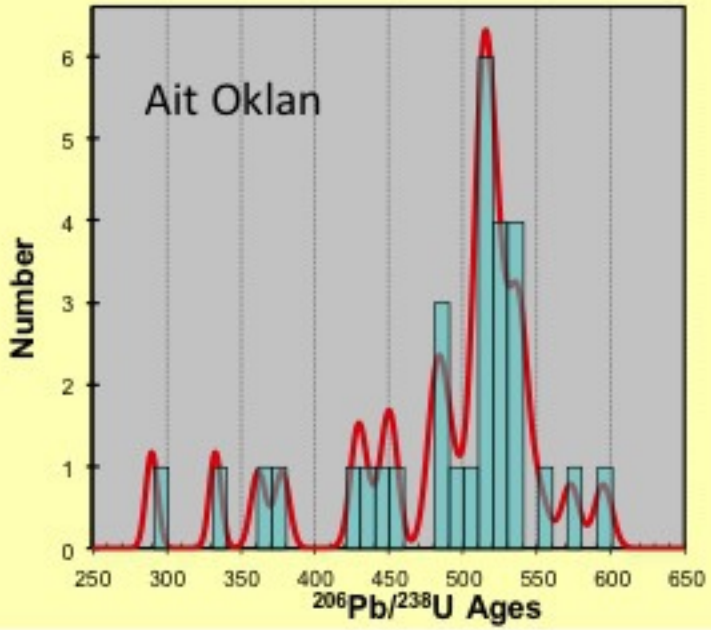
Ait Oklan
Number
0
1
2
3
4
5
6
250
300
350
400
450
500
550
600
650
206Pb/238U Ages

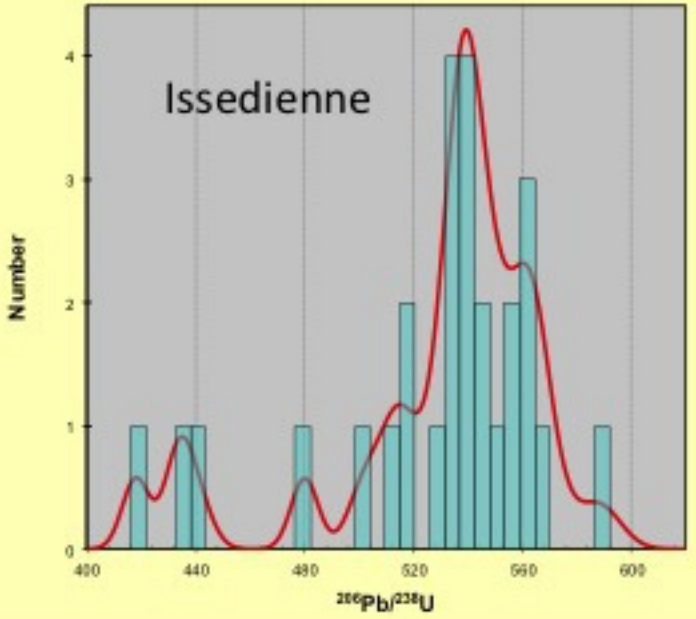
Issedienne
Number
0
1
2
3
4
400
440
480
520
560
600
206Pb/238U

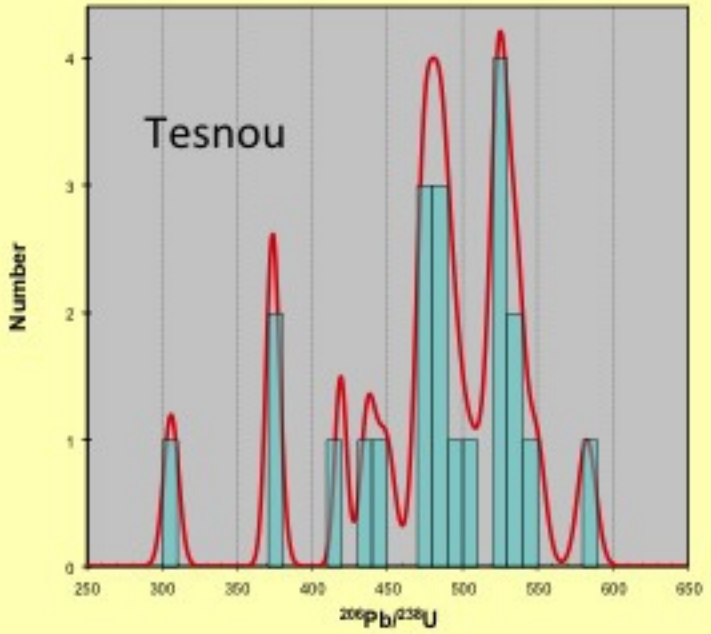
Tesnou
Number
0
1
2
3
4
250
300
350
400
450
500
550
600
650
206Pb/238U

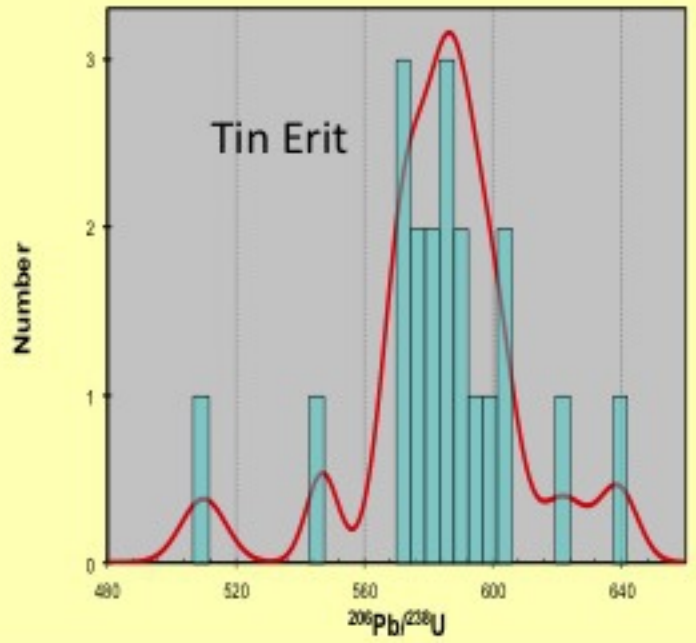
Tin Erit
Number
0
1
2
3
480
520
560
600
640
206Pb/238U

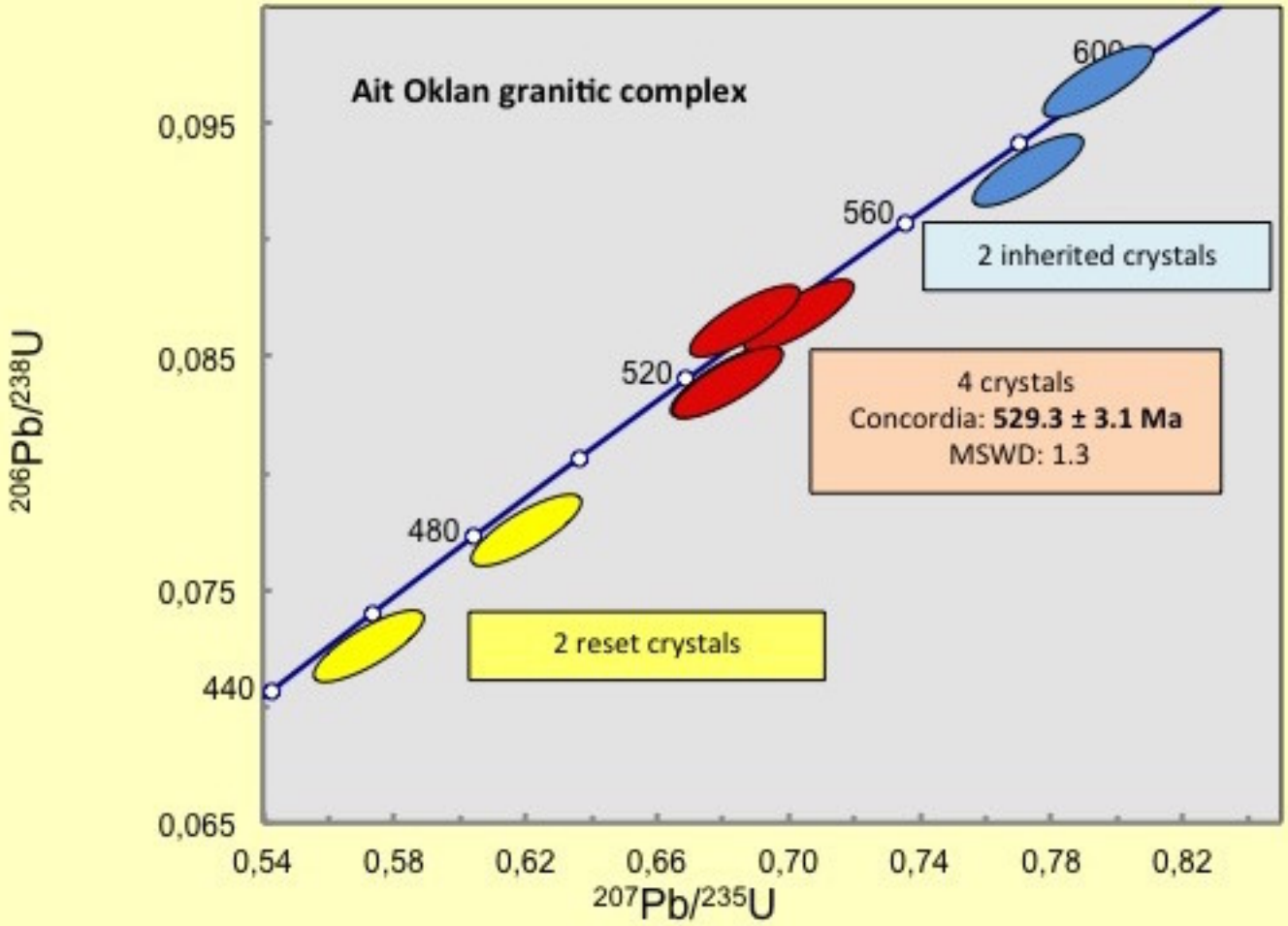
Ait Oklan granitic complex
600
560
520
480
440
2 inherited crystals
4 crystals
Concordia: 529.3 ± 3.1 Ma
MSWD: 1.3
2 reset crystals
0,095
0,085
0,075
0,065
0,54
0,58
0,62
0,66
0,70
0,74
0,78
0,82
206Pb/238U
207Pb/235U

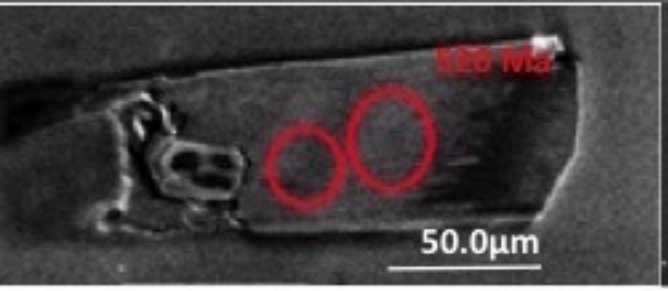

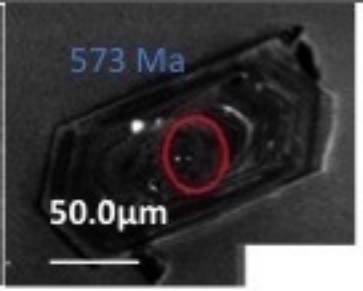

15 concordant

17 inherited (P2)

5 inherited (S24-P2)

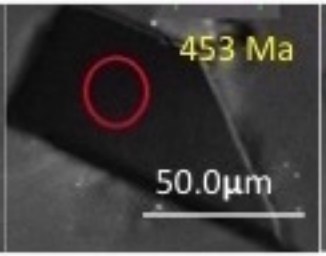

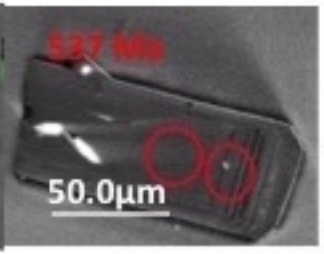

19 reset

20 reset

28 concordant (P1)

40 concordant(S25)

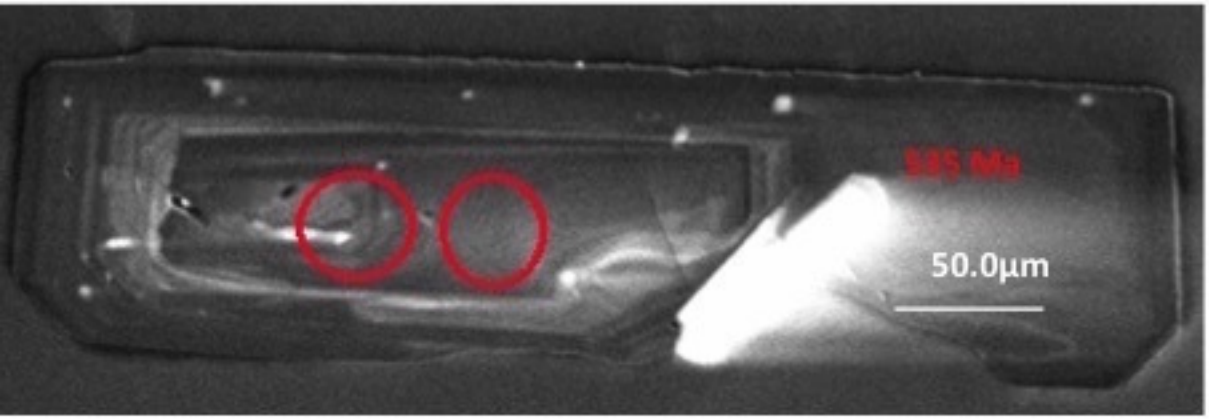

44 concordant (S25)

Ait Oklan

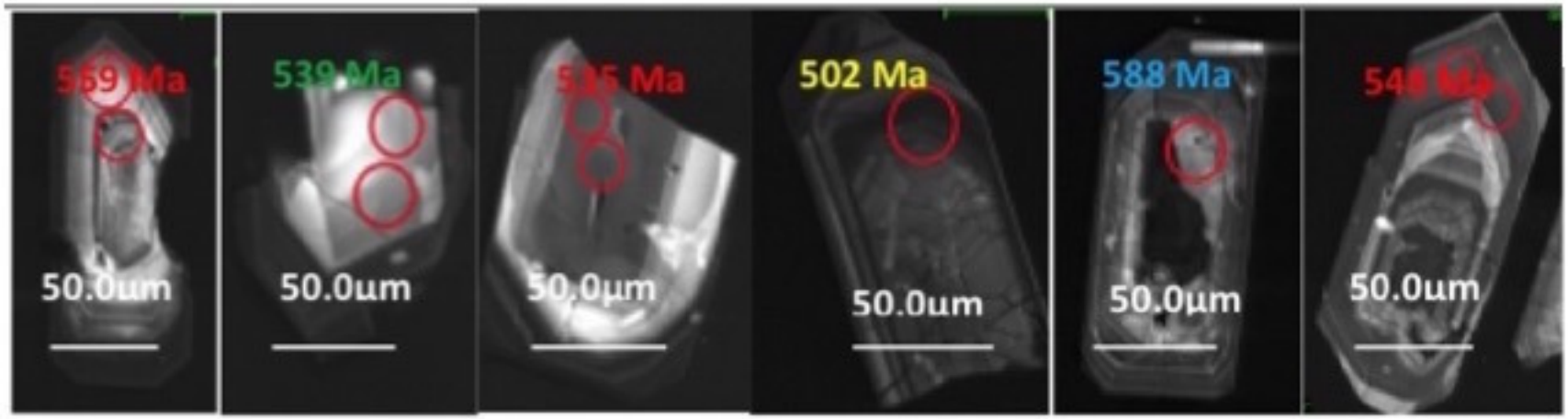

2 concordant (P2) 3 concordant 4 concordants (S14) 6 reset(S25-P1) 10 inherited(S14) 11 concordant(S25-P5)

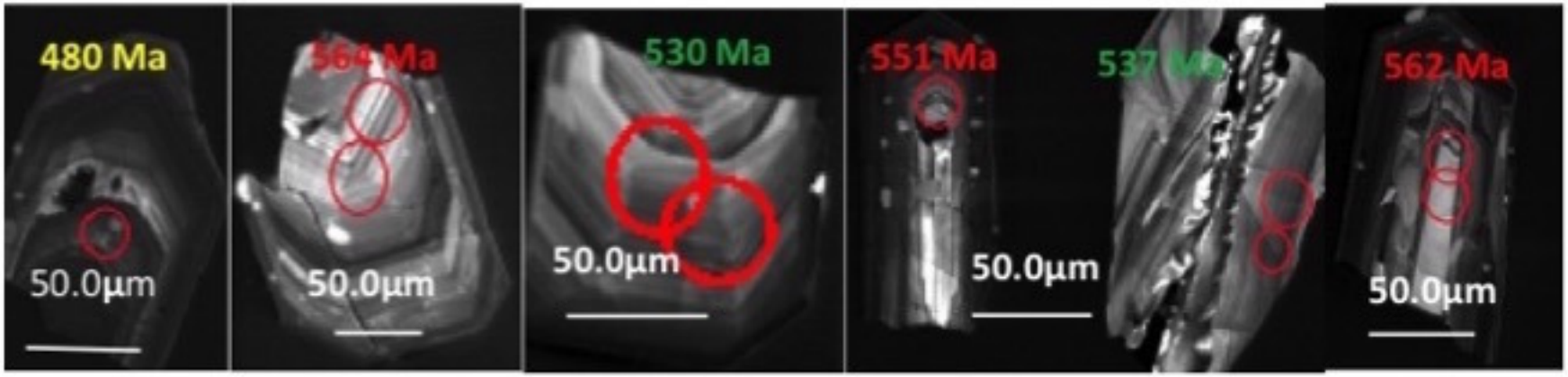

22 reset(P2) 25 concordant(S24) 40 concordant (S24) 45(P2) and 46 concordant 49 concordant(P2)

Issedienne

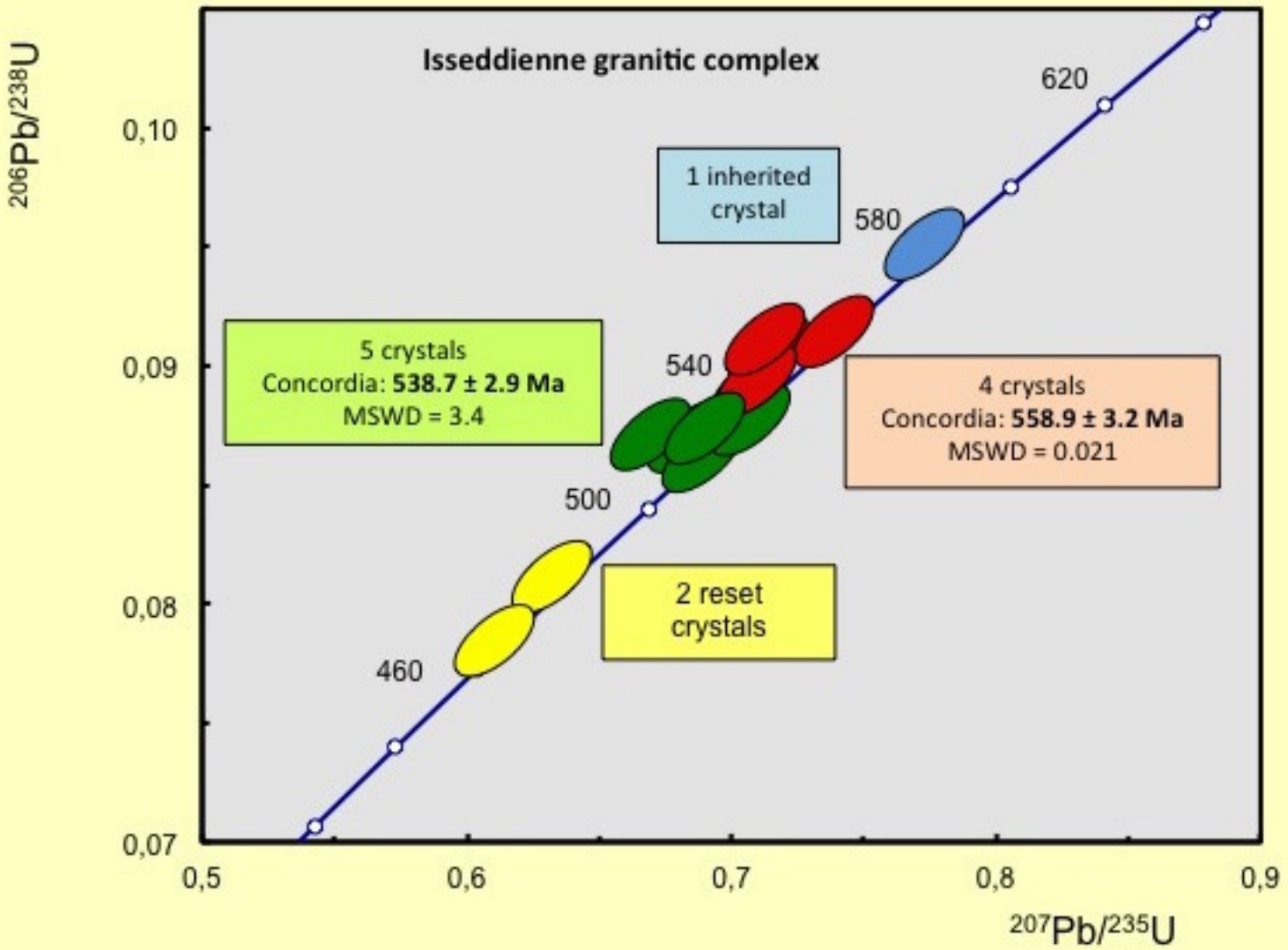
Isseddienne granitic complex
1 inherited crystal
5 crystals
Concordia: 538.7 ± 2.9 Ma
MSWD = 3.4
4 crystals
Concordia: 558.9 ± 3.2 Ma
MSWD = 0.021
2 reset crystals
620
580
540
500
460
0,10
0,09
0,08
0,07
0,5
0,6
0,7
0,8
0,9
206Pb/238U
207Pb/235U

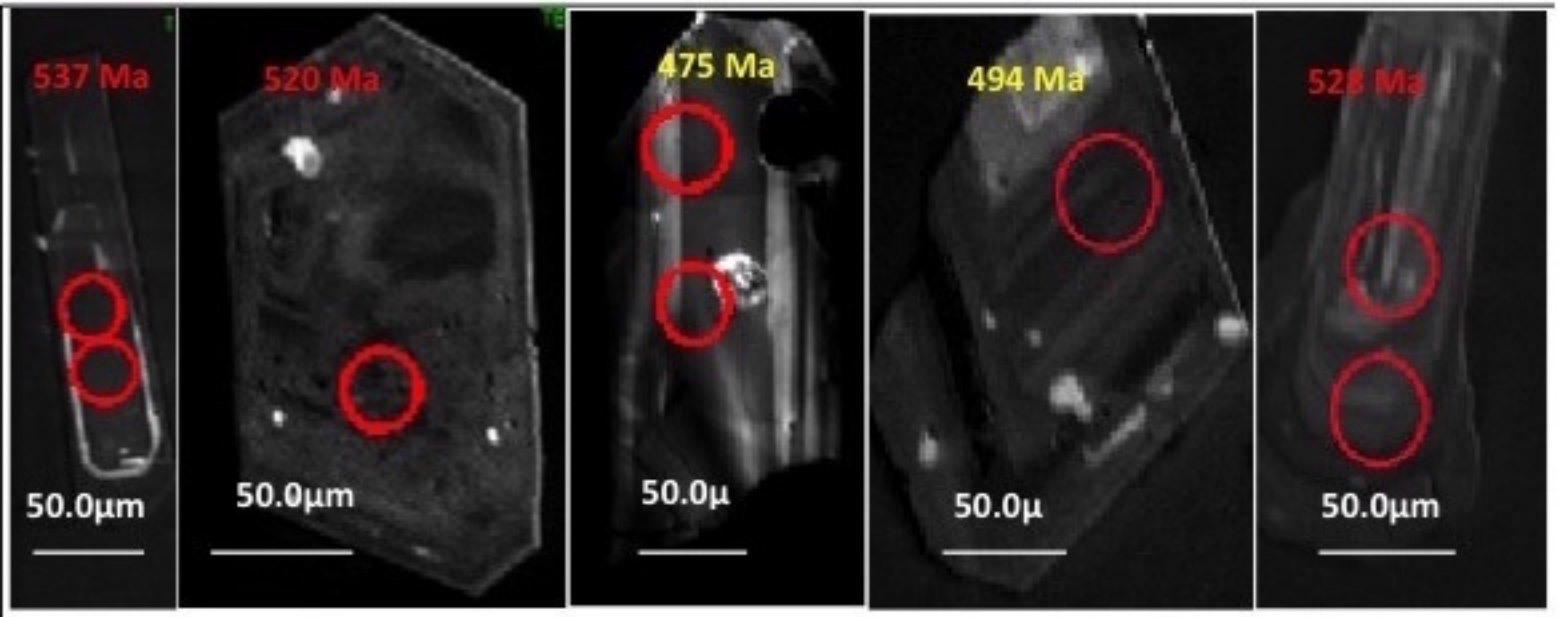

2 concordant(S25)3 concordant(P5) 4 reset 11 reset 14concordant

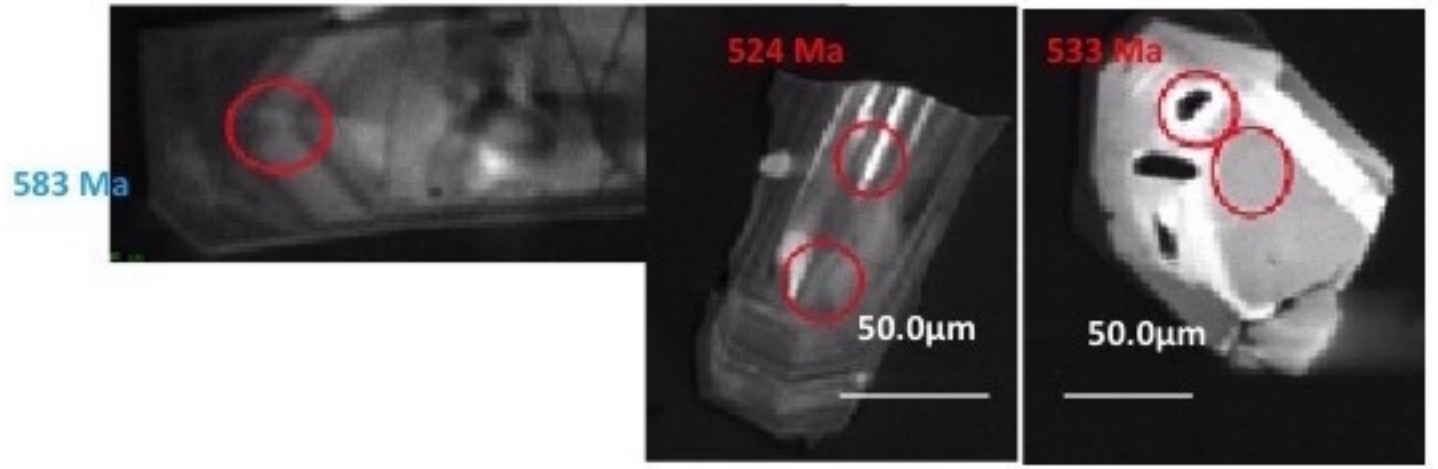

18 inherited (G1) 22 concordant (S14) 28 concordant (S24)

Tesnou

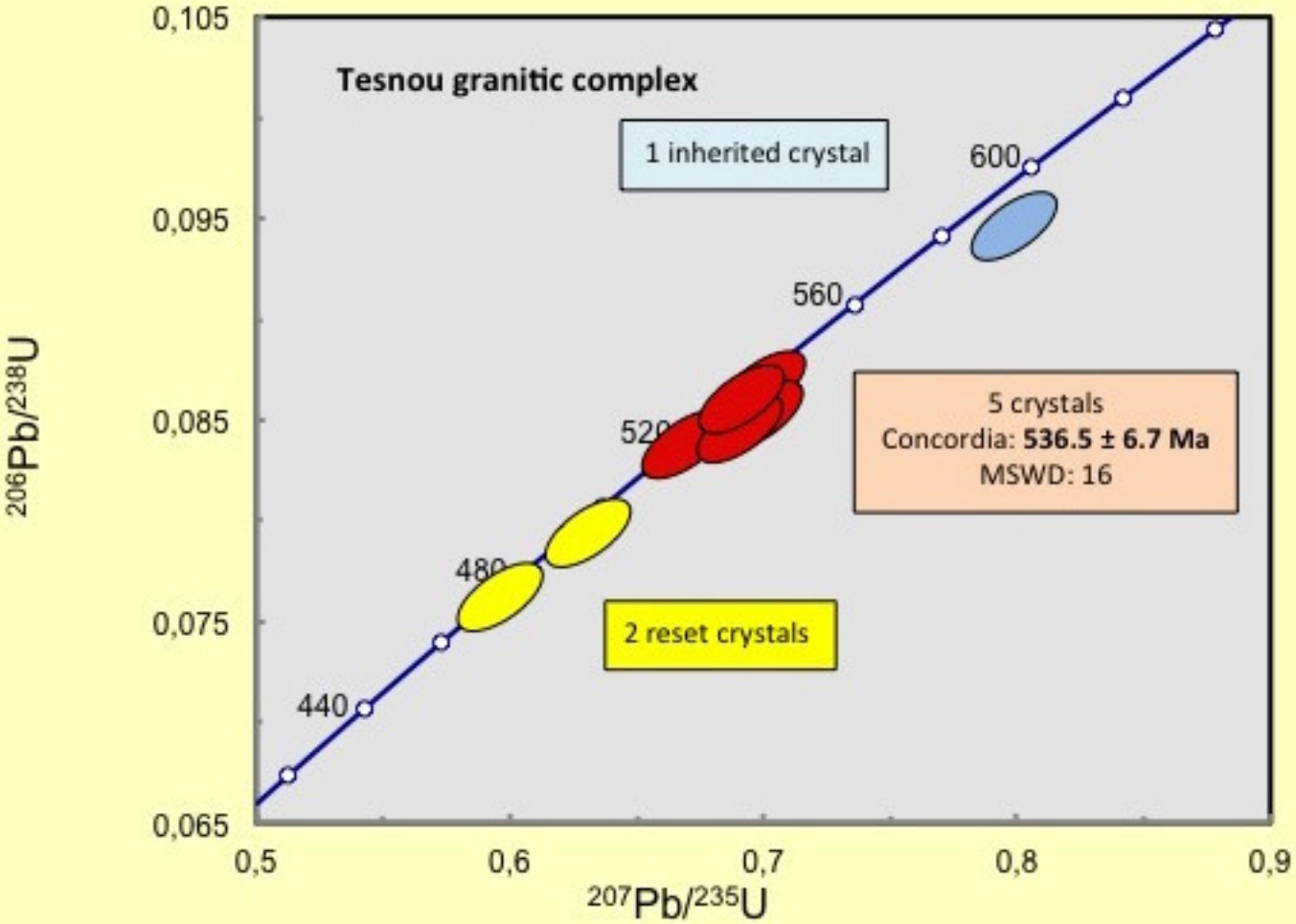
Tesnou granitic complex
1 inherited crystal
5 crystals
Concordia: 536.5 ± 6.7 Ma
MSWD: 16
2 reset crystals
600
560
520
480
440
0,105
0,095
0,085
0,075
0,065
0,5
0,6
0,7
0,8
0,9
206Pb/238U
207Pb/235U

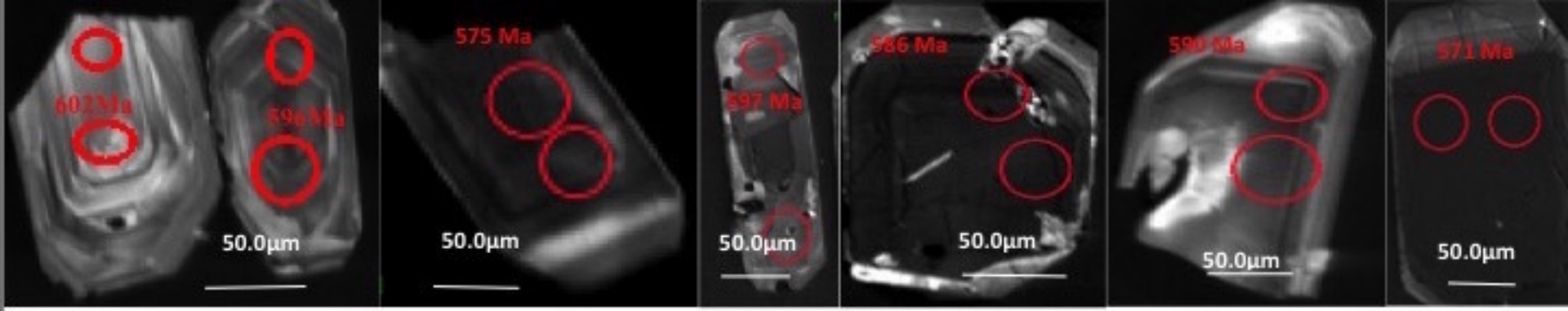

3 and 4 concordant(S14) 6 concordant(P5-T13) 7 concordant(D-K1) 12 concordant(D-K1) 14 concordant(P5-T13) 8 concordant((P5)

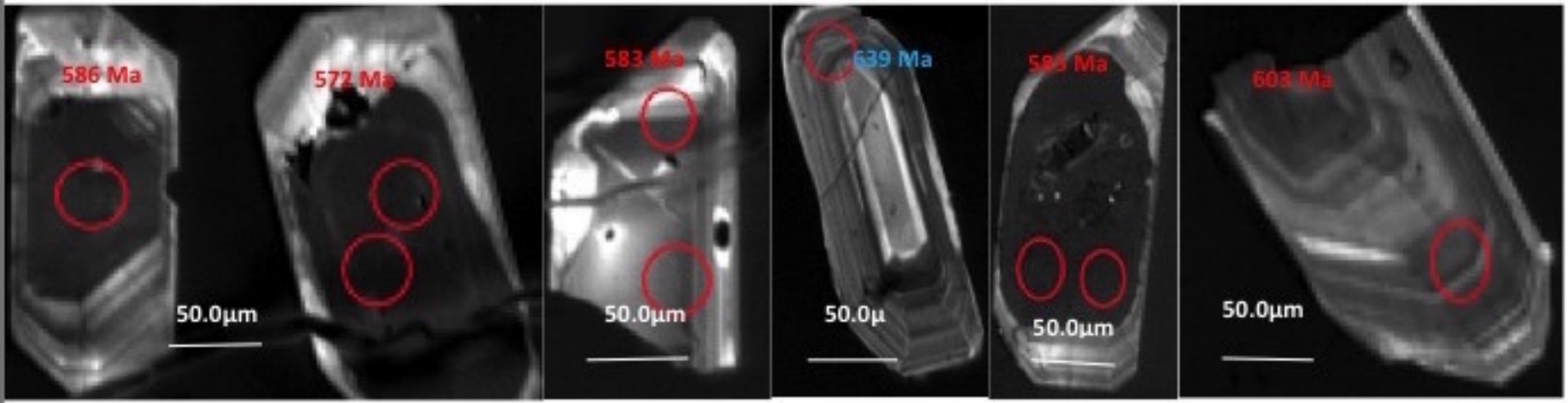

17(S24) et 18(P5) concordant 19 concordant 21 inherited(S14) 25 concordant(S25) 28 concordant(S25)

Tin Erit

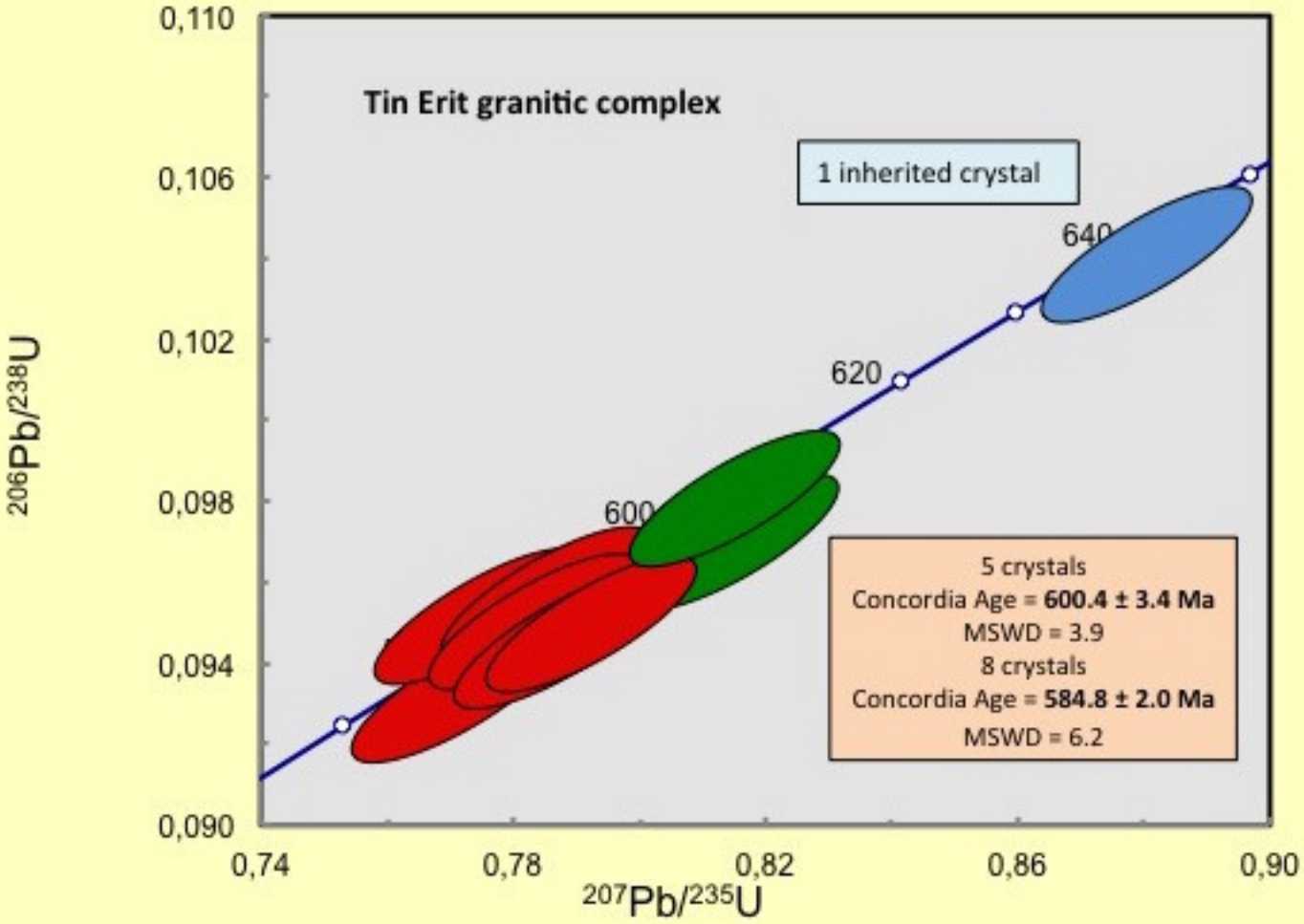
Tin Erit granitic complex
1 inherited crystal
640
620
600
5 crystals
Concordia Age = 600.4 ± 3.4 Ma
MSWD = 3.9
8 crystals
Concordia Age = 584.8 ± 2.0 Ma
MSWD = 6.2
0,110
0,106
0,102
0,098
0,094
0,090
0,74
0,78
0,82
0,86
0,90
206Pb/238U
207Pb/235U

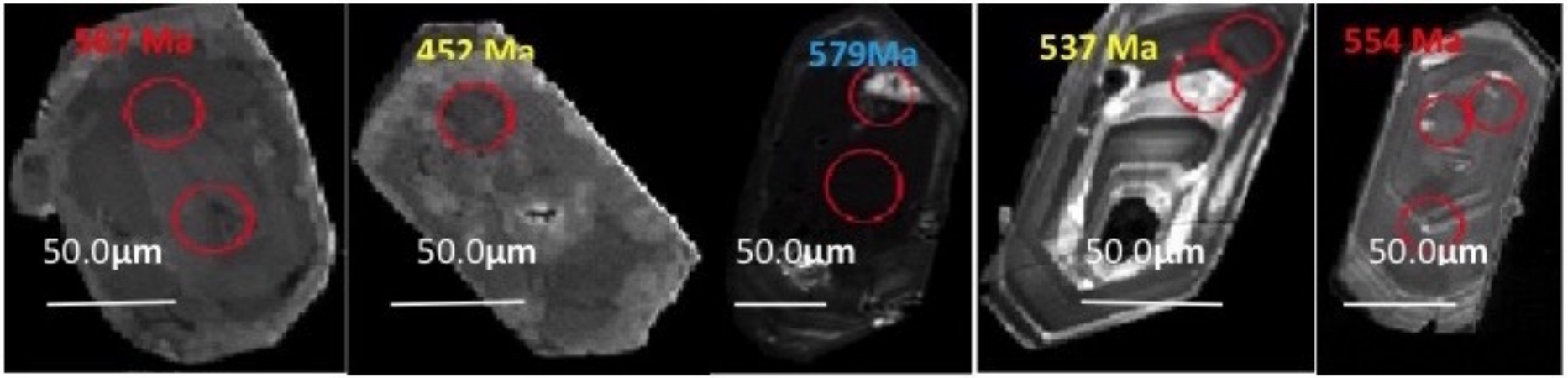

1concordant 3 reset(G1) 13 inherited(S25) 14reset(G1) 16 concordant(S25)

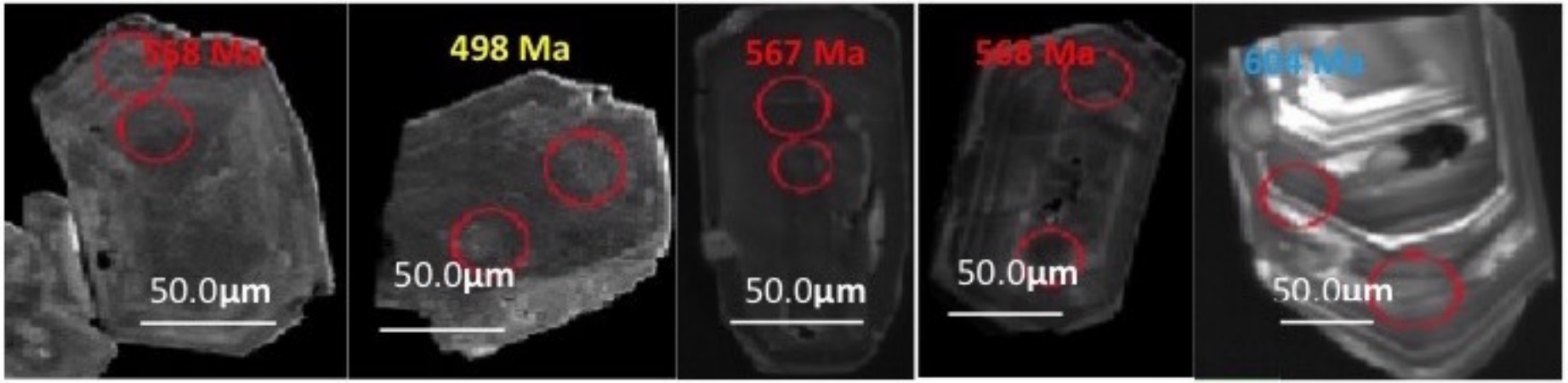

19 concordant, 21 reset 47 concordant 48 concordant(D-P5) 50 inherited(S25-P1)

Tihoiiarene

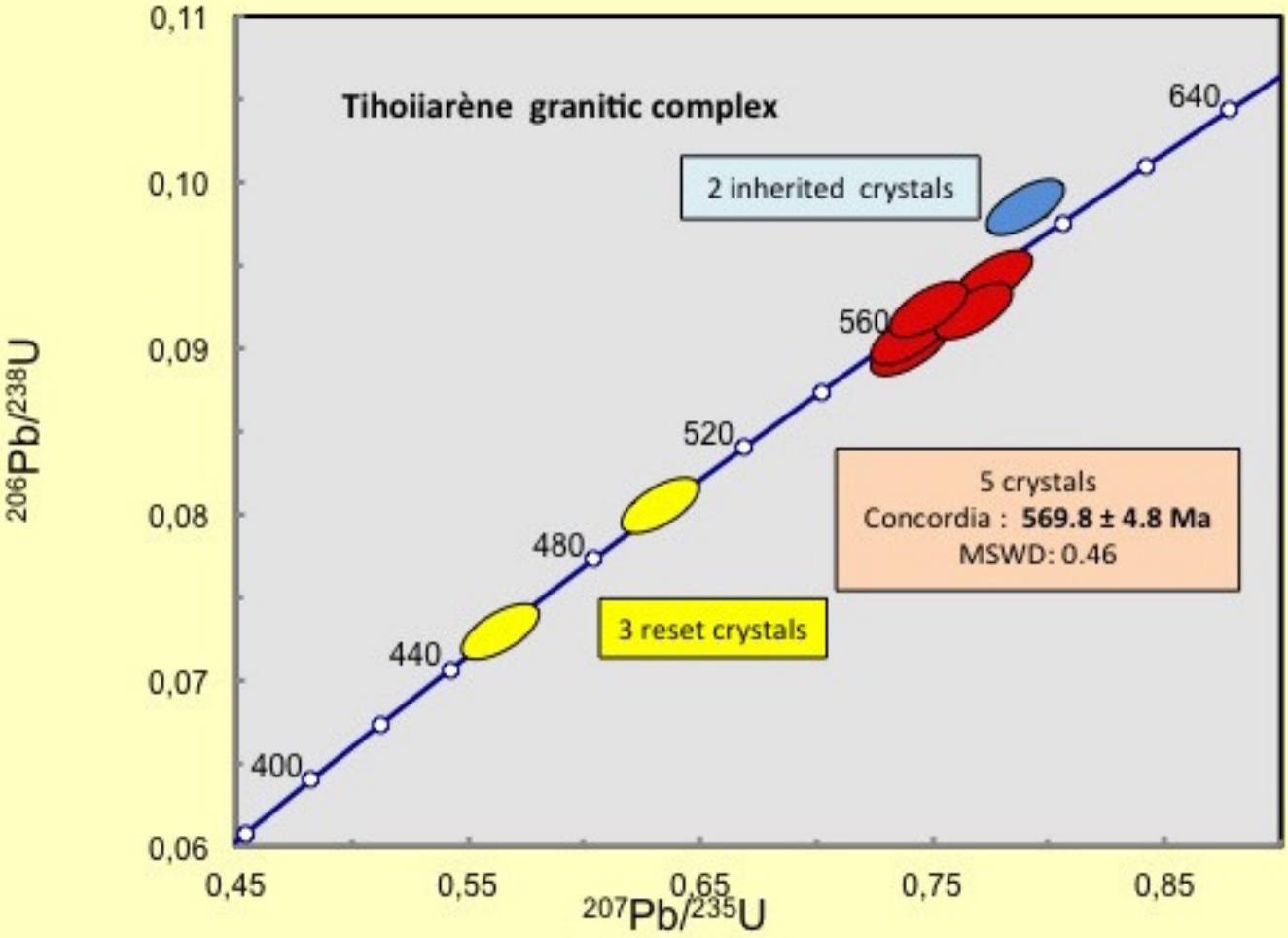
Tihoiiarène granitic complex
2 inherited crystals
5 crystals
Concordia : 569.8 ± 4.8 Ma
MSWD: 0.46
3 reset crystals
640
560
520
480
440
400
0,11
0,10
0,09
0,08
0,07
0,06
0,45
0,55
0,65
0,75
0,85
206Pb/238U
207Pb/235U

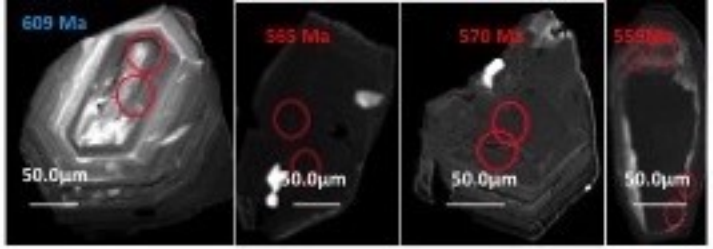

1 inherited (P) 2 concordant 5 concordant 10C concordant (J4)

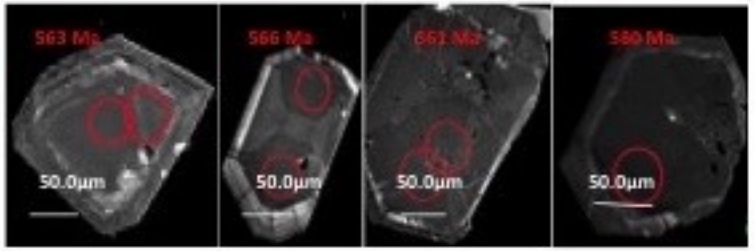

12 concordant 13 concordant(S25) 14 concordant 17 concordant(P5)

Tioueine

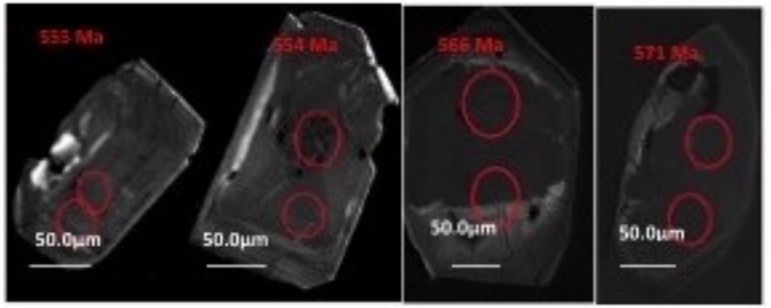

25 concordant (D) 26 concordant (D-T14) 30 concordant(D) 32 concordant (D)

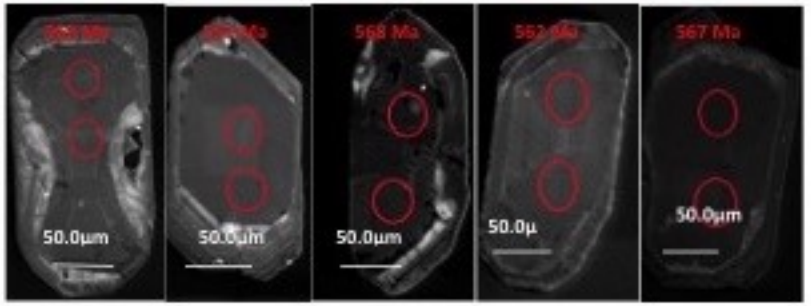

33 concordant(D) 34 concordant (S25) 37 concordant(D) 40 concordant 43 concordant(D)

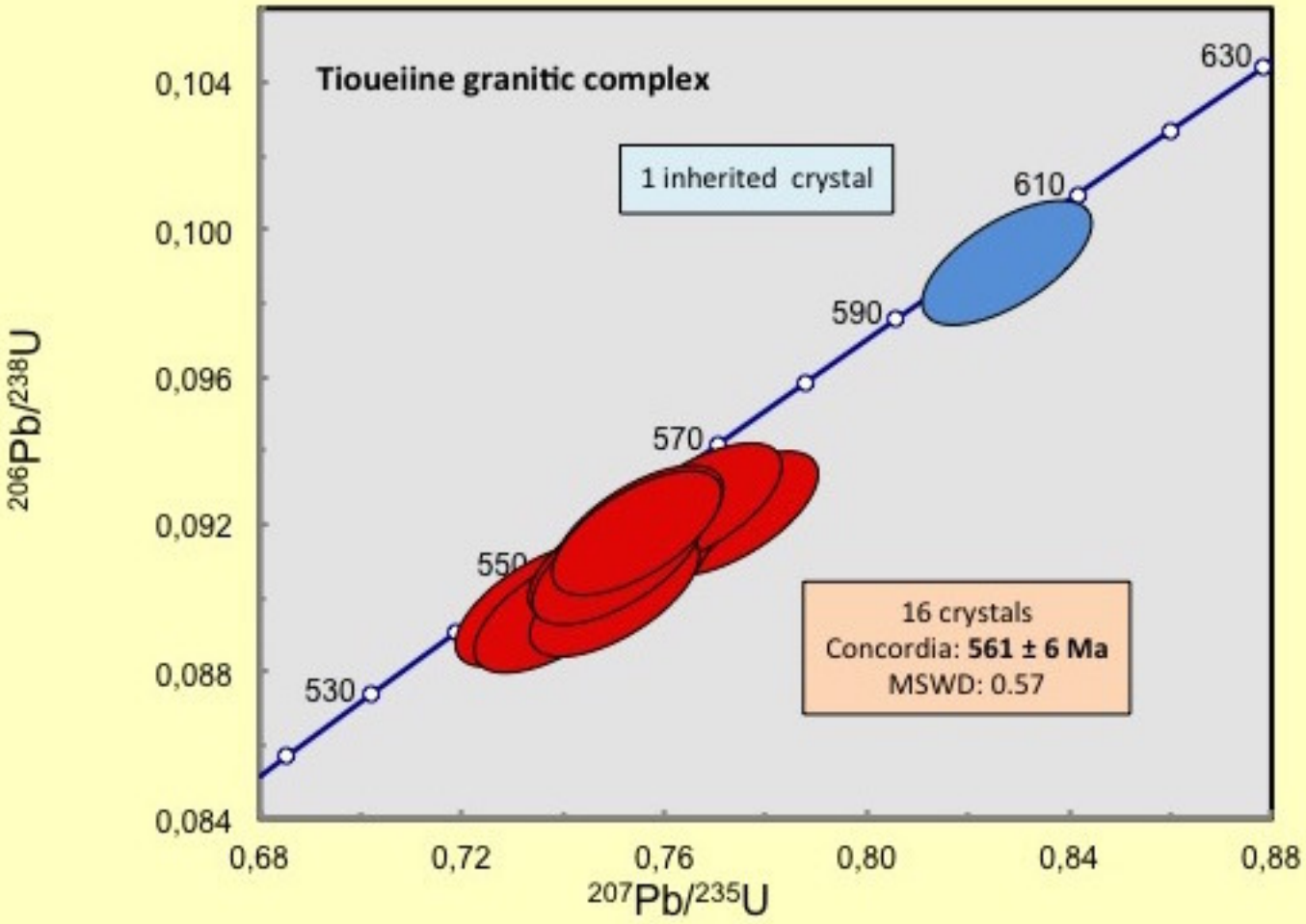
Tioueiine granitic complex
1 inherited crystal
16 crystals
Concordia: 561 ± 6 Ma
MSWD: 0.57
630
610
590
570
550
530
0,104
0,100
0,096
0,092
0,088
0,084
0,68
0,72
0,76
0,80
0,84
0,88
206Pb/238U
207Pb/235U

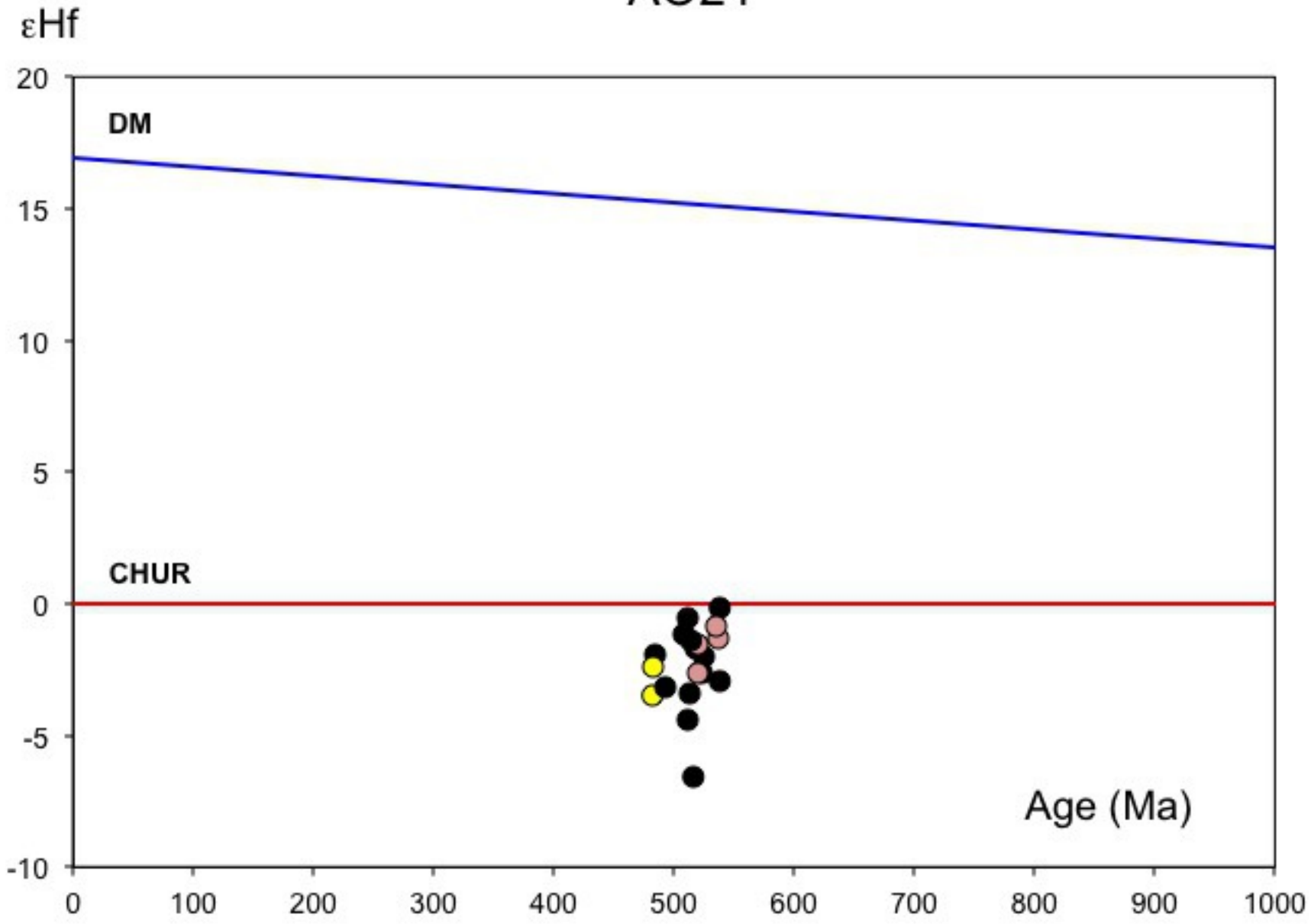
AO24
εHf
20
15
10
5
0
-5
-10
DM
CHUR
0
100
200
300
400
500
600
700
800
900
1000
Age (Ma)

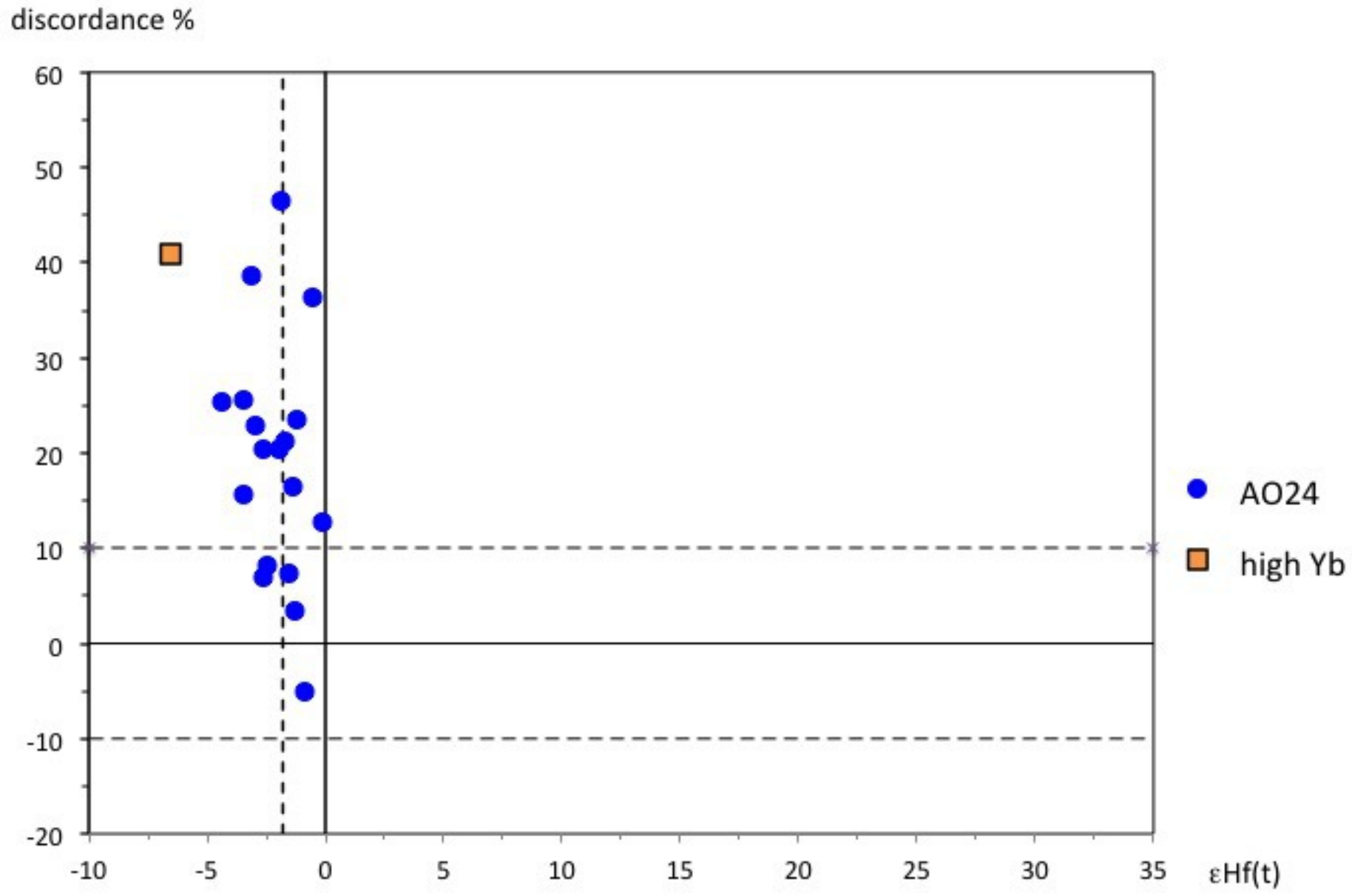
discordance %
60
50
40
30
20
10
0
-10
-20
-10
-5
0
5
10
15
20
25
30
35
εHf(t)
AO24
high Yb

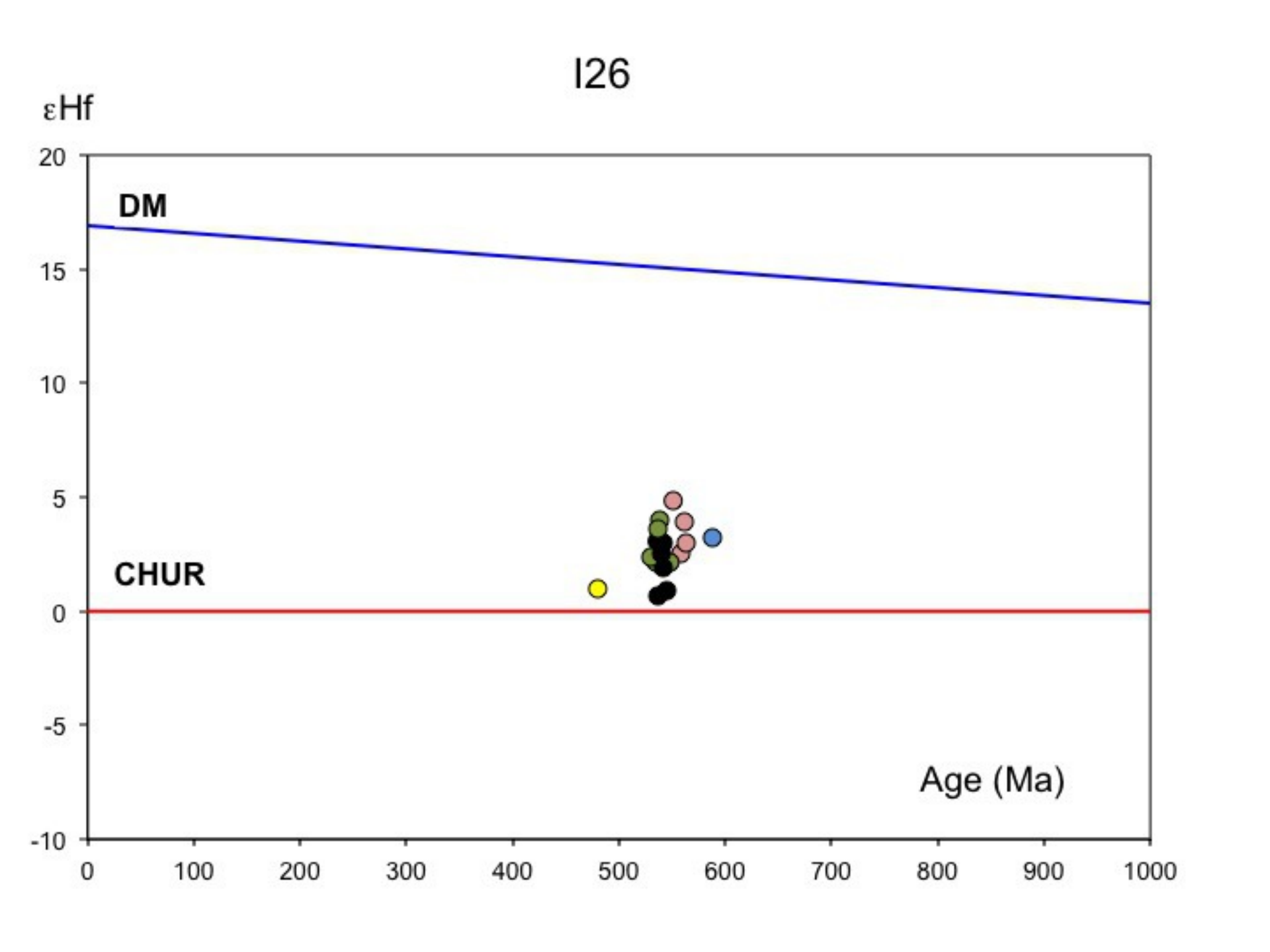
I26
εHf
20
15
10
5
0
-5
-10
DM
CHUR
0
100
200
300
400
500
600
700
800
900
1000
Age (Ma)

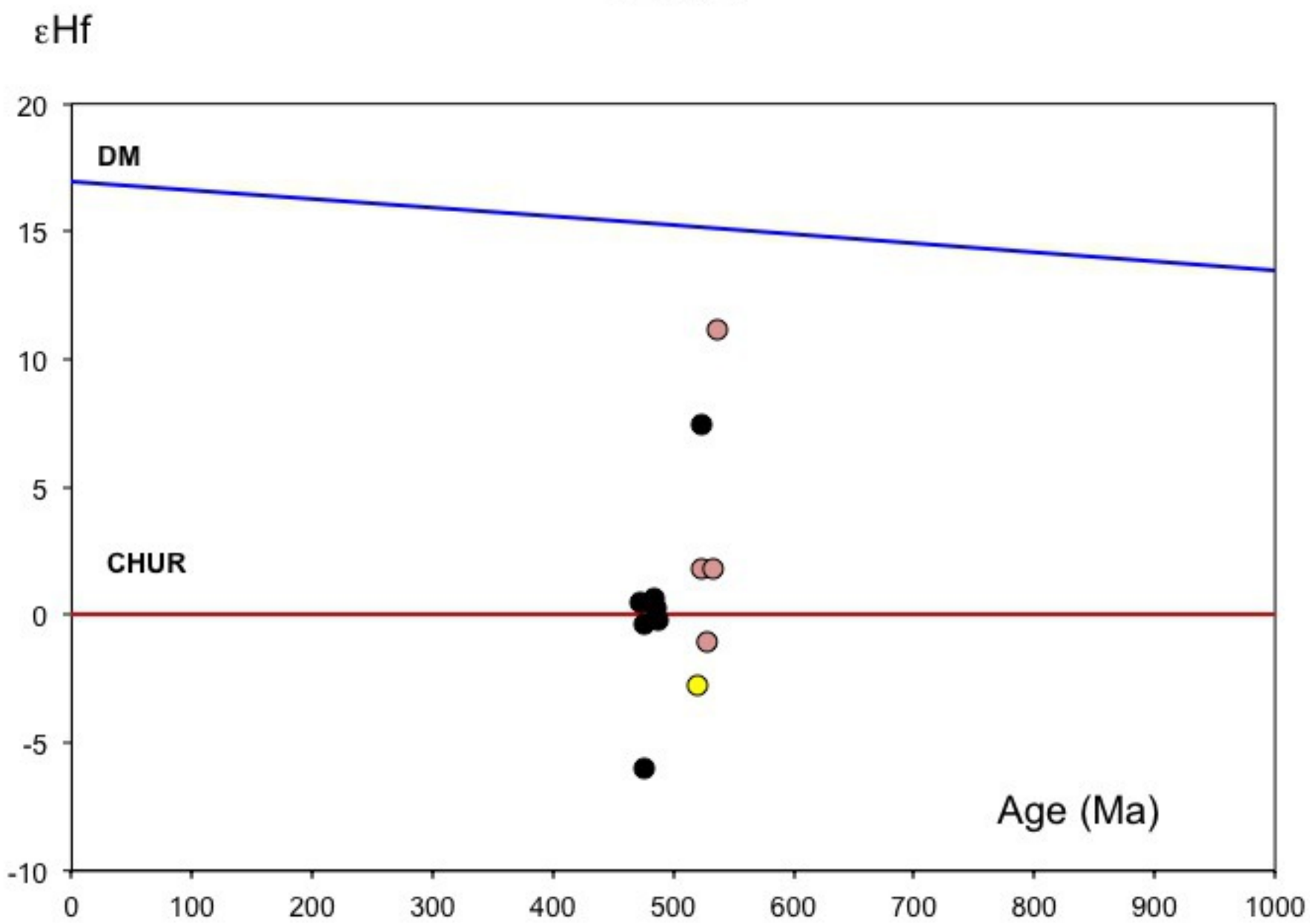
TES52
εHf
20
15
10
5
0
-5
-10
DM
CHUR
0
100
200
300
400
500
600
700
800
900
1000
Age (Ma)

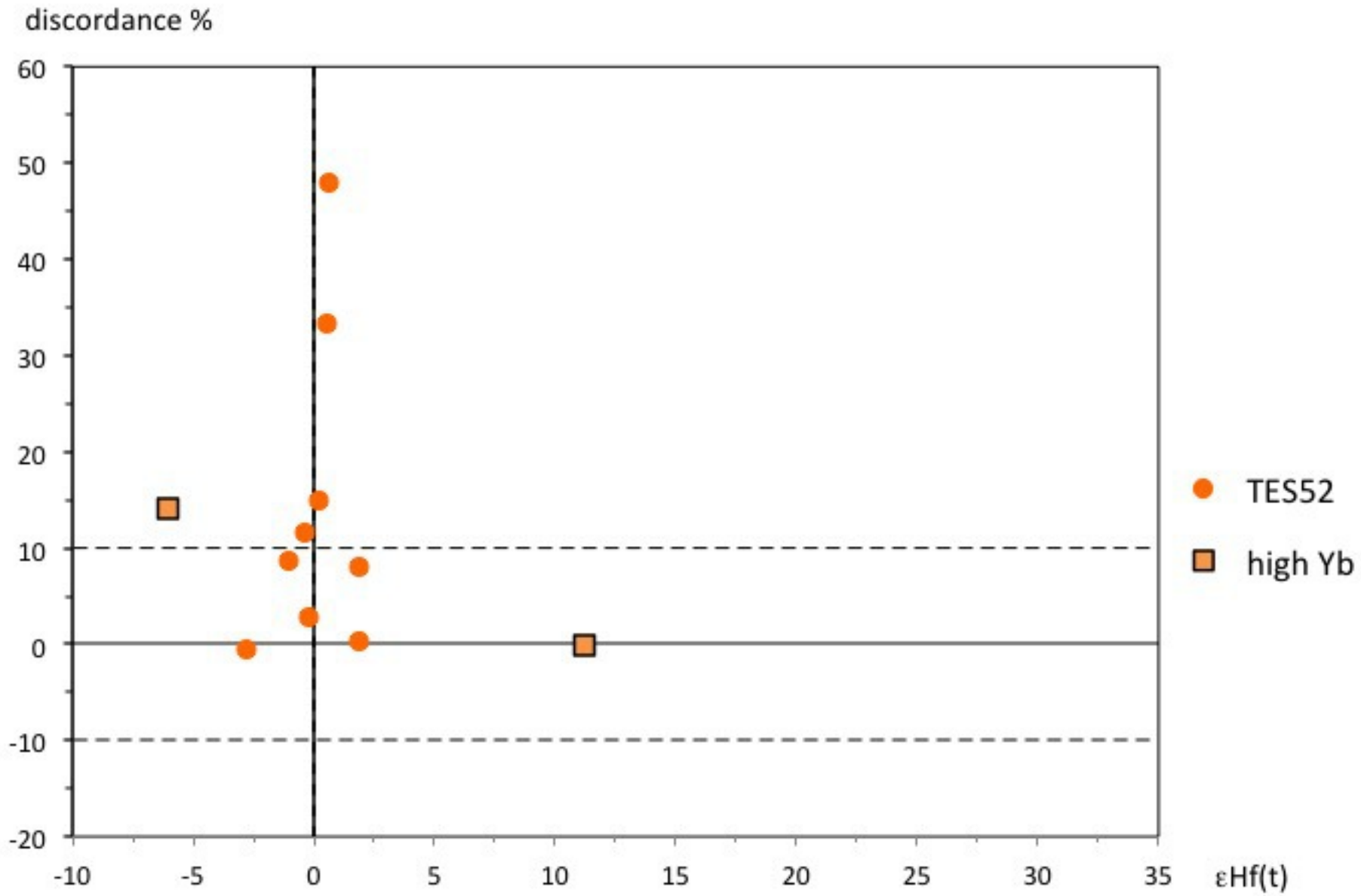
discordance %
60
50
40
30
20
10
0
-10
-20
-10
-5
0
5
10
15
20
25
30
35
εHf(t)
TES52
high Yb

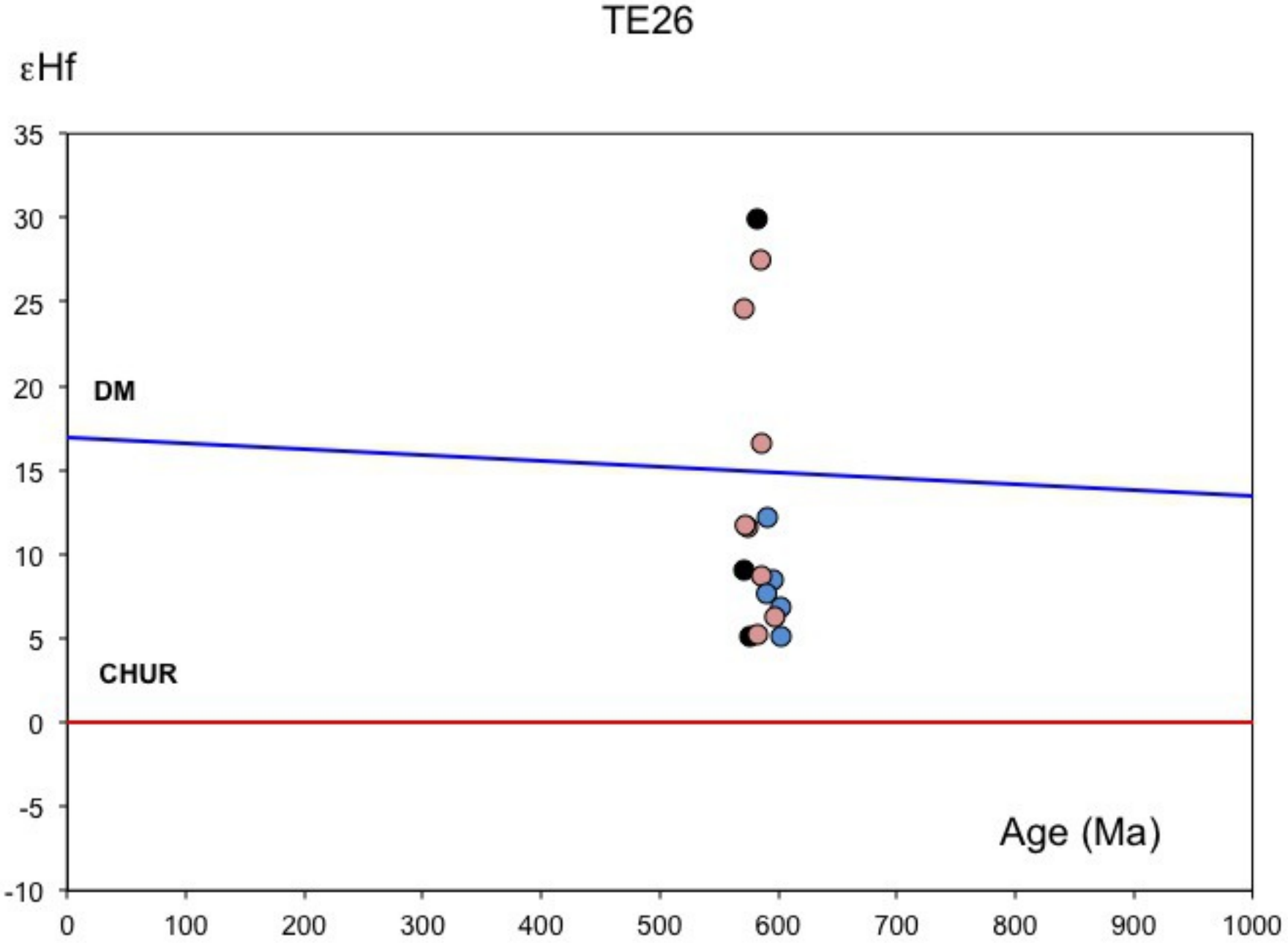
TE26
εHf
35
30
25
20
15
10
5
0
-5
-10
DM
CHUR
Age (Ma)
0
100
200
300
400
500
600
700
800
900
1000

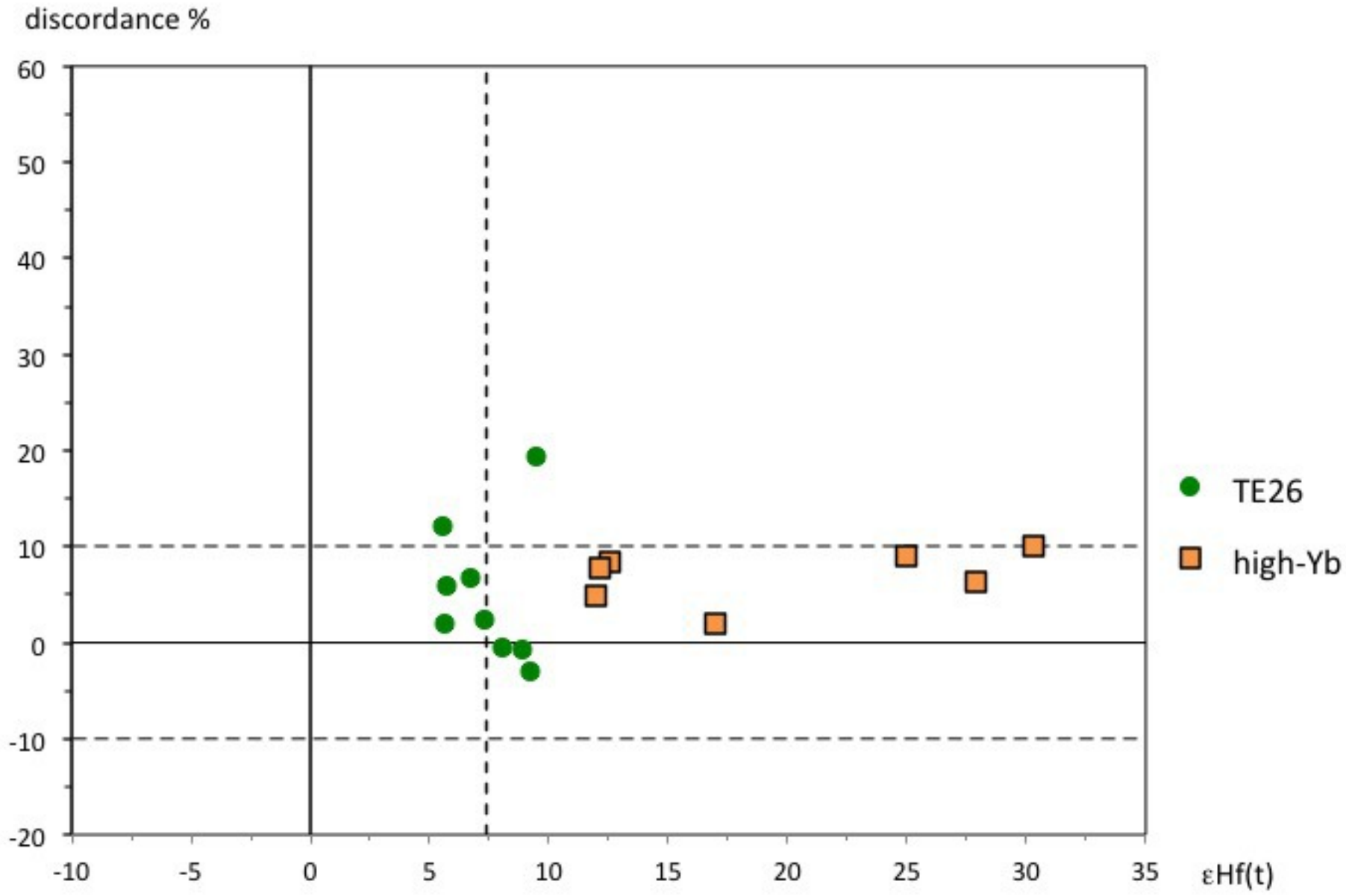
discordance %
60
50
40
30
20
10
0
-10
-20
-10
-5
0
5
10
15
20
25
30
35
εHf(t)
TE26
high-Yb

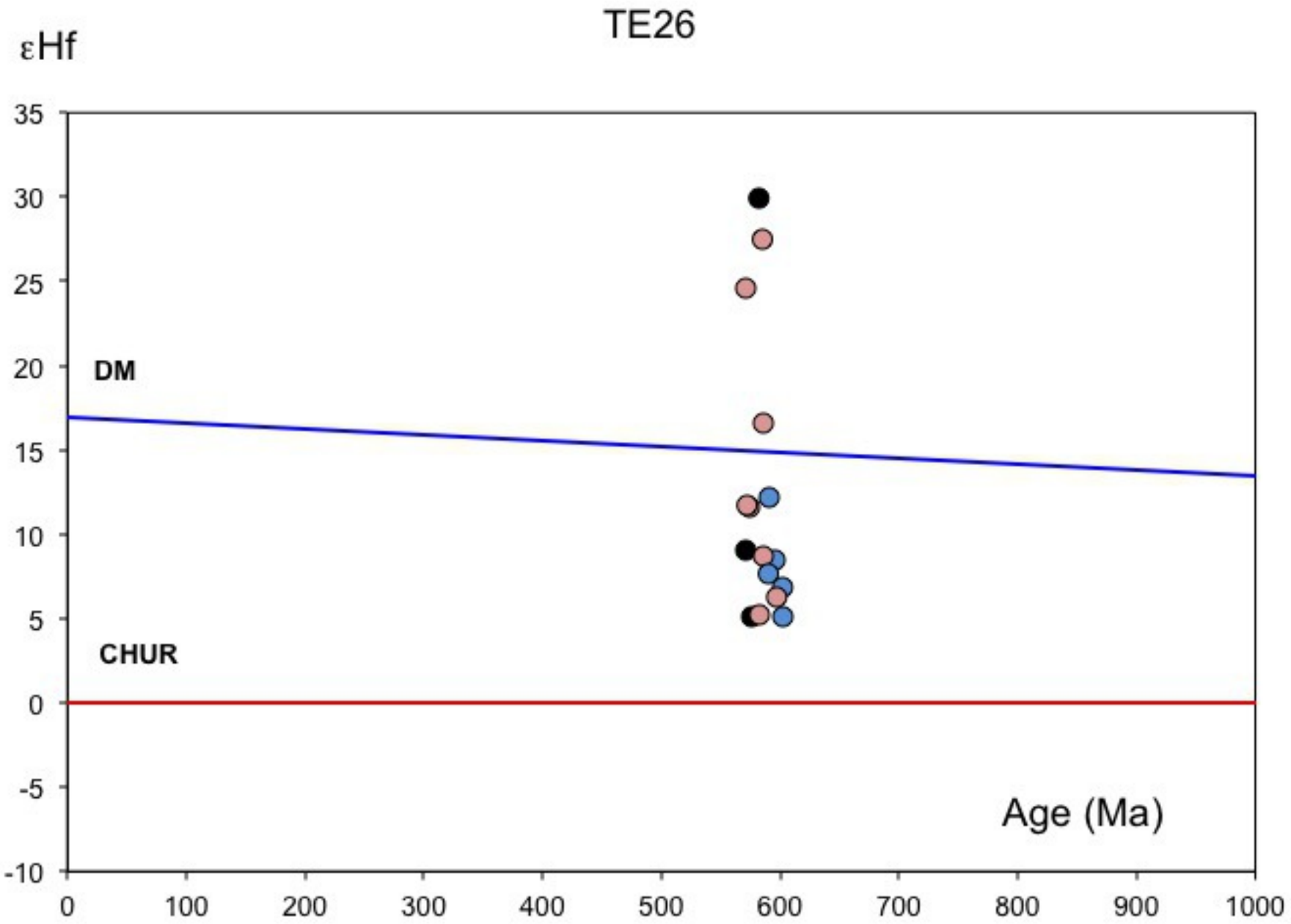
TE26
εHf
35
30
25
20
15
10
5
0
-5
-10
DM
CHUR
Age (Ma)
0
100
200
300
400
500
600
700
800
900
1000

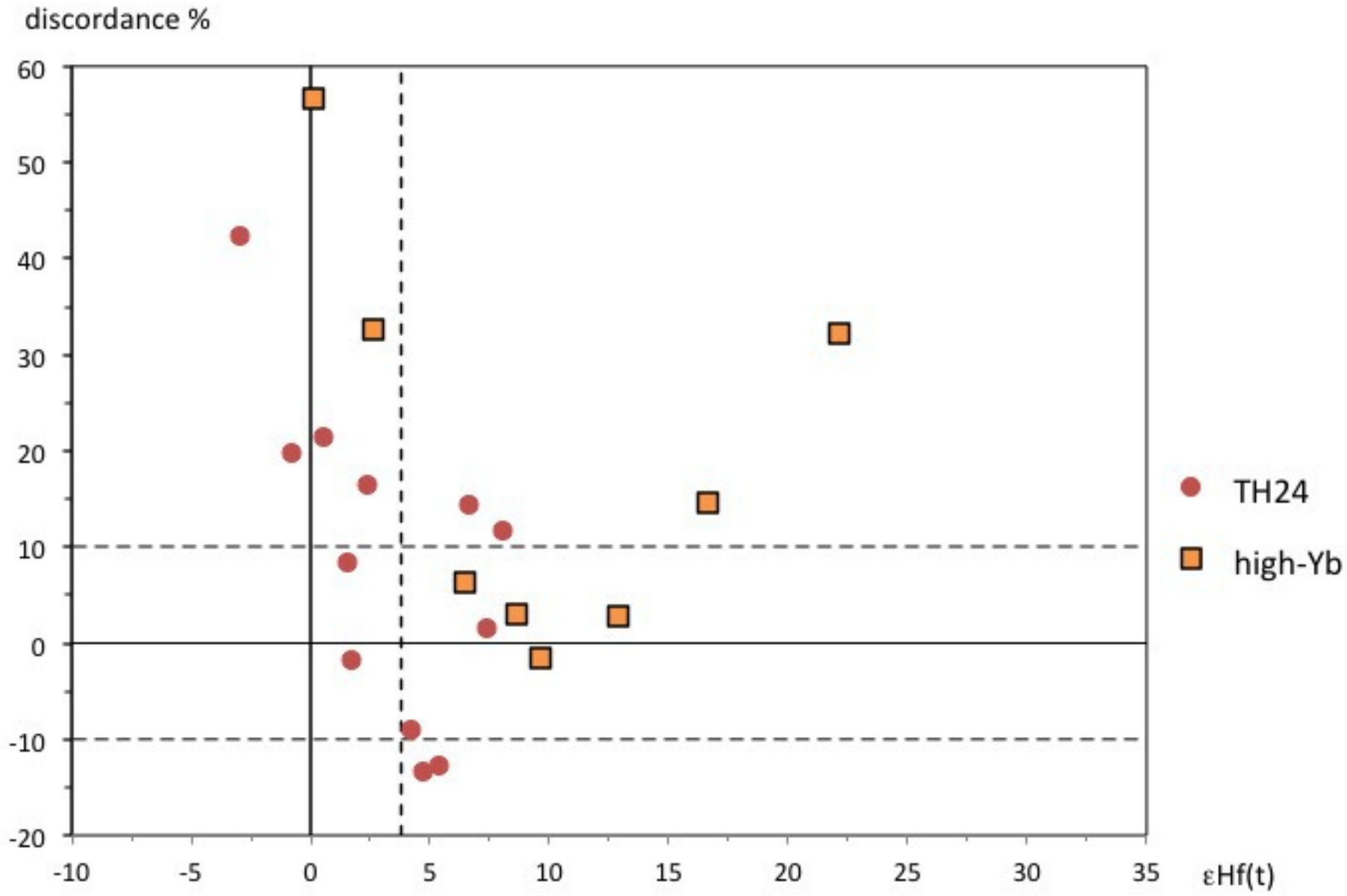
discordance %
60
50
40
30
20
10
0
-10
-20
-10
-5
0
5
10
15
20
25
30
35
εHf(t)
TH24
high-Yb

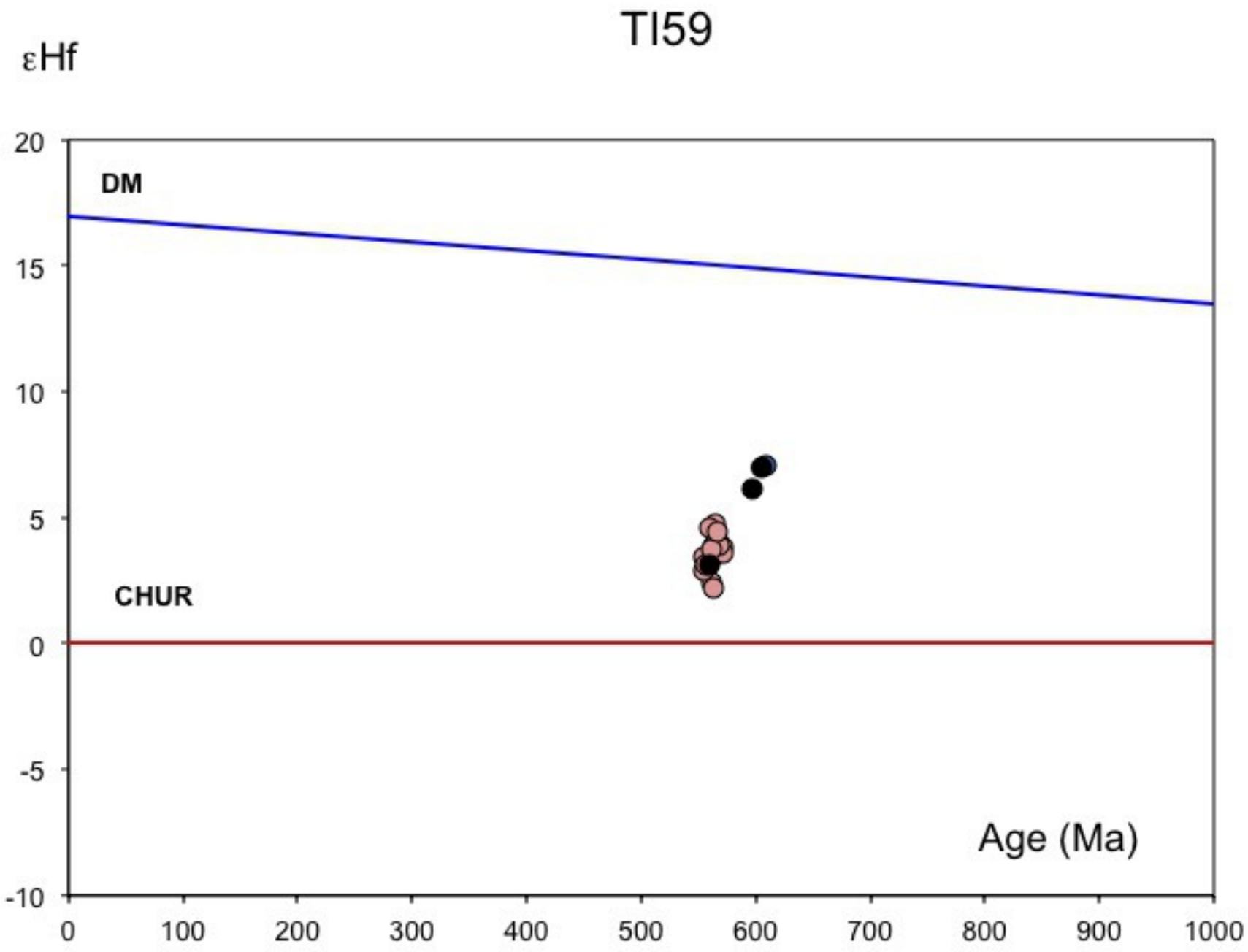
TI59
εHf
20
15
10
5
0
-5
-10
DM
CHUR
Age (Ma)
0
100
200
300
400
500
600
700
800
900
1000

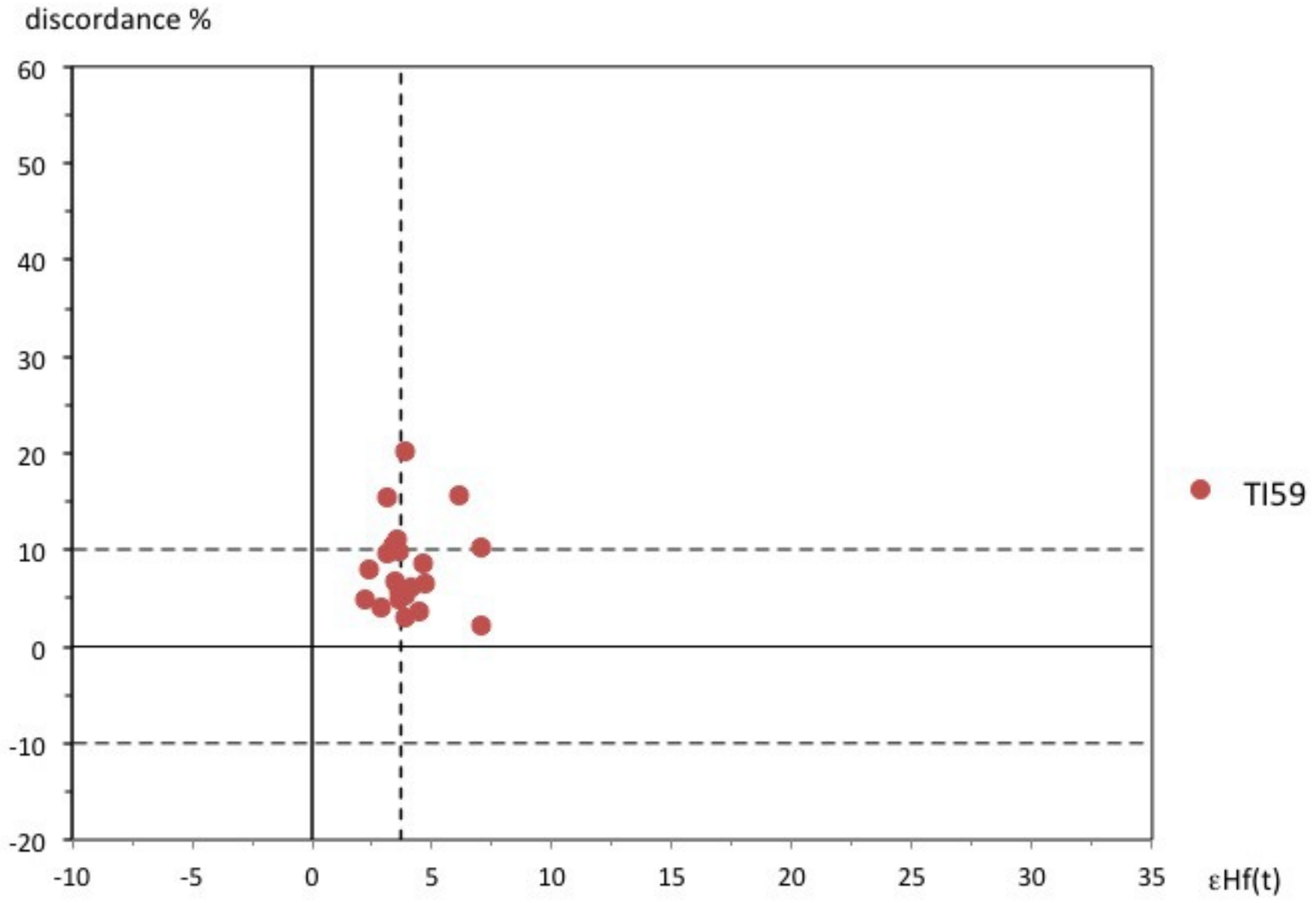
discordance %
60
50
40
30
20
10
0
-10
-20
-10
-5
0
5
10
15
20
25
30
35
εHf(t)
TI59

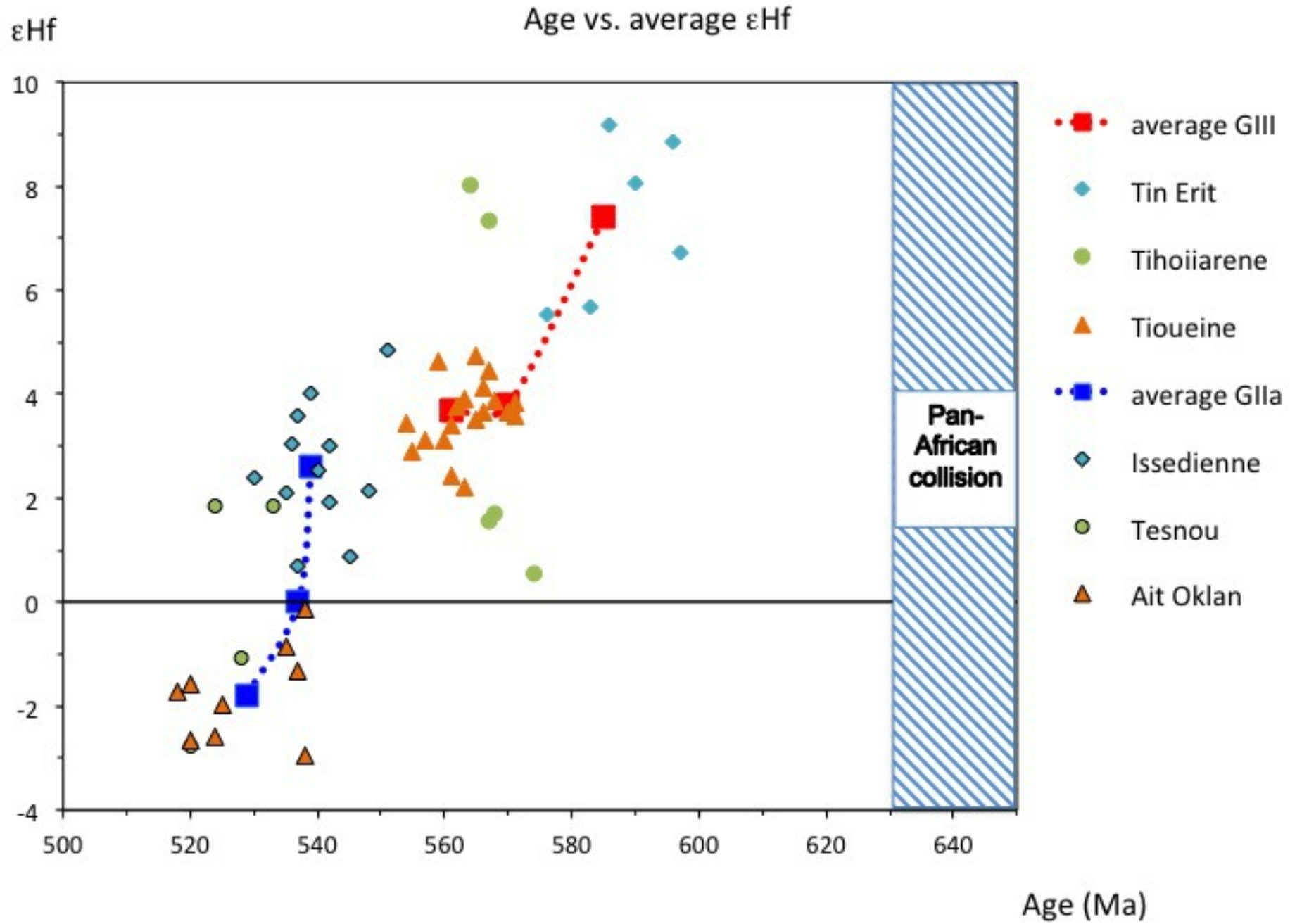
Age vs. average εHf
εHf
10
8
6
4
2
0
-2
-4
500
520
540
560
580
600
620
640
Age (Ma)
Pan-African collision
average GIII
Tin Erit
Tihoiiarene
Tioueine
average GIIa
Issedienne
Tesnou
Ait Oklan

Table 1. The Taourirt granitic suite of Hoggar, Algeria, as of 2003.

Rock types		gabbro and diorite (stocks, enclaves) G I monzogranite G IIa monzogranite and syenogranite G IIb alaskite (alkali feldspar granite) G III alkali feldspar syenite and granite	
Rock-forming mineralogy		G I quartz + K-feldspar + plagioclase + edenite-hornblende + biotite G IIa quartz + K-feldspar + plagioclase + biotite ± hornblende G IIb quartz + K-feldspar + albite + protolithionite-zinnwaldite G III alkali feldspar ± quartz ± plagioclase + hedenbergite + hastingsite-hornblende + biotite ± grünerite ± riebeckite	
Accessory mineralogy		G I zircon + allanite + titanite + ilmenite + magnetite + apatite G IIa zircon + allanite + titanite + ilmenite + magnetite + apatite + thorite + fergusonite + monazite + xenotime G IIb zircon + allanite + titanite + fluorite + topaz ± tourmaline ± garnet G III zircon + thorite + allanite + chevkinite + ilmenite + magnetite + apatite + fluorite	
Major element chemistry	SiO_2	G I 69 – 73 wt % G IIa 70 – 76.5 wt % G IIb ≤ 78 wt % G III 65 – 69 (syenite) and 73 – 77 wt %	
	CaO	G I 1.2 – 2.2 wt % G IIa 0.8 – 1.8 wt % G IIb < 0.02 wt % G III 2 – 2.5 (syenite) and 0.5 v 0.9 wt %	
	ASI	G I metaluminous G IIa metaluminous G IIb peraluminous G III metaluminous to peralkaline	
	alkali-calcic	G I, G IIa, G IIb	
	alkaline	G III	
Trace elements (ppm)	Rb	200 – 410 (G I, G IIa, G IIb)	120 – 260 (G III)
	Ba	14 – 800	37 – 600
	Th	20 – 85	15 – 60
	Zr	65 – 300	180 – 1200
	Y	22 – 140	40 – 60
REE patterns	La (ppm)	10 – 80 (G I, G IIa, G IIb)	35 – 280 (GIII)
	$(La/Yb)_N$	0.6 – 10	13 – 30
	Eu/Eu*	0.02 – 0.75 (G I, G IIa, G IIb)	0.04 – 0.16 (GIII)

		gull wing shape tetrad effects in G IIb only	gull wing shape no tetrad effects
Isotopic ratios	Sr_i εNd(525 Ma)	from 0.703 to 0.723 from -1.25 to -9.75	
Isotopic ages	590 – 520 Ma		
References	Azzouni-Sekkal and Boissonnas, 1993; Azzouni-Sekkal and Bonin, 1998; Azzouni-Sekkal et al., 2003; Bonin et al., 1998; Cheilletz et al., 1993.		

Table 2: U-Pb isotopic data

Sample: AO24
Ait Oklan

				R A T I O S (common-Pb corrected)								A G E S (common-Pb corrected, Ma)									
Analysis No.	Th (ppm)	U (ppm)	Th/U	$^{207}Pb/^{206}Pb$	± 1s	$^{207}Pb/^{235}U$	± 1s	$^{206}Pb/^{238}U$	± 1s	$^{208}Pb/^{232}Th$	± 1s	$^{207}Pb/^{206}Pb$	± 1s	$^{207}Pb/^{235}U$	± 1s	$^{206}Pb/^{238}U$	± 1s	$^{208}Pb/^{232}Th$	± 1s	Disc. %	Correction type
AO24-01	1249	8962	0.14	0.05900	0.00081	0.631	0.009	0.07758	0.00097	0.02432	0.00050	567	31	497	6	482	6	486	10	15.7	None
AO24-03	2986	17945	0.17	0.06211	0.00130	0.708	0.013	0.08271	0.00090	0.02544	0.00037	678	46	544	8	512	5	508	7	25.4	Disc
AO24-04	1755	2495	0.70	0.06542	0.00091	0.746	0.011	0.08266	0.00102	0.01256	0.00026	788	30	566	7	512	6	252	5	36.4	None
AO24-05	673	1272	0.53	0.05948	0.00090	0.793	0.012	0.09675	0.00109	0.02788	0.00065	585	34	593	7	595	6	556	13	-1.9	None
AO24-06	6790	5919	1.15	0.06740	0.00084	0.774	0.010	0.08327	0.00098	0.02498	0.00044	850	27	582	6	516	6	499	9	40.9	None
AO24-08	833	2495	0.33	0.06152	0.00255	0.696	0.027	0.08201	0.00121	0.02525	0.00040	658	91	536	16	508	7	504	8	23.6	Disc
AO24-09	1123	3391	0.33	0.06140	0.00093	0.718	0.012	0.08479	0.00107	0.02435	0.00060	653	33	549	7	525	6	486	12	20.5	None
AO24-10	626	997	0.63	0.06837	0.00180	0.736	0.019	0.07818	0.00118	0.01653	0.00077	880	56	560	11	485	7	331	15	46.6	None
AO24-11	1738	4314	0.40	0.06537	0.00140	0.717	0.016	0.07955	0.00111	0.01416	0.00059	786	46	549	9	493	7	284	12	38.7	None
AO24-12	1426	2697	0.53	0.06132	0.00159	0.715	0.019	0.08464	0.00126	0.02018	0.00104	650	57	548	11	524	7	404	21	20.4	None
AO24-13	580	877	0.66	0.06244	0.00099	0.749	0.012	0.08705	0.00096	0.01851	0.00046	689	35	568	7	538	6	371	9	22.9	None
AO24-14	1267	3850	0.33	0.06087	0.00104	0.749	0.013	0.08928	0.00114	0.02349	0.00066	635	38	568	8	551	7	469	13	13.7	None
AO24-15	1640	8272	0.20	0.05873	0.00168	0.681	0.017	0.08404	0.00112	0.02602	0.00037	557	64	527	10	520	7	519	7	6.9	Disc
AO24-17	1090	3898	0.28	0.06023	0.00078	0.772	0.010	0.09299	0.00099	0.05074	0.00102	612	29	581	6	573	6	1000	20	6.6	None
AO24-18	1469	3265	0.45	0.06131	0.00098	0.707	0.012	0.08367	0.00108	0.01819	0.00047	650	35	543	7	518	6	364	9	21.2	None
AO24-19	1589	7381	0.22	0.05785	0.00190	0.620	0.018	0.07775	0.00112	0.02411	0.00037	524	74	490	11	483	7	482	7	8.2	Disc
AO24-20	613	2299	0.27	0.05700	0.00123	0.572	0.011	0.07284	0.00078	0.02263	0.00026	491	49	460	7	453	5	452	5	8.1	Disc
AO24-21	1034	908	1.14	0.06742	0.00186	0.645	0.018	0.06945	0.00108	0.00674	0.00030	851	59	506	11	433	7	136	6	50.8	None
AO24-22	2309	5608	0.41	0.06523	0.00116	0.618	0.011	0.06877	0.00090	0.01760	0.00053	782	38	489	7	429	5	353	11	46.7	None
AO24-24	1323	3562	0.37	0.06024	0.00111	0.723	0.013	0.08700	0.00109	0.02309	0.00076	612	41	552	8	538	6	461	15	12.7	None
AO24-28	1050	1922	0.55	0.05880	0.00072	0.681	0.009	0.08401	0.00098	0.01943	0.00030	560	27	527	5	520	6	389	6	7.4	None
AO24-29	2291	17177	0.13	0.05575	0.00150	0.354	0.008	0.04600	0.00062	0.01433	0.00023	442	61	307	6	290	4	288	5	35.3	Disc
AO24-31	2075	11410	0.18	0.05989	0.00088	0.499	0.008	0.06043	0.00078	0.01913	0.00045	600	33	411	5	378	5	383	9	38.0	None
AO24-32	1546	3641	0.42	0.06215	0.00104	0.709	0.012	0.08280	0.00104	0.02038	0.00057	679	37	544	7	513	6	408	11	25.5	None
AO24-34	855	3718	0.23	0.05992	0.00131	0.595	0.011	0.07197	0.00084	0.02223	0.00030	601	48	474	7	448	5	444	6	26.3	Disc
AO24-35	3033	8950	0.34	0.06019	0.00141	0.689	0.016	0.08306	0.00120	0.02490	0.00110	610	52	532	10	514	7	497	22	16.4	None
AO24-36	4801	27552	0.17	0.06010	0.00120	0.479	0.010	0.05779	0.00079	0.01874	0.00071	607	44	397	7	362	5	375	14	41.5	None
AO24-38	1920	10532	0.18	0.05244	0.00137	0.384	0.009	0.05310	0.00067	0.01666	0.00024	305	61	330	6	333	4	334	5	-9.6	Disc
AO24-40	1341	3710	0.36	0.05869	0.00092	0.703	0.012	0.08685	0.00111	0.02516	0.00066	556	35	540	7	537	7	502	13	3.5	None
AO24-44	660	2033	0.32	0.05749	0.00120	0.686	0.015	0.08661	0.00120	0.02599	0.00097	510	47	531	9	535	7	519	19	-5.1	None

Sample: I26
Isseddienne

				R A T I O S (common-Pb corrected)								A G E S (common-Pb corrected, Ma)									
Analysis No.	Th (ppm)	U (ppm)	Th/U	$^{207}Pb/^{206}Pb$	± 1s	$^{207}Pb/^{235}U$	± 1s	$^{206}Pb/^{238}U$	± 1s	$^{208}Pb/^{232}Th$	± 1s	$^{207}Pb/^{206}Pb$	± 1s	$^{207}Pb/^{235}U$	± 1s	$^{206}Pb/^{238}U$	± 1s	$^{208}Pb/^{232}Th$	± 1s	Disc. %	Correction type
I26-01	396	1208	0.33	0.05720	0.00512	0.536	0.047	0.06799	0.00113	0.02111	0.00048	499	204	436	31	424	7	422	10	15.6	Disc
I26-02	129	153	0.85	0.05844	0.00111	0.730	0.014	0.09055	0.00112	0.03098	0.00063	546	42	556	8	559	7	617	12	-2.4	None
I26-03	420	382	1.10	0.05943	0.00088	0.715	0.011	0.08729	0.00102	0.02795	0.00052	583	33	548	6	539	6	557	10	7.8	None
I26-04	108	110	0.99	0.05830	0.00145	0.695	0.017	0.08652	0.00120	0.02694	0.00064	541	56	536	10	535	7	537	13	1.2	None
I26-06	806	1992	0.40	0.05612	0.00168	0.626	0.017	0.08093	0.00102	0.02519	0.00033	457	68	494	11	502	6	503	6	-10.2	Disc
I26-07	585	699	0.84	0.06177	0.00135	0.706	0.015	0.08285	0.00109	0.03028	0.00110	666	48	542	9	513	6	603	22	23.9	None
I26-10	1242	5040	0.25	0.06037	0.00246	0.795	0.030	0.09549	0.00138	0.02947	0.00049	617	90	594	17	588	8	587	10	4.9	Disc
I26-11	400	815	0.49	0.05896	0.00090	0.722	0.011	0.08877	0.00105	0.02847	0.00068	566	34	552	7	548	6	567	13	3.2	None
I26-12	5874	7788	0.75	0.10792	0.00465	1.356	0.055	0.09114	0.00141	0.02641	0.00041	1765	81	870	24	562	8	527	8	71.1	Disc
I26-14	325	286	1.14	0.06953	0.00272	0.869	0.033	0.09066	0.00164	0.02830	0.00162	915	82	635	18	559	10	564	32	40.5	None
I26-17	384	830	0.46	0.06039	0.00102	0.734	0.013	0.08818	0.00110	0.03014	0.00074	618	37	559	7	545	7	600	15	12.3	None
I26-18	192	347	0.55	0.06028	0.00122	0.722	0.014	0.08687	0.00103	0.02864	0.00090	614	45	552	8	537	6	571	18	13.0	None
I26-21	78	133	0.59	0.06704	0.00163	0.772	0.019	0.08357	0.00119	0.03197	0.00081	839	52	581	11	517	7	636	16	39.9	None
I26-22C	9534	10187	0.94	0.05727	0.00081	0.610	0.009	0.07731	0.00089	0.02489	0.00058	502	32	484	6	480	5	497	11	4.5	None
I26-22R	676	1837	0.37	0.06619	0.00108	0.611	0.010	0.06696	0.00079	0.03014	0.00082	812	35	484	6	418	5	600	16	50.2	None
I26-23	287	1467	0.20	0.05692	0.00141	0.680	0.015	0.08664	0.00110	0.02692	0.00037	488	56	527	9	536	6	537	7	-10.1	Disc
I26-25	194	463	0.42	0.06004	0.00099	0.757	0.013	0.09143	0.00109	0.02993	0.00076	605	36	572	7	564	6	596	15	7.1	None
I26-27	269	920	0.29	0.06525	0.00288	0.800	0.033	0.08886	0.00129	0.02718	0.00051	783	95	597	19	549	8	542	10	31.1	Disc
I26-28	606	442	1.37	0.07245	0.00221	0.703	0.021	0.07043	0.00103	0.02504	0.00144	999	63	541	12	439	6	500	28	58.0	None
I26-31	316	305	1.04	0.07842	0.00386	0.909	0.043	0.08404	0.00173	0.03304	0.00277	1158	100	656	23	520	10	657	54	57.3	None
I26-32	273	455	0.60	0.06096	0.00095	0.737	0.012	0.08765	0.00109	0.03028	0.00058	638	34	560	7	542	6	603	11	15.7	None
I26-33	559	892	0.63	0.05903	0.00328	0.662	0.036	0.08138	0.00117	0.02518	0.00040	568	124	516	22	504	7	503	8	11.7	Disc
I26-35	338	939	0.36	0.06736	0.00119	0.645	0.012	0.06947	0.00090	0.03351	0.00084	849	38	505	7	433	5	666	16	50.6	None
I26-37	41	54	0.76	0.06072	0.00166	0.734	0.020	0.08768	0.00122	0.03250	0.00080	629	60	559	11	542	7	646	16	14.5	None
I26-38	5149	7775	0.66	0.06266	0.00150	0.794	0.019	0.09194	0.00130	0.02990	0.00134	697	52	594	11	567	8	595	26	19.4	None
I26-40	152	301	0.50	0.05944	0.00098	0.702	0.012	0.08562	0.00105	0.02847	0.00060	583	37	540	7	530	6	567	12	9.6	None
I26-43	13	3	3.96	0.67012	0.11630	23.143	3.091	0.25047	0.02776	0.06122	0.01325	4668	266	3233	130	1441	143	1201	252	76.4	Disc
I26-44	211	357	0.59	0.05995	0.00097	0.722	0.012	0.08733	0.00105	0.02734	0.00060	602	36	552	7	540	6	545	12	10.8	None
I26-45	244	430	0.57	0.05892	0.00100	0.724	0.013	0.08918	0.00110	0.02820	0.00068	564	38	553	7	551	7	562	13	2.5	None
I26-46	102	315	0.32	0.05863	0.00146	0.703	0.015	0.08693	0.00105	0.02692	0.00034	553	56	540	9	537	6	537	7	3.0	Disc
I26-49	67	165	0.40	0.05797	0.00285	0.728	0.034	0.09107	0.00143	0.02824	0.00048	528	111	555	20	562	8	563	9	-6.6	Disc

Sample: TES52
Tesnou

				R A T I O S (common-Pb corrected)								A G E S (common-Pb corrected, Ma)									
Analysis No.	Th (ppm)	U (ppm)	Th/U	$^{207}Pb/^{206}Pb$	± 1s	$^{207}Pb/^{235}U$	± 1s	$^{206}Pb/^{238}U$	± 1s	$^{208}Pb/^{232}Th$	± 1s	$^{207}Pb/^{206}Pb$	± 1s	$^{207}Pb/^{235}U$	± 1s	$^{206}Pb/^{238}U$	± 1s	$^{208}Pb/^{232}Th$	± 1s	Disc. %	Correction type
TES52-01	282	706	0.40	0.06344	0.00108	0.741	0.012	0.08473	0.00089	0.02307	0.00061	723	37	563	7	524	5	461	12	28.6	None
TES52-02	358	1150	0.31	0.05836	0.00083	0.699	0.010	0.08687	0.00090	0.03034	0.00063	543	32	538	6	537	5	604	12	1.2	None
TES52-03	102	197	0.52	0.05773	0.00213	0.668	0.023	0.08397	0.00117	0.02605	0.00036	519	83	520	14	520	7	520	7	-0.1	Disc
TES52-04	5511	41833	0.13	0.05652	0.00064	0.596	0.007	0.07649	0.00085	0.02548	0.00036	473	26	475	5	475	5	509	7	-0.5	None
TES52-06	1526	7095	0.22	0.05946	0.00099	0.668	0.012	0.08154	0.00110	0.02424	0.00066	584	37	520	7	505	7	484	13	14.0	None
TES52-07	109	883	0.12	0.05933	0.00159	0.641	0.015	0.07834	0.00095	0.02422	0.00033	579	59	503	9	486	6	484	7	16.7	Disc
TES52-09	586	4954	0.12	0.05906	0.00179	0.640	0.017	0.07858	0.00115	0.02431	0.00039	569	68	502	11	488	7	486	8	14.9	Disc
TES52-11	730	4382	0.17	0.05743	0.00136	0.631	0.013	0.07963	0.00100	0.02472	0.00033	508	53	496	8	494	6	494	6	2.9	Disc
TES52-14	290	1018	0.28	0.05926	0.00083	0.698	0.010	0.08542	0.00103	0.02712	0.00054	577	31	538	6	528	6	541	11	8.7	None
TES52-17	599	1353	0.44	0.07966	0.00169	0.654	0.013	0.05953	0.00073	0.03043	0.00107	1189	43	511	8	373	4	606	21	70.6	None
TES52-18	303	928	0.33	0.06109	0.00088	0.797	0.012	0.09466	0.00110	0.03010	0.00059	642	32	595	7	583	6	599	12	9.7	None
TES52-19	609	695	0.88	0.07584	0.00145	0.733	0.014	0.07012	0.00084	0.02646	0.00071	1091	39	559	8	437	5	528	14	62.0	None
TES52-21	290	1026	0.28	0.06604	0.00117	0.810	0.014	0.08895	0.00103	0.02489	0.00069	808	38	603	8	549	6	497	14	33.3	None
TES52-22	209	618	0.34	0.05905	0.00200	0.690	0.022	0.08474	0.00099	0.02622	0.00033	569	75	533	13	524	6	523	6	8.1	Disc
TES52-23	968	5253	0.18	0.05818	0.00181	0.539	0.016	0.06716	0.00074	0.02082	0.00030	536	70	438	10	419	4	416	6	22.6	Disc
TES52-25	1041	3271	0.32	0.06905	0.00120	0.742	0.013	0.07798	0.00091	0.02403	0.00071	900	37	564	7	484	5	480	14	48.0	None
TES52-26	1750	8658	0.20	0.06268	0.00178	0.659	0.016	0.07621	0.00103	0.02342	0.00034	698	62	514	10	473	6	468	7	33.3	Disc
TES52-28	93	164	0.57	0.05813	0.00142	0.691	0.017	0.08618	0.00123	0.02686	0.00071	535	55	533	10	533	7	536	14	0.3	None
TES52-30	814	2709	0.30	0.06734	0.00153	0.669	0.015	0.07208	0.00093	0.01631	0.00066	848	48	520	9	449	6	327	13	48.7	None
TES52-31	1153	2922	0.39	0.06123	0.00340	0.410	0.022	0.04858	0.00075	0.01497	0.00025	647	122	349	16	306	5	300	5	54.0	Disc
TES52-32	243	528	0.46	0.08010	0.00173	0.662	0.014	0.05992	0.00078	0.03476	0.00113	1199	44	516	9	375	5	691	22	70.7	None
TES52-38	1165	6659	0.17	0.05815	0.00176	0.614	0.017	0.07661	0.00102	0.02375	0.00036	535	68	486	10	476	6	474	7	11.5	Disc

Sample: TE26
Tin Erit

				R A T I O S (common-Pb corrected)								A G E S (common-Pb corrected, Ma)									
Analysis No.	Th (ppm)	U (ppm)	Th/U	$^{207}Pb/^{206}Pb$	± 1s	$^{207}Pb/^{235}U$	± 1s	$^{206}Pb/^{238}U$	± 1s	$^{208}Pb/^{232}Th$	± 1s	$^{207}Pb/^{206}Pb$	± 1s	$^{207}Pb/^{235}U$	± 1s	$^{206}Pb/^{238}U$	± 1s	$^{208}Pb/^{232}Th$	± 1s	Disc. %	Correction type
TE26-01	480	1159	0.41	0.06281	0.00086	0.803	0.010	0.09268	0.00094	0.03291	0.00062	702	30	598	6	571	6	654	12	19.4	None
TE26-02	4355	6387	0.68	0.06644	0.00097	0.811	0.011	0.08857	0.00090	0.03165	0.00071	820	31	603	6	547	5	630	14	34.7	None
TE26-03	68	127	0.54	0.06035	0.00105	0.814	0.014	0.09785	0.00118	0.03100	0.00057	616	38	605	8	602	7	617	11	2.4	None
TE26-04	160	378	0.42	0.05967	0.00087	0.797	0.012	0.09691	0.00114	0.03088	0.00056	592	32	595	7	596	7	615	11	-0.8	None
TE26-05	602	558	1.08	0.06331	0.00111	0.884	0.016	0.10131	0.00126	0.03275	0.00079	719	38	643	9	622	7	651	15	14.1	None
TE26-06	648	1375	0.47	0.05999	0.00178	0.772	0.021	0.09332	0.00119	0.02882	0.00036	603	66	581	12	575	7	574	7	4.9	Disc
TE26-07	118	319	0.37	0.06096	0.00082	0.816	0.011	0.09706	0.00107	0.03075	0.00051	638	30	606	6	597	6	612	10	6.7	None
TE26-08	3700	6993	0.53	0.06060	0.00082	0.774	0.011	0.09259	0.00113	0.02936	0.00059	625	30	582	7	571	7	585	12	9.1	None
TE26-09	886	1955	0.45	0.06108	0.00077	0.808	0.010	0.09600	0.00104	0.03100	0.00052	642	28	602	6	591	6	617	10	8.3	None
TE26-12	517	1296	0.40	0.05907	0.00148	0.776	0.020	0.09524	0.00143	0.02932	0.00122	570	56	583	11	586	8	584	24	-3.1	None
TE26-14	217	332	0.65	0.05953	0.00077	0.786	0.010	0.09577	0.00103	0.03088	0.00040	587	29	589	6	590	6	615	8	-0.5	None
TE26-15	159	485	0.33	0.06135	0.00161	0.790	0.021	0.09344	0.00144	0.02836	0.00085	652	58	591	12	576	8	565	17	12.2	None
TE26-17	2255	2256	1.00	0.05980	0.00069	0.784	0.010	0.09511	0.00109	0.03104	0.00040	596	26	588	6	586	6	618	8	1.9	None
TE26-18	1328	3076	0.43	0.06039	0.00072	0.772	0.010	0.09278	0.00108	0.03137	0.00045	618	26	581	6	572	6	624	9	7.7	None
TE26-19	199	355	0.56	0.06041	0.00092	0.788	0.013	0.09464	0.00118	0.03067	0.00046	618	34	590	7	583	7	611	9	6.0	None
TE26-21	151	193	0.78	0.06138	0.00091	0.881	0.013	0.10412	0.00108	0.03343	0.00049	653	33	642	7	639	6	665	10	2.3	None
TE26-24	1034	3107	0.33	0.06923	0.00123	0.786	0.015	0.08232	0.00115	0.03514	0.00089	906	37	589	9	510	7	698	17	45.4	None
TE26-25	1117	2196	0.51	0.06053	0.00066	0.793	0.009	0.09505	0.00104	0.03161	0.00036	623	24	593	5	585	6	629	7	6.3	None
TE26-26	7853	15165	0.52	0.06115	0.00072	0.797	0.011	0.09454	0.00117	0.02986	0.00044	645	26	595	6	582	7	595	9	10.1	None
TE26-28	156	362	0.43	0.06031	0.00074	0.816	0.010	0.09813	0.00104	0.03150	0.00040	615	27	606	6	603	6	627	8	1.9	None
TH24-36	12800	30519	0.42	0.06426	0.00349	0.522	0.027	0.05895	0.00088	0.01806	0.00031	750	118	427	18	369	5	362	6	52.2	Disc
TH24-42	4302	16838	0.26	0.06013	0.00069	0.659	0.009	0.07952	0.00104	0.02412	0.00039	608	25	514	6	493	6	482	8	19.7	None
TH24-46	532	1276	0.42	0.06253	0.00118	0.837	0.016	0.09704	0.00131	0.03394	0.00102	692	41	618	9	597	8	675	20	14.3	None
TH24-47	212	521	0.41	0.06037	0.00069	0.765	0.010	0.09197	0.00118	0.03206	0.00045	617	25	577	6	567	7	638	9	8.4	None
TH24-48	1042	3268	0.32	0.05876	0.00066	0.746	0.010	0.09208	0.00116	0.03091	0.00044	558	25	566	6	568	7	615	9	-1.8	None
TH24-49	975	2323	0.42	0.06341	0.00116	0.814	0.016	0.09311	0.00129	0.03408	0.00103	722	40	605	9	574	8	677	20	21.5	None
TH24-50	207	554	0.37	0.05816	0.00088	0.788	0.013	0.09825	0.00124	0.03216	0.00064	536	34	590	7	604	7	640	13	-13.3	None
TH24-52	302	711	0.43	0.05976	0.00574	0.665	0.062	0.08073	0.00170	0.02494	0.00056	595	216	518	38	500	10	498	11	16.5	Disc
TH24-54	8270	21283	0.39	0.19468	0.00322	1.103	0.020	0.04112	0.00056	0.07387	0.00207	2782	28	755	9	260	3	1441	39	92.4	None
TH24-56	693	2424	0.29	0.08083	0.02635	0.162	0.053	0.01457	0.00053	0.00435	0.00054	1217	712	153	46	93	3	88	11	93.0	Disc

Sample: TH 24
table 5

				R A T I O S (common-Pb corrected)								A G E S (common-Pb corrected, Ma)									
Analysis No.	Th (ppm)	U (ppm)	Th/U	$^{207}Pb/^{206}Pb$	± 1s	$^{207}Pb/^{235}U$	± 1s	$^{206}Pb/^{238}U$	± 1s	$^{208}Pb/^{232}Th$	± 1s	$^{207}Pb/^{206}Pb$	± 1s	$^{207}Pb/^{235}U$	± 1s	$^{206}Pb/^{238}U$	± 1s	$^{208}Pb/^{232}Th$	± 1s	Disc. %	Correction type
TH24-01	1943	8288	0.23	0.05922	0.00079	0.751	0.011	0.09192	0.00120	0.03081	0.00064	575	30	569	7	567	7	613	13	1.5	None
TH24-03	3669	13755	0.27	0.05605	0.00159	0.562	0.014	0.07268	0.00097	0.02263	0.00030	454	64	453	9	452	6	452	6	0.5	Disc
TH24-04	23425	24363	0.96	0.11129	0.00547	0.354	0.016	0.02308	0.00039	0.00666	0.00011	1821	91	308	12	147	2	134	2	92.9	Disc
TH24-05	2553	9406	0.27	0.06238	0.00095	0.799	0.013	0.09287	0.00117	0.03279	0.00079	687	33	596	7	572	7	652	15	17.4	None
TH24-10	751	3038	0.25	0.06971	0.00133	0.849	0.017	0.08831	0.00123	0.03832	0.00128	920	40	624	9	546	7	760	25	42.4	None
TH24-11	2314	8277	0.28	0.10037	0.00216	0.833	0.018	0.06018	0.00087	0.04419	0.00174	1631	41	615	10	377	5	874	34	79.1	None
TH24-13	2631	5096	0.52	0.05975	0.00134	0.774	0.018	0.09398	0.00143	0.03109	0.00123	595	50	582	10	579	8	619	24	2.8	None
TH24-14	162	484	0.34	0.05708	0.00223	0.684	0.025	0.08691	0.00114	0.02700	0.00037	495	88	529	15	537	7	538	7	-9.0	Disc
TH24-15	689	1999	0.34	0.06088	0.00090	0.768	0.012	0.09144	0.00119	0.03217	0.00074	635	33	578	7	564	7	640	14	11.7	None
TH24-16	434	1886	0.23	0.05962	0.00091	0.738	0.012	0.08977	0.00120	0.03115	0.00076	590	34	561	7	554	7	620	15	6.3	None
TH24-17	249	485	0.51	0.06570	0.00192	0.808	0.024	0.08942	0.00146	0.03619	0.00195	797	63	601	13	552	9	719	38	32.2	None
TH24-18	11470	27872	0.41	0.05975	0.00183	0.771	0.024	0.09369	0.00157	0.02690	0.00093	595	68	580	13	577	9	537	18	3.2	None
TH24-19	21364	40522	0.53	0.05920	0.00065	0.738	0.010	0.09044	0.00117	0.02956	0.00044	574	24	561	6	558	7	589	9	3.0	None
TH24-21	3755	7666	0.49	0.05697	0.00188	0.631	0.019	0.08027	0.00107	0.02494	0.00031	491	75	496	12	498	6	498	6	-1.5	Disc
TH24-22	145	441	0.33	0.06266	0.00519	0.842	0.068	0.09745	0.00184	0.02994	0.00059	697	183	620	37	599	11	596	12	14.6	Disc
TH24-26	1996	8171	0.24	0.05794	0.00311	0.768	0.039	0.09613	0.00153	0.02981	0.00047	528	121	579	23	592	9	594	9	-12.7	Disc
TH24-27	2988	7290	0.41	0.07827	0.00088	0.814	0.011	0.07543	0.00097	0.03264	0.00049	1154	23	605	6	469	6	649	10	61.5	None
TH24-32	26618	45162	0.59	0.07585	0.00180	0.834	0.020	0.07987	0.00121	0.04055	0.00144	1091	49	616	11	495	7	803	28	56.7	None
TH24-33	430	1570	0.27	0.07267	0.00107	0.918	0.015	0.09169	0.00125	0.03954	0.00068	1005	31	661	8	566	7	784	13	45.7	None
TH24-34	510	2287	0.22	0.06846	0.00094	0.932	0.014	0.09878	0.00132	0.04275	0.00089	883	29	669	8	607	8	846	17	32.7	None
TH24-36	12800	30519	0.42	0.06426	0.00349	0.522	0.027	0.05895	0.00088	0.01806	0.00031	750	118	427	18	369	5	362	6	52.2	Disc
TH24-42	4302	16838	0.26	0.06013	0.00069	0.659	0.009	0.07952	0.00104	0.02412	0.00039	608	25	514	6	493	6	482	8	19.7	None
TH24-46	532	1276	0.42	0.06253	0.00118	0.837	0.016	0.09704	0.00131	0.03394	0.00102	692	41	618	9	597	8	675	20	14.3	None
TH24-47	212	521	0.41	0.06037	0.00069	0.765	0.010	0.09197	0.00118	0.03206	0.00045	617	25	577	6	567	7	638	9	8.4	None
TH24-48	1042	3268	0.32	0.05876	0.00066	0.746	0.010	0.09208	0.00116	0.03091	0.00044	558	25	566	6	568	7	615	9	-1.8	None
TH24-49	975	2323	0.42	0.06341	0.00116	0.814	0.016	0.09311	0.00129	0.03408	0.00103	722	40	605	9	574	8	677	20	21.5	None
TH24-50	207	554	0.37	0.05816	0.00088	0.788	0.013	0.09825	0.00124	0.03216	0.00064	536	34	590	7	604	7	640	13	-13.3	None
TH24-52	302	711	0.43	0.05976	0.00574	0.665	0.062	0.08073	0.00170	0.02494	0.00056	595	216	518	38	500	10	498	11	16.5	Disc
TH24-54	8270	21283	0.39	0.19468	0.00322	1.103	0.020	0.04112	0.00056	0.07387	0.00207	2782	28	755	9	260	3	1441	39	92.4	None
TH24-56	693	2424	0.29	0.08083	0.02635	0.162	0.053	0.01457	0.00053	0.00435	0.00054	1217	712	153	46	93	3	88	11	93.0	Disc

Sample: TI59
Table 6

				R A T I O S (common-Pb corrected)								A G E S (common-Pb corrected, Ma)									
Analysis No.	Th (ppm)	U (ppm)	Th/U	$^{207}Pb/^{206}Pb$	± 1s	$^{207}Pb/^{235}U$	± 1s	$^{206}Pb/^{238}U$	± 1s	$^{208}Pb/^{232}Th$	± 1s	$^{207}Pb/^{206}Pb$	± 1s	$^{207}Pb/^{235}U$	± 1s	$^{206}Pb/^{238}U$	± 1s	$^{208}Pb/^{232}Th$	± 1s	Disc. %	Correction type
TI59-01	72	154	0.47	0.06052	0.00078	0.827	0.011	0.09913	0.00110	0.03110	0.00046	622	28	612	6	609	6	619	9	2.2	None
TI59-02	2375	4456	0.53	0.05997	0.00073	0.758	0.010	0.09163	0.00115	0.02807	0.00049	602	27	573	6	565	7	560	10	6.5	None
TI59-03	243	510	0.48	0.10881	0.00137	1.410	0.019	0.09399	0.00108	0.06205	0.00107	1780	23	893	8	579	6	1217	20	70.4	None
TI59-05	3624	5570	0.65	0.06071	0.00074	0.773	0.011	0.09241	0.00114	0.02809	0.00049	629	27	582	6	570	7	560	10	9.8	None
TI59-06	3716	5395	0.69	0.06057	0.00068	0.760	0.009	0.09097	0.00105	0.02848	0.00042	624	25	574	5	561	6	568	8	10.5	None
TI59-07	335	514	0.65	0.06284	0.00111	0.841	0.016	0.09710	0.00133	0.03187	0.00087	703	38	620	9	597	8	634	17	15.7	None
TI59-08	3504	7185	0.49	0.06078	0.00097	0.767	0.013	0.09153	0.00124	0.02768	0.00077	631	35	578	8	565	7	552	15	11.1	None
TI59-10C	2360	3759	0.63	0.06017	0.00073	0.752	0.009	0.09059	0.00098	0.02804	0.00047	610	27	569	5	559	6	559	9	8.7	None
TI59-10R	483	1526	0.32	0.06190	0.00168	0.839	0.022	0.09834	0.00149	0.03500	0.00180	671	59	619	12	605	9	695	35	10.3	None
TI59-11	2268	4112	0.55	0.06151	0.00072	0.769	0.009	0.09071	0.00100	0.03006	0.00049	657	26	579	5	560	6	599	10	15.5	None
TI59-12	5705	8637	0.66	0.05970	0.00073	0.751	0.011	0.09120	0.00117	0.02803	0.00050	593	27	569	6	563	7	559	10	5.3	None
TI59-13	2409	4314	0.56	0.05994	0.00071	0.758	0.010	0.09174	0.00113	0.02918	0.00048	601	26	573	6	566	7	581	9	6.2	None
TI59-14	3484	6053	0.58	0.06009	0.00065	0.753	0.009	0.09090	0.00105	0.02878	0.00039	607	24	570	5	561	6	573	8	7.9	None
TI59-15	2152	4508	0.48	0.06902	0.00132	0.822	0.016	0.08641	0.00120	0.03338	0.00109	899	40	609	9	534	7	664	21	42.3	None
TI59-17	2931	5615	0.52	0.06042	0.00087	0.785	0.013	0.09418	0.00125	0.02941	0.00067	619	32	588	7	580	7	586	13	6.5	None
TI59-18	2654	5011	0.53	0.06761	0.00111	0.812	0.013	0.08707	0.00101	0.03427	0.00096	857	35	603	7	538	6	681	19	38.7	None
TI59-19	2404	4032	0.60	0.06355	0.00114	0.784	0.015	0.08943	0.00122	0.02907	0.00087	727	39	588	8	552	7	579	17	25.1	None
TI59-20	2310	4555	0.51	0.06302	0.00146	0.805	0.019	0.09269	0.00140	0.02822	0.00112	709	50	600	11	571	8	562	22	20.3	None
TI59-25	3029	5506	0.55	0.05929	0.00067	0.735	0.009	0.08997	0.00103	0.02820	0.00043	578	25	560	5	555	6	562	8	4.1	None
TI59-26	5613	7183	0.78	0.05970	0.00076	0.739	0.010	0.08981	0.00109	0.02803	0.00054	593	28	562	6	554	6	559	11	6.8	None
TI59-27	2514	4295	0.59	0.06025	0.00078	0.733	0.010	0.08826	0.00098	0.02775	0.00053	613	29	558	6	545	6	553	10	11.5	None
TI59-28	466	1727	0.27	0.06611	0.00109	0.784	0.013	0.08607	0.00104	0.03968	0.00105	810	35	588	7	532	6	787	20	35.7	None
TI59-30	2001	3780	0.53	0.05973	0.00064	0.756	0.009	0.09180	0.00104	0.02870	0.00037	594	24	572	5	566	6	572	7	4.9	None
TI59-32	1679	3832	0.44	0.06000	0.00065	0.766	0.009	0.09263	0.00101	0.02944	0.00039	604	24	578	5	571	6	586	8	5.6	None
TI59-33	3682	5149	0.72	0.05962	0.00073	0.750	0.009	0.09123	0.00098	0.02868	0.00049	590	27	568	5	563	6	572	10	4.8	None
TI59-34	1733	3372	0.51	0.06029	0.00071	0.750	0.010	0.09024	0.00110	0.02924	0.00048	614	26	568	6	557	7	583	9	9.7	None
TI59-35	1710	3050	0.56	0.06061	0.00069	0.734	0.009	0.08781	0.00097	0.02885	0.00042	625	25	559	5	543	6	575	8	13.8	None
TI59-37	3714	7640	0.49	0.05949	0.00085	0.755	0.012	0.09203	0.00120	0.03034	0.00072	585	32	571	7	568	7	604	14	3.1	None
TI59-40	4162	6302	0.66	0.05976	0.00074	0.751	0.010	0.09110	0.00108	0.02950	0.00053	595	27	569	6	562	6	588	10	5.8	None
TI59-43	3108	5861	0.53	0.05955	0.00087	0.754	0.012	0.09189	0.00119	0.03028	0.00074	587	32	571	7	567	7	603	15	3.7	None

Table 3 Zircon Hf isotopic data

Sample: AO24 Ait Oklan

Analysis No.	Th (ppm)	U (ppm)	Th/U	Age (Ma)	$^{176}Hf/^{177}Hf$	1 se	$^{176}Lu/^{177}Hf$	$^{176}Yb/^{177}Hf$	T(DM) (Ga)	T(DM) (crustal)	epsilon Hf	discordance %
AO24-01	1249	8962	0.14	482	0.282396	0.000007	0.002334	0.06945	1.21	1.62	-3.4	15.7
AO24-03	2986	17945	0.17	512	0.282356	0.000008	0.002754	0.08502	1.28	1.70	-4.4	25.4
AO24-04	1755	2495	0.70	512	0.282454	0.000006	0.001618	0.05021	1.11	1.46	-0.5	36.4
AO24-06	6790	5919	1.15	516	0.282351	0.000016	0.008842	0.31026	1.55	1.84	-6.6	40.9
AO24-08	833	2495	0.33	508	0.282442	0.000008	0.002066	0.06299	1.14	1.50	-1.2	23.6
AO24-09	1123	3391	0.33	525	0.282412	0.000008	0.002315	0.07791	1.19	1.56	-2.0	20.5
AO24-10	626	997	0.63	485	0.282431	0.000011	0.001601	0.05119	1.14	1.52	-1.9	46.6
AO24-11	1738	4314	0.40	493	0.282395	0.000006	0.002056	0.06071	1.20	1.61	-3.2	38.7
AO24-12	1426	2697	0.53	524	0.282387	0.000009	0.001489	0.04587	1.20	1.60	-2.6	20.4
AO24-13	580	877	0.66	538	0.282368	0.000006	0.001431	0.04567	1.22	1.63	-3.0	22.9
AO24-15	1640	8272	0.20	520	0.282398	0.000009	0.002501	0.08433	1.22	1.60	-2.6	6.9
AO24-18	1469	3265	0.45	518	0.282415	0.000006	0.001424	0.04208	1.16	1.54	-1.7	21.2
AO24-19	1589	7381	0.22	483	0.282415	0.000007	0.001297	0.04063	1.15	1.55	-2.4	8.2
AO24-24	1323	3562	0.37	538	0.282449	0.000007	0.001578	0.04799	1.12	1.45	-0.1	12.7
AO24-28	1050	1922	0.55	520	0.282421	0.000006	0.001767	0.05700	1.16	1.53	-1.6	7.4
AO24-32	1546	3641	0.42	513	0.282382	0.000008	0.002734	0.08837	1.25	1.64	-3.4	25.5
AO24-35	3033	8950	0.34	514	0.282441	0.000012	0.002922	0.09400	1.17	1.51	-1.4	16.4
AO24-40	1341	3710	0.36	537	0.282420	0.000009	0.001948	0.06264	1.17	1.53	-1.3	3.5
AO24-44	660	2033	0.32	535	0.282431	0.000008	0.001636	0.05199	1.14	1.50	-0.9	-5.1

Sample: I26 Isseddienne

Analysis No.	Th (ppm)	U (ppm)	Th/U	Age (Ma)	$^{176}Hf/^{177}Hf$	1 se	$^{176}Lu/^{177}Hf$	$^{176}Yb/^{177}Hf$	T(DM) (Ga)	T(DM) (crustal)	epsilon Hf	discordance %
I26-02	129	153	0.85	559	0.282514	0.000011	0.001825	0.05211	1.03	1.31	2.5	-2.4
I26-03	420	382	1.10	539	0.282566	0.000009	0.001600	0.04575	0.95	1.20	4.0	7.8
I26-04	108	110	0.99	535	0.282510	0.000008	0.001097	0.02993	1.02	1.31	2.1	1.2
I26-10	1242	5040	0.25	588	0.282516	0.000006	0.001642	0.04679	1.02	1.28	3.3	4.9
I26-11	400	815	0.49	548	0.282504	0.000010	0.001177	0.03169	1.03	1.32	2.2	3.2
I26-17	384	830	0.46	545	0.282473	0.000008	0.001521	0.03952	1.08	1.40	0.9	12.3
I26-18	192	347	0.55	537	0.282469	0.000007	0.001191	0.03025	1.08	1.40	0.7	13.0
I26-22c	9534	10187	0.94	480	0.282523	0.000008	0.002392	0.07763	1.04	1.34	1.0	4.5
I26-23	287	1467	0.20	536	0.282533	0.000015	0.000874	0.02839	0.98	1.26	3.0	-10.1
I26-25	194	463	0.42	564	0.282517	0.000007	0.001014	0.03191	1.01	1.28	3.0	7.1
I26-32	273	455	0.60	542	0.282502	0.000008	0.001307	0.04187	1.03	1.33	1.9	15.7
I26-37	41	54	0.76	542	0.282535	0.000009	0.001545	0.05023	1.00	1.26	3.0	14.5
I26-40	152	301	0.50	530	0.282520	0.000007	0.001026	0.03001	1.00	1.29	2.4	9.6
I26-44	211	357	0.59	540	0.282523	0.000006	0.001530	0.04817	1.01	1.29	2.5	10.8
I26-45	244	430	0.57	551	0.282575	0.000007	0.000885	0.02859	0.92	1.16	4.8	2.5
I26-46	102	315	0.32	537	0.282547	0.000009	0.000798	0.02335	0.96	1.22	3.6	3.0
I26-49	67	165	0.40	562	0.282546	0.000007	0.001169	0.03674	0.97	1.22	4.0	-6.6

Sample: TES52 Tesnou

Analysis No.	Th (ppm)	U (ppm)	Th/U	Age (Ma)	$^{176}Hf/^{177}Hf$	1 se	$^{176}Lu/^{177}Hf$	$^{176}Yb/^{177}Hf$	T(DM) (Ga)	T(DM) (crustal)	epsilon Hf	discordance %
TES52-01	282	706	0.40	524	0.282679	0.000013	0.002303	0.10301	0.81	0.98	7.5	28.6
TES52-03	358	1150	0.31	537	0.282792	0.000014	0.003800	0.16241	0.68	0.75	11.2	-0.1
TES52-04	102	197	0.52	520	0.282383	0.000007	0.001325	0.04812	1.20	1.60	-2.8	-0.5
TES52-06	5511	41833	0.13	475	0.282397	0.000018	0.010145	0.37453	1.54	1.77	-6.0	14.0
TES52-09	109	883	0.12	486	0.282505	0.000012	0.003168	0.11632	1.08	1.39	0.2	14.9
TES52-10	586	4954	0.12	488	0.282480	0.000006	0.001970	0.06342	1.08	1.42	-0.2	2.9
TES52-14	290	1018	0.28	528	0.282427	0.000013	0.001418	0.05066	1.14	1.50	-1.1	8.7
TES52-22	209	618	0.34	524	0.282514	0.000011	0.001631	0.05479	1.03	1.32	1.8	8.1
TES52-25	1041	3271	0.32	484	0.282506	0.000017	0.001949	0.07464	1.05	1.37	0.6	48.0
TES52-26	1750	8658	0.20	473	0.282515	0.000011	0.002536	0.09762	1.05	1.37	0.5	33.3
TES52-28	93	164	0.57	533	0.282499	0.000011	0.000655	0.02486	1.02	1.33	1.8	0.3
TES52-38	1165	6659	0.17	476	0.282480	0.000005	0.001697	0.05832	1.08	1.42	-0.4	11.5

Sample: TE26 Tin Erit

Analysis No.	Th (ppm)	U (ppm)	Th/U	Age (Ma)	$^{176}Hf/^{177}Hf$	1 se	$^{176}Lu/^{177}Hf$	$^{176}Yb/^{177}Hf$	T(DM) (Ga)	T(DM) (crustal)	epsilon Hf	discordance %
TE26-01	480	1159	0.41	571	0.282682	0.000026	0.001012	0.04687	0.78	0.91	9.4	19.4
TE26-03	68	127	0.54	602	0.282602	0.000021	0.000951	0.03849	0.89	1.07	7.3	2.4
TE26-04	160	378	0.42	596	0.282654	0.000009	0.001371	0.04290	0.83	0.97	8.9	-0.8
TE26-06	648	1375	0.47	575	0.282761	0.000026	0.001881	0.09015	0.69	0.76	12.0	4.9
TE26-07	118	319	0.37	597	0.282589	0.000011	0.000994	0.04203	0.91	1.10	6.7	6.7
TE26-08	3700	6993	0.53	571	0.283179	0.000021	0.006370	0.30487	0.11	-0.06	24.9	9.1
TE26-09	886	1955	0.45	591	0.282781	0.000016	0.003007	0.14389	0.68	0.73	12.6	8.3
TE26-12	517	1296	0.40	586	0.282675	0.000015	0.001899	0.08971	0.81	0.94	9.2	-3.1
TE26-14	217	332	0.65	590	0.282639	0.000015	0.001701	0.07151	0.86	1.01	8.1	-0.5
TE26-15	159	485	0.33	576	0.282566	0.000009	0.000784	0.03376	0.93	1.16	5.5	12.2
TE26-17	2255	2256	1.00	586	0.282917	0.000030	0.003889	0.15797	0.50	0.46	16.9	1.9
TE26-18	1328	3076	0.43	572	0.282778	0.000014	0.002857	0.13049	0.68	0.75	12.1	7.7
TE26-19	199	355	0.56	583	0.282569	0.000012	0.001104	0.03890	0.94	1.16	5.7	6.0
TE26-25	1117	2196	0.51	585	0.283249	0.000035	0.005848	0.29581	0.00	-0.24	27.9	6.3
TE26-26	7853	15165	0.52	582	0.283333	0.000040	0.007195	0.36380	-0.14	-0.39	30.3	10.1
TE26-28	156	362	0.43	603	0.282554	0.000012	0.001092	0.04912	0.96	1.18	5.6	1.9

Sample TH 24 Tihoiiarène

Analysis No.	Th (ppm)	U (ppm)	Th/U	Age (Ma)	$^{176}Hf/^{177}Hf$	1 se	$^{176}Lu/^{177}Hf$	$^{176}Yb/^{177}Hf$	T(DM) (Ga)	T(DM) (crustal)	epsilon Hf	discordance %
TH24-01	1943	8288	0.23	567	0.282660	0.000010	0.003139	0.14327	0.86	1.01	7.3	1.5
TH24-10	751	3038	0.25	546	0.282370	0.000059	0.002017	0.09043	1.24	1.63	-2.9	42.4
TH24-13	2631	5096	0.52	579	0.282802	0.000020	0.002567	0.11293	0.64	0.68	12.8	2.8
TH24-14	162	484	0.34	537	0.282569	0.000006	0.001331	0.05838	0.94	1.19	4.2	-9.0
TH24-15	689	1999	0.34	564	0.282668	0.000007	0.001956	0.07902	0.82	0.97	8.0	11.7
TH24-16.2	434	1886	0.23	554	0.282634	0.000013	0.002307	0.09232	0.88	1.06	6.5	6.3
TH24-17	249	485	0.51	552	0.283079	0.000035	0.002400	0.09726	0.25	0.08	22.2	32.2
TH24-19.2	21364	40522	0.53	558	0.282711	0.000018	0.004185	0.16882	0.81	0.93	8.6	3.0
TH24-21.2	3755	7666	0.49	498	0.282821	0.000028	0.009408	0.35123	0.76	0.83	9.6	-1.5
TH24-22.2	145	441	0.33	599	0.282983	0.000310	0.010284	0.43861	0.49	0.47	16.6	14.6
TH24-26	1996	8171	0.24	592	0.282578	0.000017	0.001958	0.10411	0.95	1.15	5.4	-12.7
TH24-32	26618	45162	0.59	495	0.282498	0.000015	0.003345	0.18515	1.10	1.41	0.1	56.7
TH24-34	510	2287	0.22	607	0.282507	0.000011	0.003320	0.17962	1.09	1.33	2.7	32.7
TH24-42	4302	16838	0.26	493	0.282481	0.000016	0.004105	0.19985	1.15	1.46	-0.8	19.7
TH24-46	532	1276	0.42	597	0.282618	0.000011	0.002640	0.13339	0.91	1.08	6.7	14.3
TH24-47	212	521	0.41	567	0.282488	0.000011	0.002358	0.11402	1.08	1.37	1.6	8.4
TH24-48	1042	3268	0.32	568	0.282492	0.000015	0.002417	0.10537	1.08	1.36	1.7	-1.8
TH24-49	975	2323	0.42	574	0.282466	0.000010	0.003285	0.13860	1.14	1.44	0.6	21.5
TH24-50	207	554	0.37	604	0.282544	0.000008	0.001420	0.06355	0.98	1.21	4.7	-13.3
TH24-52	302	711	0.43	500	0.282541	0.000015	0.001476	0.06306	0.99	1.27	2.3	16.5
									0.91			

Sample: TI59 Tioueiine

Analysis No.	Th (ppm)	U (ppm)	Th/U	Age (Ma)	$^{176}Hf/^{177}Hf$	1 se	$^{176}Lu/^{177}Hf$	$^{176}Yb/^{177}Hf$	T(DM) (Ga)	T(DM) (crustal)	epsilon Hf	discordance %
TI59-01	72	154	0.47	609	0.282599	0.000006	0.000606	0.01809	0.88	1.06	7.1	2.2
TI59-02	2375	4456	0.53	565	0.282576	0.000007	0.002103	0.07556	0.95	1.17	4.7	6.5
TI59-05	3624	5570	0.65	570	0.282558	0.000007	0.003533	0.13051	1.02	1.25	3.6	9.8
TI59-06	3716	5395	0.69	561	0.282556	0.000008	0.003506	0.13025	1.02	1.25	3.4	10.5
TI59-07	335	514	0.65	597	0.282592	0.000008	0.001698	0.05711	0.92	1.11	6.1	15.7
TI59-08	3504	7185	0.49	565	0.282547	0.000007	0.002624	0.09812	1.01	1.25	3.5	11.1
TI59-10c	2360	3759	0.63	559	0.282584	0.000008	0.002794	0.10153	0.96	1.18	4.6	8.7
TI59-10r	483	1526	0.32	605	0.282609	0.000007	0.001400	0.04538	0.89	1.06	7.0	10.3
TI59-11	2268	4112	0.55	560	0.282545	0.000008	0.003243	0.12195	1.03	1.27	3.1	15.5
TI59-12	5705	8637	0.66	563	0.282565	0.000010	0.003172	0.10879	1.00	1.23	3.9	5.3
TI59-13	2409	4314	0.56	566	0.282569	0.000015	0.003083	0.12235	0.99	1.21	4.1	6.2
TI59-14	3484	6053	0.58	561	0.282526	0.000009	0.003324	0.12659	1.06	1.32	2.4	7.9
TI59-20	2310	4555	0.51	571	0.282560	0.000012	0.003236	0.11707	1.01	1.23	3.9	20.3
TI59-25	3029	5506	0.55	555	0.282540	0.000008	0.003066	0.11236	1.03	1.28	2.9	4.1
TI59-26	5613	7183	0.78	554	0.282563	0.000010	0.003719	0.14765	1.02	1.25	3.4	6.8
TI59-30	2001	3780	0.53	566	0.282555	0.000008	0.003058	0.10540	1.01	1.24	3.6	4.9
TI59-32	1679	3832	0.44	571	0.282551	0.000008	0.003095	0.11517	1.02	1.25	3.6	5.6
TI59-33	3682	5149	0.72	563	0.282524	0.000010	0.003822	0.14222	1.08	1.33	2.2	4.8
TI59-34	1733	3372	0.51	557	0.282542	0.000008	0.002725	0.10162	1.02	1.27	3.1	9.7
TI59-37	3714	7640	0.49	568	0.282550	0.000012	0.002096	0.08010	0.99	1.23	3.9	3.1
TI59-40	4162	6302	0.66	562	0.282561	0.000006	0.003080	0.11351	1.00	1.23	3.8	5.8
TI59-43	3108	5861	0.53	567	0.282579	0.000017	0.003191	0.12541	0.98	1.19	4.5	3.7